Alma Mater Studiorum · Universita' di Bologna

Dottorato di ricerca in Ingegneria Elettrotecnica-Ciclo XXIX

Settore Concorsuale di afferenza: 09E2
Settore scientifico disciplinare: ING IND/33

FUNDAMENTAL STUDY AND MODELING OF NANOFLUIDS

Fabrizio Negri

Tutor:
Prof. Andrea Cavallini

Coordinatore:
Prof. Domenico Casadei

ANNO ACCADEMICO 2016-2017

A mia madre...
che grazie ai suoi sacrifici
mi ha permesso di raggiungere questo traguardo.

To my mother...
who lets me reach this goal
thanks to all her sacrifices.

Table of Contents

List of Figures

Abstract of the thesis

In spite of all the recent studies (see e.g. [1], [2], [3]), the insulating materials employed for high voltage (HV) transformer manufacturing are still those in use since several decades. Economic (development costs) and strategic issues (uncertainty about design rules and long-term performance) are the reasons for a general hostility of small manufacturers to technological changes. In a specular way, big market players with significant $R\&D$ expenditures are interested in improving the transformer technology and acquire a monopolistic position.
For the fluid insulation, mineral oil (MO) still dominates thanks to its excellent dielectric and cooling performances [5]. However, being MO a carcinogenic agent, the electric industry searched alternatives for applications where environmental concerns are of greater concern (e.g., offshore equipment, trains). In this context, many efforts have been done to study green fluids, mostly natural and synthetic esters, to replace MO [6]. However, green alternatives have a low resistance to electrical discharge propagation [7]. Therefore, they are used nowadays almost exclusively for medium voltage equipment and remain a niche product.
Despite the predominance of MO, industry is interested in liquid dielectrics with enhanced cooling properties. If available, these fluids could reduce the insulation volumes and increase the power densities, thus becoming a driver for a market revolution.
Some researchers [8], [9] have started to experiment with MO-based nanofluids (i.e., colloidal solutions of nanoparticles in a base fluid), with the aim of improving the MO heat exchange capabilities. Common sense suggests that the dispersion of conductive particles in an insulating liquids tends to reduce the dielectric withstand properties of the fluid. On the contrary, nanofluids show enhanced properties explained by the electrical properties of the nanoparticles (in particular, electron attachment properties) under the condition that nanoparticles are well dispersed inside the base fluid. Therefore, a good dispersion of nanoparticles is a key point to pursue to manufacture a good nanodielectric. It is not easy to understand how to obtain a good, stable dispersion of the nanoparticles; a logical starting point is avoid using nanofluids with high concentration of nanoparticles. This way, the mean free path between nanoparticles increases weakening the van der Waals attractive forces. Since these forces might lead to nanoparticle aggregation, lower concentrations favor the stability of nanoparticles within the fluid. A second key point, after the fluid stability requirement, is the insulating performance. Researchers have started to study nanofluids because of their outstanding thermal properties, but these fluids should be excellent also regarding all the electrical properties, ranging from the power losses to the discharge propagation resistance. Furthermore, these properties, if proved,

shall also be stable during time, that is, they should not be affected by aging too much. The aim of this thesis is hence to give an answer to all of these questions:

1. what is the best nanofluid concentration in terms of electrical properties and stability?
2. what are the basic properties of nanofluids compared to those of mineral oil?
3. how do these properties change with time, or, what about the long term stability?
4. are there any risks for the nanofluid stability?

Since the world of nanodielectrics, and that of nanofluid too, is too wide, we have limited our investigation to the field of mineral oil-based nanofluids, where the added nanoparticles have been magnetite (Fe_3O_4).
The following chapters are structured in the following way:

- chapter one starts with a brief introduction to the features an insulating liquid shall possess and then introduces mineral oils, which are still the most used insulating fluids. Their basic properties in terms of discharge and aging resistance are reported and discussed;
- chapter two contains the first results about nanofluids. First, a general introduction about the manufacturing process of nanofluids is reported, and then some literature studies are discussed. Later on, some electrical tests are discussed, considering the already published works about nanofluids. Finally, Schlieren imaging results are presented to discuss the discharge development in nanofluids.
- chapter three is the first theoretical chapter, with the aim to propose a mathematical model to give the basis to a general idea about the nanoparticle interaction with the injected charge; in this chapter we would like to prove that nanoparticles are likely to create a homocharge layer close to the HV electrode injecting charge;
- chapter four presents the results of an investigation about slow voltage waveforms ($50\,Hz$ sinusoidal and DC). Breakdown and partial discharge issues are studied and reported. At the end of the chapter some important key points are introduced, opening the second part of the thesis;
- chapter five is the second theoretical chapter, presenting different models with the aim to derive an analytical expression for the electric field distribution close to the nanoparticles, which is claimed to be the responsible of all the phenomena taking place in their proximity;
- chapter six can be considered the most important one of the thesis in the sense that contains the most important results. First, a comparative study is carried out to understand the injection of charge carriers from electrodes of different polarities to the nanofluid; later on we have compared the conductive behavior of a low concentration nanofluid with a higher concentration one, verifying the existence of different conduction

modes.
At the end of the chapter we have discussed a non stable behavior of nanofluids, when exposed to highly non uniform fields;

- chapter seven contains some experimental results about the dielectric properties of nanofluids (relative permittivity and AC conductivity), together with some simple models able to explain them.

At the beginning of each chapter, a brief abstract will introduce its content.

Chapter 1

Introduction to mineral oil insulating fluids

Abstract

This chapter introduces the insulating fluids which are used in the electrical apparatuses.
First, a brief overview about the features an insulating liquids should own is presented, and then more attention has been given to mineral oils, because they will be the basis of the investigated nanofluids and because they are the most used insulators in power transformers and cables insulation systems. Mineral oils are not described in details, because they are quite known nowadays and there are a lot of references about them, but the main properties and theories are recalled, because they will be used in the following chapters.

Dielectric fluids are an important part of the insulation systems for a lot of types of electrical apparatuses, such as transformers, bushings, cables and capacitors. Depending on the application, different electric features are required for such insulating devices: high values of electrical permittivity are necessary to reduce the physical sizes of capacitors for instance, lower ones are desired to uniform stresses in solids-liquids composites insulations, while all should have low dissipation factors in common, to reduce energy losses and thus increase the efficiencies.
Anyway, liquids are used in these equipment not only for their electrical properties, but also for their thermal exchange ones, which can be summarized in high values of specific heat and thermal conductivity together with low viscosity values and pour points.
The different properties which are requested for insulating liquids result in a problem to define a unique fluid which can be used everywhere; synthetic fluids are usually preferred in capacitors thanks to their high dielectric constants, while hydrocarbon liquids were widely used in the past in cables, before being replaced by solid extruded insulators.
Anyway, despite what it could be thought from the above mentioned considerations, mineral oils are nowadays the most used solution in the electrical applications ([4]).

Mineral oil is a class of insulating fluids refined from petroleum crude stocks, which find their natural application in transformer insulation, because of their optimal electrical properties and good thermal exchange ones. Even if they are not environmental friendly, it is estimated that in the US, at the end of the last century, more than two billion gallons were present inside transformers ([4]). Some transformer manufacturers, in order to overcome the environmental criticalities of mineral oils, have started to investigate and use vegetable fluids, but it has been demonstrated that they can be used only for distribution applications ([7]), because of their low electrical withstand properties at large gaps which are necessary for high voltages.

Fig. 1.1 represents the working scheme of a general petroleum refinery. With-

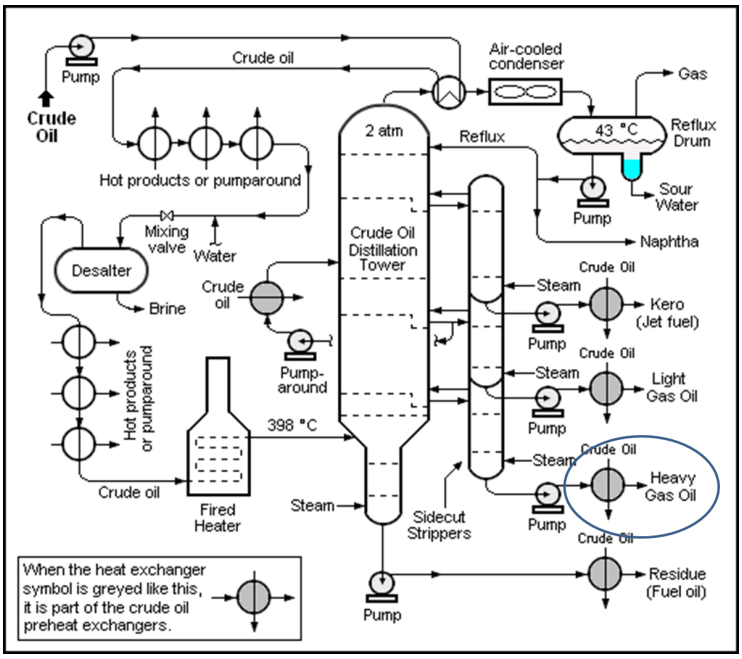

Figure 1.1: General scheme of a petroluem refinery (the mineral oil step is circled).

out entering the details of each step of the refinement process, we can easily see that mineral oils are the results of the first step of the distillation procedure, according to a defined boiling temperature range, which depends on the nature of the mineral oil the refinery wants to produce ([10]). Mineral oils indeed, being manufactured starting from crude oil, share most of the chemical properties with it; as reported in fig. 1.2, they are a mixture of paraffinic (chemical formula $C_{2n}H_{2n+2}$), nafthenic (chemical formula $C_{2n}H_{2n}$) and aromatic compounds (chemical formula C_nH_n), whose ratio defines their macroscopic behavior. In particular, aromatic compounds are usually a minor part and a mineral oil can be "'paraffinic"' or "'naphtenic"' depending on which of the other components is the prevailing.

"'Paraffinic"' oils are more viscous in general, but they have higher boiling temperatures (and thus higher distillation temperatures), while "'naphtenic"' ones are less viscous and with lower boiling temperatures.

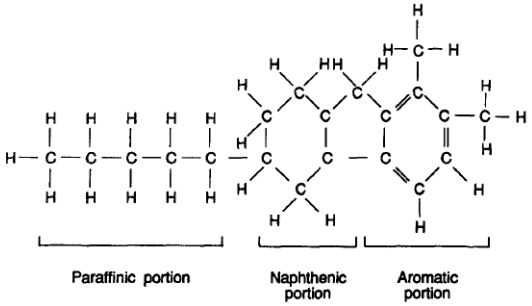

Figure 1.2: Example of a possible molecule structure of mineral oil (after [4]).

It is clear from this consideration that the majority, but not the totality of the in service transformers, are insulated with "'naphtenic"' mineral oils, because of the better heat exchange capabilities due to a reduced viscosity. If the "'paraffinic"' and "'naphtenic"' content of the oil mainly influences the thermal exchange properties of mineral oil, different considerations have to be made about the "'aromatic"' content, even if, as already said, it is the minor part. A lot of studies in the past ([11]-[12]) have confirmed that the aromatics components have a remarkable influence on the pre-breakdown (streamer) propagation properties of insulating fluids. In particular, aromatics are characterized by two properties:

- "'Low ionization potential"': it means that it is easy to ionize an aromatic component. This feature is related to the positive streamer propagation, which relies on the ionization properties of the medium in which it propagates;
- "'High electronegativity"': this is related to the negative streamer initiation, which is facilitated since such behavior tends to extract electrons from the electrodes surfaces.

1.1 Streamer propagation theory (after [12])

This section describes the results obtained by Devins in [12], which analyzed the pre-breakdown phenomena related to different types of insulating fluids, including transformer oils. As already anticipated in the previous paragraph, pre-breakdown phenomena are usually referred as streamers and their study is mainly focused on two of their properties:

1. "'Initiation"', i.e. how they originate inside the fluids;
2. "'Propagation"', that is if and how they reach the opposite electrode.

Usually, we are more interested in propagation issues, because they are likely to lead to the streamer-to-leader transition, thus causing the breakdown of the insulator. Since divergent field configurations are likely to highlight the "'propagation"' mode of the streamers, a lot of studies, including [12], are focused on this particular experimental condition. In the following, we summarize the results obtained by Devins about the positive and negative streamer propagation

inside mineral oil, because they will be referred to in the following chapters. Before doing that, it is necessary to point out that Devins did not study the relation between the streamer propagation and voltage, which is for instance reviewed in [11], but he only limited himself to study the basic mechanisms leading to the streamer propagation.

1.1.1 Positive streamer propagation mode

In the case in which the high voltage electrode creating the field inside the insulating liquid is positively charged, it is clear that no electron injection can take place; thus, a pre-breakdown phenomenon is evidently not initiated from charge injection. In order for a streamer to start, it is necessary that a free electron is available inside the fluid, and this is usually liberated by random processes including field ionization or natural cosmic rays or radioactivity ([14], [15], [11]). The free electron is then accelerated towards the positive electrode, increasing the electric field which in turn becomes so high to induce a more deterministic field ionization, which is the responsible of the generation of an avalanche process, as it is possible to see from fig. 1.3. This picture, besides clarifying the

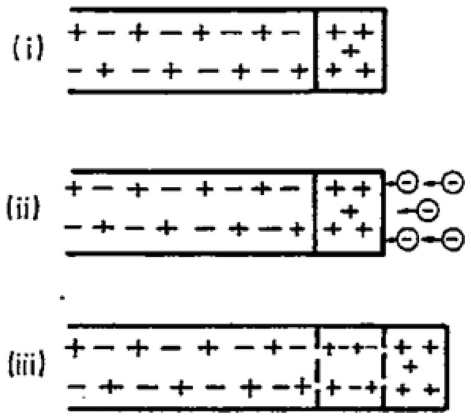

Figure 1.3: Positive streamer general propagation mechanism (after [13]). The positively charged tip is the head of the streamer.

positive streamer initiation and propagation mechanism, lets understand why it is usually reported that positive streamers are filamentary (1) and very fast (2):

1. "'filamentary"': this is due to the fact that the process proceeds via local ionization where the field is above the ionization threshold and it is not induced, as it will be shown in the following, by charge extraction from the electrodes;

2. "'fast"': this is connected to the field increase due to the presence of a filamentary charged structure (the streamer itself). Since the streamer increases the electrical field (needle effect), the ionization process goes further at a higher rate than at the beginning.

Fig. 1.4 shows some acquisitions taken from [12], which refer to shadowgraph images of a positive streamer propagating inside a "'naphtenic"' transformer

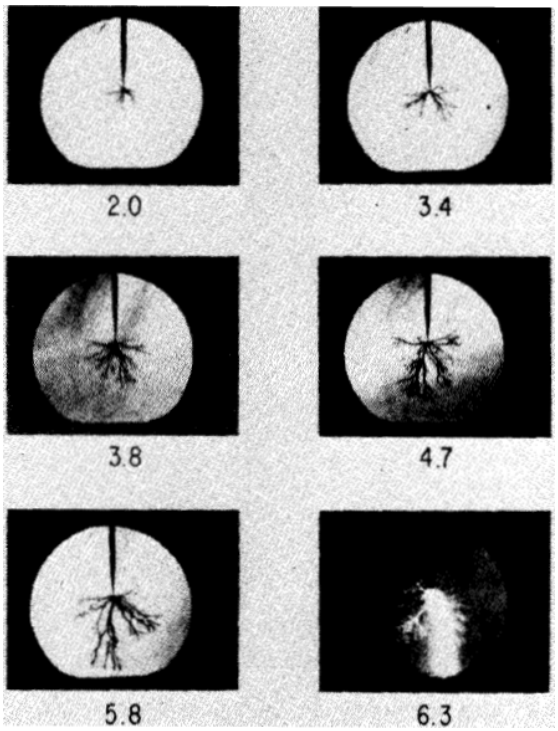

Figure 1.4: Positive streamer acquisitions (shadowgraph technique). Each image refer to a specific time instant after the streamer initiation [microseconds] (after [12]).

oil subjected to rectangular step voltage, which later on converts to a leader, causing the complete breakdown of the insulating gap. It is possible to see that, as reported in the previous considerations, the streamer shape is nearly filamentary.

The nature of positive streamers, which has now been clarified, helps understand why in the previous section aromatics were said to facilitate the streamer propagation: being easily ionized, they speed up the avalanche process, leading to a lower voltage breakdown. A simple model suggested by Devins in [12], based on the Zener ionization theory[1], lets estimate the streamer propagation velocity as:

$$v = r_0 \sqrt{\frac{ae^3 {E_0}^3}{\pi m \epsilon^3}} \frac{n}{c} \, erfc\left(\sqrt{\frac{\pi^2 maW^2}{h_0 e E_0}}\right) \tag{1.1}$$

where:

1. r_0 represents the streamer radius which has been modeled as a conductive cylindrical channel;

2. a represents the average molecular separation;

[1]The Zener ionization theory should be applied only to solid insulation materials and not to fluids, but it is anyway sufficient to catch some important aspects of the liquid state, too. For a more detailed quantitative description of the problem, refer to [16].

3. e represents the elementary charge;
4. h represents the Planck constant;
5. m represents the electron mass;
6. W represents the liquid phase ionization potential (band gap);
7. E_0 represents the electric field at the streamer tip;
8. n represents the molecule density;
9. c represents the concentration of positive and negative carriers;
10. $erfc$ represents the complementary error function, defined as:

$$erfc(x) = \frac{2}{\sqrt{\pi}} \int_0^{+\infty} e^{-t^2} dt \tag{1.2}$$

Looking at the parameter ϵ in equation 1.1, it is then evident that a reduction of the liquid phase ionization potential due to the presence of aromatics can favour the streamer propagation.

1.1.2 Negative streamer propagation mode

Negative streamers, i.e. pre-breakdwon phenomena taking place when the high voltage electrodes are negatively charged, are somehow different. In this case indeed, when the maximum electric field exceeds the injection threshold, electrons are injected inside the insulating fluid ([11], [12], [17]). The interactions between the injected charge and the molecules of the liquid is then able to raise locally the temperature till the evaporation ([14], [18]). In this way a gas bubble is usually generated and, because of the electrical permittivity mismatch between the air and the liquid, the electric field inside the bubble is higher than in the fluid, letting the electrons to gain sufficient energy to ionize later the liquids molecules. Electrons release indeed the acquired energy to the fluid via attachment reactions, as schematically represented in fig. 1.5.

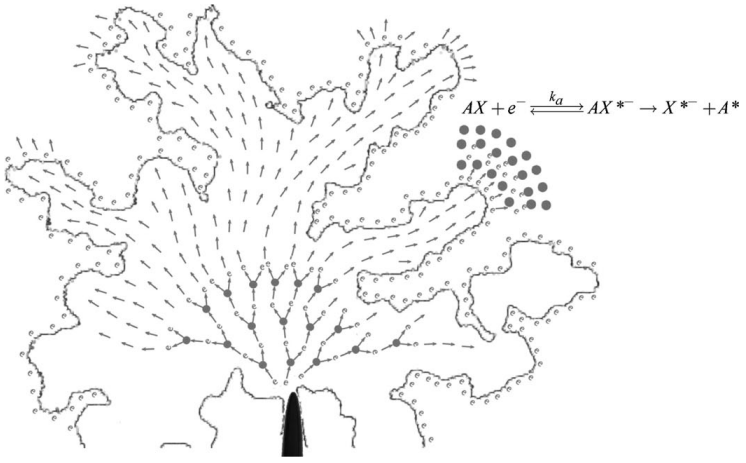

Figure 1.5: Negative streamer propagation mechanism, after [19].

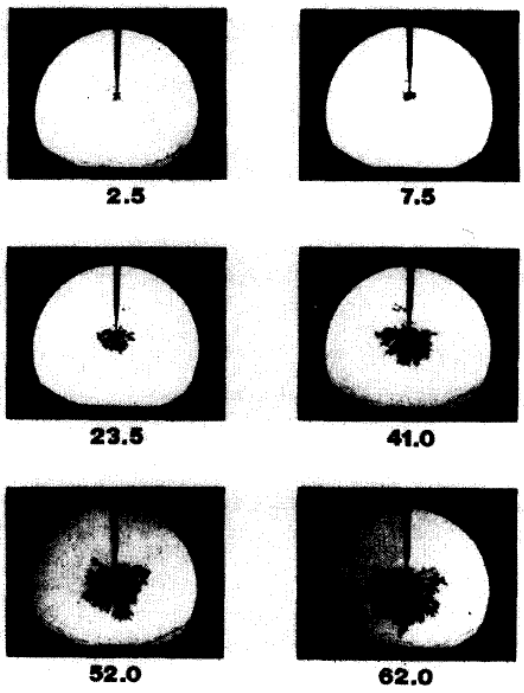

Figure 1.6: Negative streamer acquisitions (shadowgraph technique). Each image refer to a specific time instant after the streamer initiation [microseconds] (after [12]).

This energy exchange phenomenon increases the size of the original bubble, giving rise to an avalanche process which tends to be bushier than the previous described one. Generally speaking, negative streamers have a bushy shape and a lower speed than positive streamers, as it is possible to see from fig. 1.6.

The reduced, and non uniform speed of the negative streamer, has been explained by Chadband and Wrigth in [20], who calculated the electrical field distribution generated by a growing conducting sphere (a schematic model of the streamer growth) and found that the field at its edge goes through a minimum at approximately 60% of the gap.

In order to explain the results obtained from the observation about the negative streamer propagation, Devins ([12]) formulated the following "'two step model"':

- electron injection and trapping: during this first step, electrons are injected and trapped at the gas-liquid interface, as it is possible to see from fig. 1.5. The extracted electron concentration and its distance from the high voltage electrode depends upon the electron scavenger concentration inside the insulating fluid. This results in a space charge layer close to the high voltage electrode, which acts as homocharge, i.e. reduces the field close to the electrode, but increase it at the streamer tip;

- ionization: once the field increase is sufficient to ionize the liquid molecule, the avalanche process can start and propagate towards the other electrode.

The "'two step model"' states that the average streamer velocity (which is at least one order of magnitude lower than the positive streamer one) can be obtained by averaging the time spent by the electrons in each phase: the higher the time in the first step, the lower the streamer propagation speed and vice versa.

Electron scavenger components, like the aromatics, are likely to reduce the time spent in the first step, because they facilitate the charge extraction. In this way, the field at the streamer tip increases faster and the streamer assumes the shape and the features of the positive one.

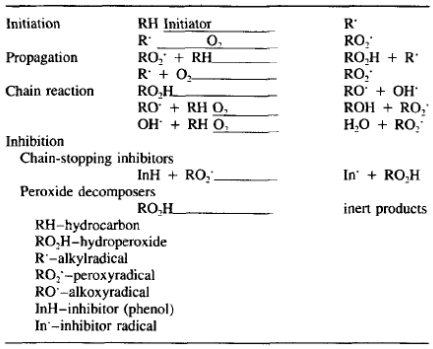

Figure 1.7: Oxidation processes in hydrocarbon oils.

The previous two sections clarify that the presence of aromatics is an index facilitating pre-breakdown mechanisms reducing in this way the withstand capability of the insulating fluids. These considerations suggest that it is necessary to reduce the aromatics concentration as mush as possible, but this is not possible for an obvious economic reason concerning the distillation process, and because aromatics can also have a positive effect for liquids. They have in fact two important positive effects:

1. they protect the insulating fluid from oxidation, and thus from ageing effects;

2. they prevent the gas bubbles formation, reducing the risk of partial discharges and their consequent ageing process.

There is a third, but minor reason why aromatics have a positive influence on insulating oils; they increase in fact the viscosity of the fluid itself and this aspect can help to hinder the effect of contaminants. Indeed, contaminants usually increase dielectric losses, unless their mobility is very low; by increasing the viscosity, the mobility of contaminants is obviously reduced, preventing them to increase the dielectric losses[2].

1.2 Mineral Oil oxidation resistance

The oxidation of insulating oils, and mineral oils in particular, results in the formation of organic weak acids, sludges (which are composed of insoluble condensed matter) and polar byproducts ([4]).
Weak acids and polar byproducts increase dielectric losses and conductive properties, and may be deleterious for the applications in which polarization currents have to be minimized (cables and transformers for instance), while sludges are able to increase locally the viscosity of the insulating liquid thus reducing its heat transfer properties creating thermal hot spots which can accelerate the

[2]This is true in the limit of temperature operations, which, as known, tend to reduce the values of the viscosity. The increase in viscosity is anyway dangerous in terms of reduced heat transfer capabilities of the insulating fluid.

dielectric degradation. Oxidation is not only due to the access of air inside the insulating liquid, but it is usually catalyzed by copper particles which are present because copper is the element though which the conductive parts of the electrical systems are usually realized. Since oxidation byproducts are dangerous for the electrical assets, aluminum has now largely replaced copper as the active material in distribution transformers and the enamels frequently used as replacements for paper insulation and current magnetic steel coating reduce the contact between oils and catalytic metals.
In [4], M. Duval explains that all the hydrocarbon insulating oils degrade according to the same oxidation mechanism, which can be summarized as follows:

1. oxygen attack on hydrocarbon molecules which result in the formation of peroxides or hydro-peroxides, which later on dissociate into reactive radicals (initiation process);

2. radicals then react with hydrocarbon molecules to form intermediate oxydation compounds as aldehydes, alcohols and ketones and new active radicals (propagation);

3. these new radicals react with hydrocarbon molecules, too, to form organic acids and polymeric sludges (chain reactions).

Fig. 1.7, which has been taken from [21], summarizes the above mentioned phenomena related to oxidation processes. The chemical composition of mineral oils obviously influences their oxidation resistance. Paraffinic and naphtenic compounds, for instance, if not protected by inhibitors, which in certain conditions can be represented by aromatics, oxidize rapidly to form organic acids. Di- and tri-aromatics are able to form phenolic structures with good antioxidant properties during the oxidation process and so are particularly favorable. These aromatic compounds oxidize rapidly, however, with the formation of oil-insoluble sludges.
Taking into account the pre-breakdown issues considerated in the previous section, a good compromise for the aromatics concentration inside mineral oils is from 5% to 15%. Fig. 1.8 helps to understand why: in this picture indeed, it is possible to see that, when the aromatics concentration is close to the aforementioned range, the "'protective"' properties have a minimum, indicating that they reach their optimum value, while the heat transfer capability and viscosity do not worsen too much.

1.3 Gas Adsorbing behavior under electrical discharges

Gas bubbles can originate inside insulating liquids as a result of thermal and electrical degradation processes. Bubbles, whatever their origin is, are characterized by a lower value of dielectric strength and electrical permittivity and are thus subjected to higher electrical stresses.
Hydrogen is for instance formed either by decomposition of oil vapors or through reactions at the oil-gas interface, and may recombine to form hydrogen gas. A H_2 bubble is eventually created, and it can increase its volume until breakdown or arcing may occur; if such phenomenon happens, the oil is said to be "'gas

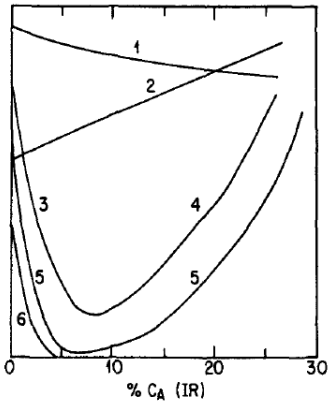

1. Specific heat, thermal conductivity
2. Viscosity, refractive index, density
3. Gas evolution
4. Gas absorption
5. Oxidation
6. Inhibitor response

Arbitrary relative ordinate units.

Figure 1.8: Influence of the aromatic content on the physical and chemical properties of mineral oils (after [4], [22], [23]).

evolving"', because there is no obstacle to the bubble formation and growth. In alternative, the oil is said to be "'gas adsorbing"', if the nascent hydrogen is reacting with oil molecules, preventing the growth of the gas bubble. Fig. 1.8 shows how the "'gas evolving"' tendency of mineral oils changes with the aromatics (polyaromatics, in particular) content. In particular, for very low aromatics concentrations, the decreasing curve tendency is due to the reduction of the gas evolving behavior due to an increase of the gas adsorbing tendency. Again, the optimum situation is reached when the final concentration is around $5 - 10\%$.

Chapter 2

Introduction to mineral oil based nanofluids

Abstract

This chapter will introduce the field of nanofluids and in particular those manufactured starting from mineral oil. These liquids are a relatively new class of insulating materials, aiming at replacing the traditional ones, because of their outstanding possibilities in terms of power densities increase.
First, a review about the preliminary results concerning ferrofluids-based nanofluids is carried on; later on in this chapter the first measurement results about our investigated fluids are reported and discussed, considering the theories presented in the previous chapter.

One of the first studies about the electrical properties of nanofluids has been reported in [24]. Generally speaking, researchers have always doubted about the possibility of adding particles inside insulating fluids, especially if they were conductive, because of the reduction of the withstand capabilities ([25]-[26] for instance). In [24] instead, the authors explored the benefits obtained by adding magnetite nanosized particles inside mineral oil, knowing that conductive nanoparticles could increase the thermal exchange properties of insulating fluids in such a way to reduce the size of the electrical equipment and so to increase their power densities ([27], [28], [29]).
Magnetite nanoparticles (Fe_3O_4) dispersed inside a blendant fluid based on organic solvents are generally referred in literature as *ferrofluids*. They were first invented in 1963 by NASA's Steve Papell as a liquid rocket fuel which could be drawn toward a pump inlet in a weightless environment by applying a magnetic field ([30]). In order to be used for final purposes, ferrofluids must necessarily have a stable behavior, i.e. magnetite nanoparticles should not agglomerate. In particular, they should behave as colloids and not suspensions, meaning that a suspension is not a stable mixture of particles and blendant fluid. It is very difficult to manufacture a stable colloid made of magnetite nanoparticles (usually the mean radius of such nanoparticles is bigger than $10\,nm$), because of the forces which tend to collect them tending to form an agglomerate. The solution which is generally adopted to produce a final usable product is the use of surfac-

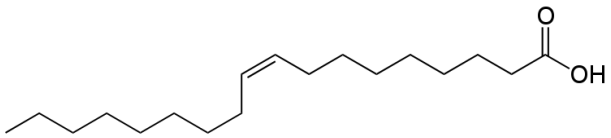

Figure 2.1: Chemical structure of oleic acids, the most used surfactant for ferrofluids manufacturing process.

tants, i.e. long chain molecules which are able to keep nanoparticles separated, preventing them to attract. From a chemical point of view surfactants are:

- oleic acid;
- tetramethylammonium hydroxide;
- soy lecithin;
- citric acid.

Oleic acid is the most used surfactant in commercial ferrofluids, and in particular it is the one which has been used in the ferrofluid which has been used to manufacture the nanofluids which are the object of this work. Without entering too much into the details of the chemical structure (which is shown in Fig. 2.1), we only say that it is a fatty acid, in which one termination is hydrophobic and the other one hydrophilic, containing the hydroxyl group OH. Fig. 2.2, which has been taken from [31], shows how surfactants act in order to prevent the Wan der Waals attractive forces to agglomerate nanoparticles.

The idea to increase the distance among nanoparticles in order to improve the colloidal solution stability can find a mathematical explanation in the Darjanguin-Landan-Verwey-Overbeek (DLVO) theory ([32]), which states that the total interaction energy of the nanoparticles, i.e. the sum of the van der Walls attraction and the electrostatic repulsion, develops an energy barrier the particles must overcome in order to aggregate. If this energy barrier is higher than 15 kT, then the nanofluid is considered stable ([33]); the increase of the mean distance

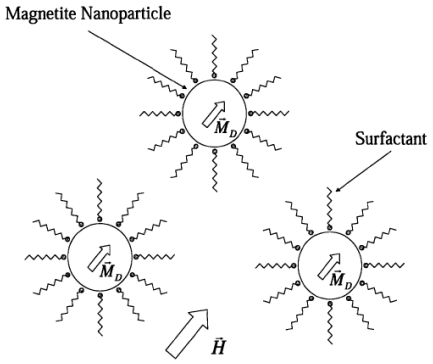

Figure 2.2: Effect of surfactants on the nanoparticles mean distance.

among nanoparticles has the obvious effect of increasing the energy barrier between them, because it shifts the balance between Wan der Walls forces and repulsive ones to the latter. Another equivalent approach to study the stability of nanoparticles inside a nanofluid has been reported in [34] and [31] and consists in the analysis of the ratio between the thermal energy kT and the attractive gravitational and magnetic energies. The result of this investigation is the maximum size nanoparticles should have to be considered stable, which is usually less than 10 nm. Commercial magnetite nanoparticles have an average radius of about $10-15\,nm$ and this causes an instability mechanism which takes place at longer times, even in the presence of surfactants.

2.1 Impulse Breakdown voltage of Nanofluids (after [24])

This section has the aim to introduce the results obtained by Seagal in [24]. In this work, there is no indication about the concentration of the nanoparticles which have been dispersed inside the mineral oil, but the authors say that they refer to the "'optimum concentration"'. Apart from this aspect, they have performed impulse ($1.2 - 50\mu s$) breakdown tests under divergent fields (needle to sphere electrode configuration), as done by Devins in [12]. In this way, they focalized their attention to the streamer (and leader) propagation features inside oil (benchmark) and the corresponding nanofluids. The results, presented in figure 2.3, refer to a $25.4\,mm$ inter-electrode gap and two different base naphtenic mineral oils: Univolt 60 and Nytro 10X. The first column, about the breakdown voltage values, clearly shows the asymmetry between positive and negative polarity; this is a quite known effect in literature, which is due to the different propagation modes of positive and negative streamers and which is explained by Devins in [12]. The different streamer propagation modes are clearly visible looking at the third column, where the average avalanche velocity is reported, showing how positive streamers are much faster than negative ones. The third and fourth rows of fig. 2.3 are relative to nanofluids manufactured starting from the previously introduced mineral oils, without any indications about the magnetite concentration. The results about this class of fluids are particularly interesting:

- under positive polarity, there is a significant increase of the withstand capabilities of the insulating fluid: the breakdown voltage is almost doubled;
- under negative polarity there is a slight reduction, even if we do not know if it is an actual reduction or if it is due to the normal scattering of the

Liquid	Gap	Breakdown Voltage, kV		Time, μs		Velocity, Km/s	
	mm	Negative Needle	Positive Needle	Negative Needle	Positive Needle	Negative Needle	Positive Needle
Univolt 60	25.4	170	86	27	12	0.94	2.10
Nytro 10X	25.4	177	88	23	16	1.10	1.59
Univolt 60 Colloid	25.4	154	157	15	26	1.69	0.98
Nytro 10X Colloid	25.4	173	156	17	25	1.49	1.02

Figure 2.3: Results of the tests presented in [24].

measurement results; in other words, we have no information about the confidence levels of the presented results.

Apart from the slight apparent reduction under negative polarity, the high increase under the positive polarity indicates that the resulting fluids have higher impulse breakdown strengths compared to mineral oil ones, that is, the contribution of the magnetite nanoparticles is evidently positive.
From Seagal work anyway, it is not possible to see if the improving behavior is concentration-dependent or not, because, as already stated in the previous statements, nothing is said about the way to produce the "'optimum"' nanofluid. The word "'optimum"' lets suppose that the behavior can be concentration-dependent, but we do not know if there is an improving trend with the concentration or not and no final conclusions can be drawn from the negative polarity. In order to give an answer to such questions, the experiments presented in [24] have been repeated with different nanofluids concentrations.

2.2 Repeated Impulse breakdown tests

Impulse breakdown tests have been performed using a Passoni Villa $600\,kV/20\,kJ$ 6 stages generator; the divergent field configuration has been obtained by using a needle ($15\,\mu m$ average radius of curvature, controlled by optic microscope) to plane electrode; gap spacing was $10\,mm$. The test procedure which has been adopted to evaluate breakdown voltage values is represented in fig. 2.4, which has been taken from [35]. The starting voltage value has always been $20\,kV$, the

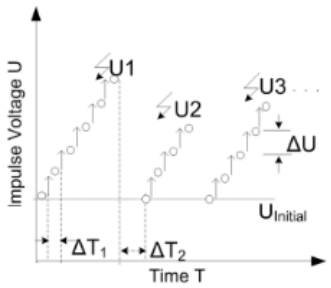

Figure 2.4: Adopted test procedure to evaluate the breakdown strength, after [35].

ΔU was $5\,kV$, the ΔT_1 time value between two unsuccessful tests was 1 minute, while the ΔT_2 time value after the electrical discharge was 5 minutes. For each sample and each polarity, 8 tests have been performed. Because of the high energy value of the HV generator, needles electrodes have been changed after each discharge, because it was impossible to protect them with series resistors. Mineral oil base fluid has been BergOil Transag G11, a naphtenic type oil which is generally used for power transformers; ferrofluid has been purchased by Magnacol, UK. Particles shape is spherical and their dimension is in the $10 - 50\,nm$ range; they are treated on the surface with oleic acid acting as surfactant to improve their dispersion; coated particles are then dispersed in a blending liquid with 50% weight concentration. Samples have prepared according to a general

rule which has been adopted for the preparation of all the samples which are object of this thesis and which is summarized in the following:

1. mineral oil filtering with a pore filter of $2\,\mu m$ pore size (24 hours);
2. mineral oil degassing, at a pressure of $50\,Pa$ for 24 hours;
3. ferrofluid dispersion, in correct mass quantity, with the help of a magnetic stirrer;
4. final nanofluid degassing ($50\,Pa$), to remove the moisture absorbed by the blendant fluid (12 hours).

The presence of oleic acid on the surface of the nanoparticles and the compatibility between mineral oil and ferrofluid, which has been proved by the Seagal's work [24], made the dispersion of nanoparticles quite easy inside mineral oil making the use of a sonicator probe unnecessary. In the case of more viscous and different fluids, such as synthetic esters, such a device is of fundamental importance to obtain well dispersed samples. The final treatment, for the moisture reduction, is also necessary to let the fluid reach a "'moisture steady state"' condition. As reported in the previous section, oleic acid is characterized by a hydrophobic (nanoparticle side) and a hydrophilic (fluid side) termination, and this aspect produces a moisture shift towards the nanoparticles, which then act as moisture trap sites. The result is a formation of a water shell close to the nanoparticles, which is able to increase the "'apparent"' relative permittivity of the nanoparticles themselves, with the effect to distort the electric field lines, as it will be shown in the following.
Four different insulating fluid samples have been tested:

- Mineral oil, hereafter referred as $FF0$;
- $0.2\,\frac{g}{L}$ nanofluid, hereafter name as $FF0.2$;
- $0.5\,\frac{g}{L}$ nanofluid, hereafter labeled as $FF0.5$;
- $1.0\,\frac{g}{L}$ nanofluid, hereafter called $FF1.0$.

The results have been elaborated through the 2 parameters Weibull distribution [36], i.e.:

$$F(V) = 1 - e^{-(\frac{V}{\alpha})^{\beta}} \tag{2.1}$$

where F indicates the cumulative breakdown voltage distribution function, V indicated the random variable of the breakdown voltages, α represents the Weibull scale parameter and β the shape parameter. Since the number of performed test is limited, the third parameter of the Weibull distribution has not been used, and the confidence intervals ($p = 0.9$) have been calculated with the Monte-Carlo pivotal method, which is the most reliable method and has been described in [36].
The elaboration results for mineral oil, presented alone in fig. 2.5, show the same results obtained by Seagal in [24] about the asymmetry between positive and negative polarity. In particular, the two Weibull distributions are characterized by the same β values, which indicated that the final breakdown is due to

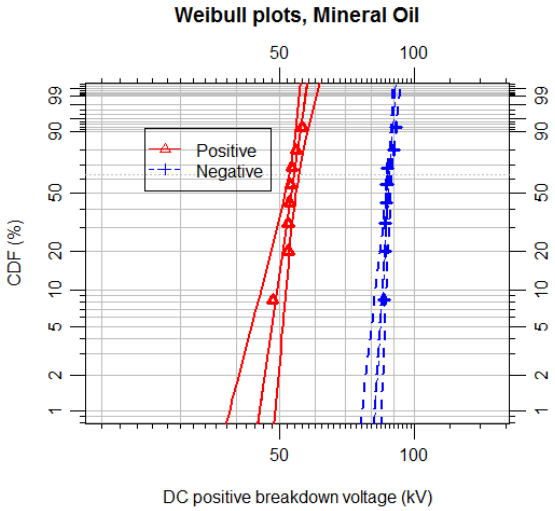

(a) *Weibull analysis for mineral oil samples.*

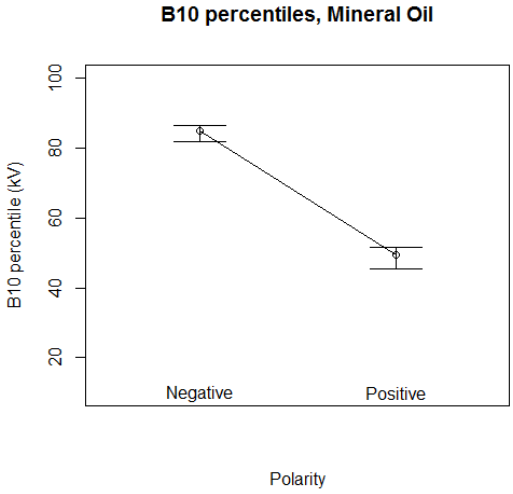

(b) $B-10$ *percentiles (and relative confidence interval) for mineral oil samples.*

Figure 2.5: Summary of the results about mineral oil samples.

the same mechanism in both cases[1], i.e. in both polarities the avalanche propagation is due to field ionization. Fig. 2.5 also reports the difference between the $B10$ (10 % probability) percentiles and relative confidence bounds; since the confidence intervals do not overlap, there is no need of a t−test to state that under negative polarity impulse voltage and divergent field, the breakdown voltage values are much higher than positive polarity ones.

[1]In [36], the author reports the studies of Weibull about the physical meaning of β, saying that this parameter reveals the breaking mechanism of the investigated apparatus.

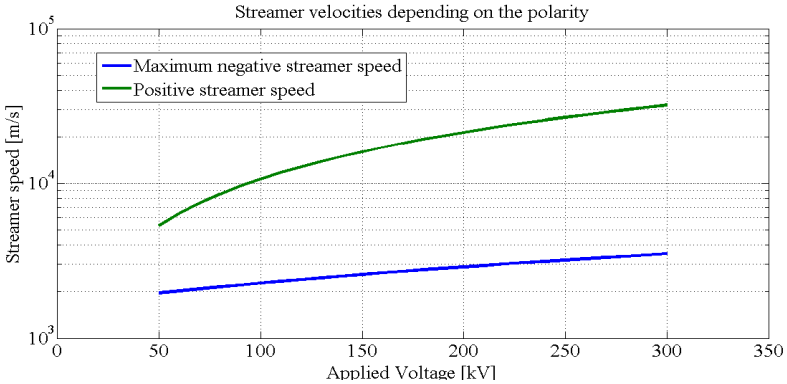

Figure 2.6: Streamer propagation speed vs applied voltage. Note that in the negative voltage case, the speed refers to the maximum one (at the needle tip).

A very simple model which helps to understand this result can be obtained remembering what it has been found by Devins in [12] and summarized in the previous chapter: positive polarity streamers are not slowed down by the avalanche shape like negative ones, but they are fastened. Generally speaking, the following equation is valid, in the case of breakdown:

$$\int_a^b dx = L \tag{2.2}$$

where L is the gap distance between the two electrodes, which are at positions a and b.
Equation 2.2 can be now rewritten considering that $dx = v(t)dt$, thus obtaining the following relationship:

$$\int_{t_1}^{t_2} vdt = L \tag{2.3}$$

At the same voltage value, but opposite polarity, the different relation speed$-$voltage is able then to explain why positive streamers are easier to lead to the final breakdown than negative ones. Devins, in [38], for small radii of curvature and a particular mineral oil (Marcol 70), found two different expression correlating the streamer propagation speed and the applied impulse voltage:

$$v = v_0 + KV \tag{2.4}$$

$$v(r) = \frac{AV}{r^2(\frac{1}{r} - \frac{1}{L})} \tag{2.5}$$

where v_0 is equal to $1.64 \cdot 10^5 \frac{cm}{s}$, K is equal to $0.62 \frac{cm}{Vs}$, A is equal to $0.016 \frac{cm^2}{Vs}$, r is the linear coordinate and L represents the gap distance.

Equation 2.4 is relative to the positive applied impulse, and shows that the propagation speed is uniform across the gap, while in equation 2.5 the second case (i.e. in the case of negative applied impulse), the propagation velocity depends on the radial coordinate[2], because of the shielding effect the

[2]For the sake of simplicity, when dealing with needle to plane geometries, it is possible to suppose that the electrode configuration is like a cylindrical capacitance.

avalanche has on itself. Equation 2.5 is represented in fig. 2.6 considering the geometrical parameters of our performed tests, and finally shows the differences in the propagation speed with the applied polarity.

The results about the nanofluids are presented in fig. 2.7 (positive polarity

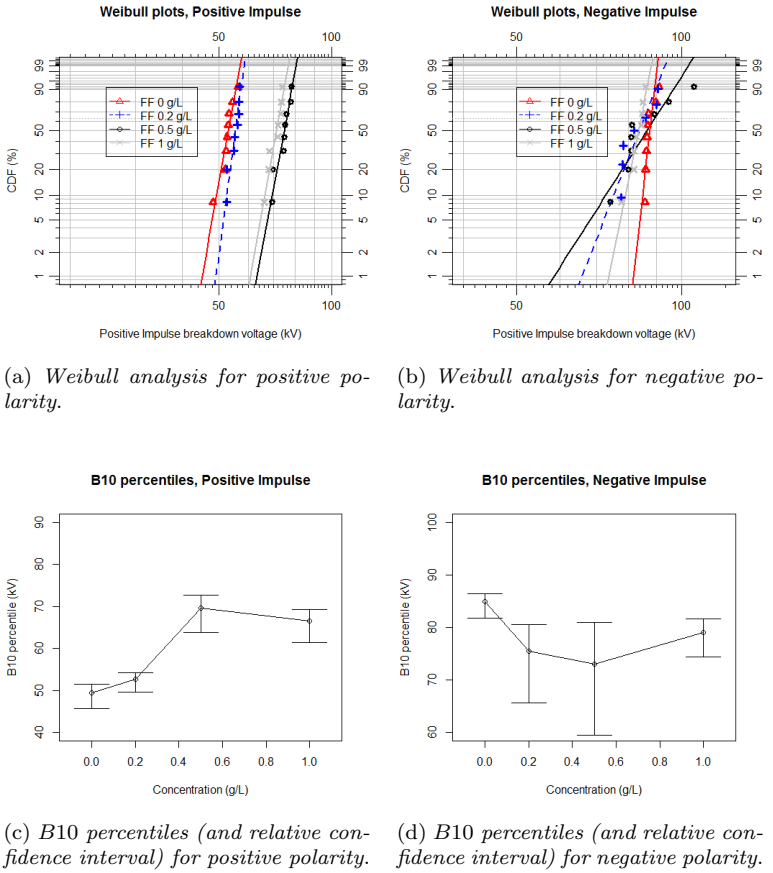

(a) *Weibull analysis for positive polarity.*

(b) *Weibull analysis for negative polarity.*

(c) *B*10 *percentiles (and relative confidence interval) for positive polarity.*

(d) *B*10 *percentiles (and relative confidence interval) for negative polarity.*

Figure 2.7: Summary of the results about impulse breakdown tests.

left, negative polarity right).

2.2.1 Positive impulse breakdown results

The results which are relative to the positive applied polarity clearly show, as in [24], the positive effect due to the addition of nanoparticles to the insulating mineral oil. Apart from the lowest concentration ($FF0.2$) in which there is a partial overlap of the confidence bounds, in the other cases there is an evident statistically significant improvement of the breakdown voltage which is due to the presence of nanoparticles. Further on, it seems, but it is not sure from a statistically point of view, that $FF0.5$ behaves better than $FF1.0$, i.e. it is not true generally speaking that the breakdown voltage increases monotonically with the nanoparticles concentration.

The explanation of the results is quite puzzling, because we do not know what

is the exact interaction between nanoparticles and hot electrons, because it involves the nanometric scale, and this is not a known matter yet. Anyway, we can try to give a possible explanation of the phenomenon, taking into account the known aspects regarding the effect of nanoparticles addition. In [31], the author made the hypothesis that magnetite nanoparticles can distort the electric field due to the high value of their relative permittivity. It is not easy to estimate the permittivity of nanosized particles, but in the case of surfactants treated nanoparticles, the formation of a water shell around them allows us to say that their relative permittivity is high and very close to that of water, that is $\epsilon_r = 81$.

The permittivity mismatch (transformer oil relative permittivity ranges from

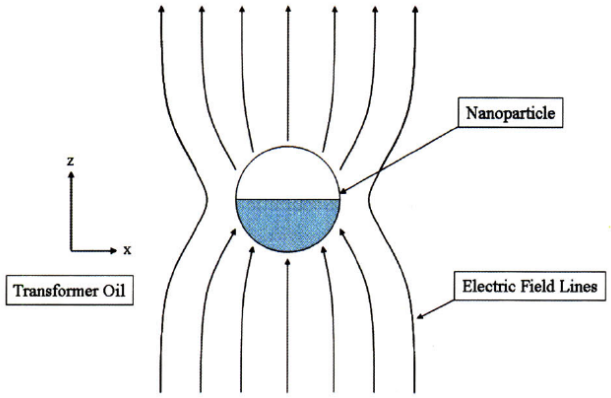

Figure 2.8: Electric field lines distortion (after [31]).

2.1 to 2.3) creates the situation depicted in fig. 2.8, where the field lines are attracted by the nanoparticles. Since the electrons speed vector is related to the field lines ($\vec{v} = \mu\vec{E}$, where μ refers to the electrons mobility), it follows that nanoparticles act as electrons (or charge carriers, generally speaking) scavengers.

Devins, in [12], analyzing the effect of aromatics on the propagation of electrical streamers, observed that the electron scavenging property does not have any influence on the positive streamer propagation, despite what we have obtained and what Seagal found in [24]. A possible explanation of this macroscopic result can be anyway found observing that the field lines distortion has an effect on the increase of the attachment cross section for hot electrons. Electrons, while propagating from the cathode to the anode, collide against nanoparticles, being trapped on their surfaces, modifying their mobility and reducing the electric field[3]. The combined effect of field reduction and mobility reduction affects the macroscopic velocity of the positive streamer ($v = \mu E$).

A quite puzzling result is the apparent worsening effect which seems to start after the $0.5\frac{g}{L}$ concentration. According to the previously mentioned mechanism, the improving effect should increase monotonically with the concentration, because a concentration increase further increases the attachment cross section and prevents the electrons velocity to raise at the propagation beginning. In

[3]They reduce the electric field because, propagating from the cathode to the anode, they act as homocharge.

this considerations, however, no mention has been done to the distance among nanoparticles, which can have a role in the charge carriers transfer dynamics. If the distance among nanoparticles is high (some tens of nanometers), it is true that they act as trapping sites, reducing the dangerousness of the electrons avalanche, but if the distance starts to reduce below ten nanometers, it is possible to activate some fast exchange charge transfer mechanisms, like tunneling effects.
These phenomena would result in a higher value of the charge carriers mobility and a reduced homocharge effect, possibly explaining the results obtained for higher concentrations nanofluids.

2.2.2 Negative impulse breakdown results

The results about negative streamers propagation are quite in agreement with [24]. Fig. 2.7 (right) shows a clear, statistically significant, breakdown voltage reduction due to the presence of nanoparticles. Even if the reduction in the mean value is not as evident as the increase in the case of positive applied polarity, the Weibull distributions fitting the experimental values are quite interesting, because they reveal a change in the β value. Unlike the positive distribution functions, which were all parallel, these ones cross revealing a change of phenomenon which they describe. In [36], the author reported that the value of β usually takes information about the breaking mechanism of the investigated system.
It is possible then, that in the negative applied polarity, nanoparticles effect is likely to change the streamer propagation mode. Again, Devins' theory can be of help in the interpretation of the results.
When a negative polarity impulse is applied, the two stage model reveals that, at the beginning, charge carriers have to be extracted from the cathode and then, when the field at the tip of the electrons cloud overcomes the ionization threshold, the avalanche can start towards the anode. Nanoparticles, with their electron scavenging effect which has been introduced in the previous subsection, are likely to reduce the time duration of the first stage, increasing in this way the propagation speed of the streamer which should then resemble the positive polarity one. Unfortunately, it has not been possible to detect the streamer shape to prove such statement, but the concentration trend seems to confirm it anyway, because the situation is the same of the previous case, where a change of trend started to take place after the $0.5\frac{g}{L}$ concentration. The loose of the electrons scavenging property of the nanofluid after that concentration makes the streamer more similar to that propagating inside transfomer oil, justifying the increase in the mean breakdown value.

2.3 Breakdown voltage under divergent fields. Slowly varying waveforms

The measurements which have been described in the previous section have been performed using an impulse generator with a high energy value. This aspect prevented us to take pictures of the discharges, because it was impossible to highlight the streamer shape during the flash-over, since all the generator en-

ergy was released after each discharge[4]. In order to take some pictures of the electrical discharges involving nanofluids, different tests have been carried out, using a different high voltage generator of lower energy. The choice of the generator fell on a Trek 30/20 power amplifier, used in combination with an Agilent 33120a function generator to generate the reference voltage. The advantage in using the Trek power amplifier instead of the Passoni Villa Impulse generator is that it is possible to limit the output current in case of breakdown ($I_{lim} = 0.1\,mA$), which also allows to reduce the number of used needles preventing the replacement after each breakdown. The disadvantage is that power amplifiers are characterized by a limited bandwidth which prevents them to generate lightning impulse waveforms. The test setup is the same of the previously described tests: needle to plane configuration, but $1\,mm$ gap spacing. Tungsten steel needles ($1\,\mu m$ radius tip and $0.5\,mm$ diameter) have been protected by a $1\,M\Omega$ resistor connected in series with the insulating fluid sample.
The following voltage waveforms have been tested:

- DC, both positive and negative polarity;
- $50\,Hz$, $250\,Hz$, $500\,Hz$ sinusoidal voltage;
- $50\,Hz$, $250\,Hz$, $500\,Hz$ square wave voltage with $50\,\mu s$ rising time (slow square voltage).

These three voltage waveforms are characterized by slow slew rates compared to the $1.2 - 50\,\mu s$ lightning impulse one, allowing space charge to be injected and influence the pre-breakdown phenomena, which are of second importance otherwise [31]. A second aspect to be considered for such applied waveforms is that moisture can play a significant role for the breakdown voltage results. Unfortunately, Karl Fisher titration techniques [37] cannot be used on nanofluids to check the moisture level after the sample manufacture and treatment, because the presence of conductive nanoparticles can produce unacceptable noise on the moisture measurement chain. Mineral oil final moisture value is, anyway, less than 5 ppm.
Schlieren images have been captured to highlight the breakdown propagation modes. They have been taken using a Z-type configuration setup ([39],[40]). The light source was a tungsten halogen low voltage lamp equipped with a rear reflector. The condenser of the optical system was a Schneider-Kreuznach Xenon 40 mm double - Gauss lens with an f=1.9 focal ratio. The light beam was reflected by two off-axis parabolic mirrors 138 mm in diameter and with an f=3.5 focal ratio. The knife edge was parallel to the needle so that the Schlieren diagnostic could record density gradients perpendicular to it. The images were detected by a PCO CCD camera equipped with a super-video-graphics array resolution with a pixel size of (6 x 6) m [40]. The camera has been triggered via a TTL signal generated by the TREK when the discharge occurred, with 1 s exposure time.
Insulating fluid samples have been manufactured according to the procedure which has been described previously in this chapter. Three different nanofluids have been prepared:

1. Mineral oil (MO), which is used as benchmark;

[4]This is also the reason why, after each measurement, the high voltage needle electrode has been changed.

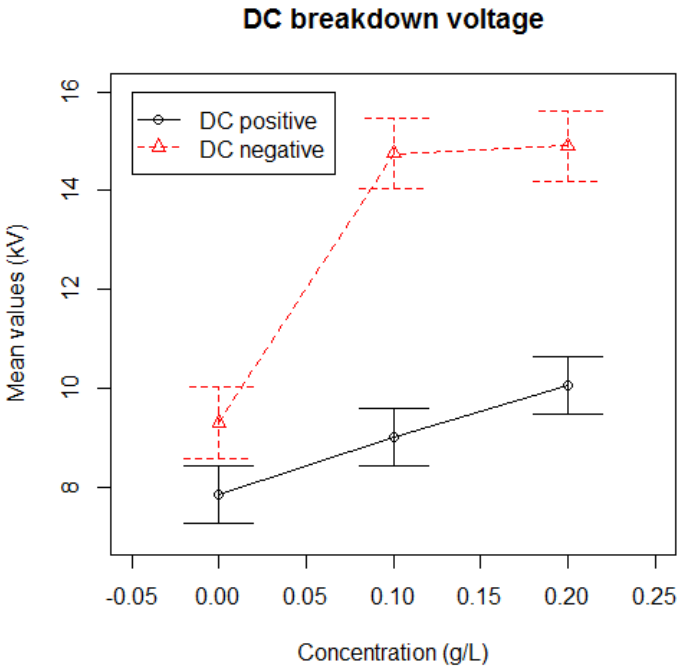

Figure 2.9: DC breakdown voltages for nanofluids under divergent conditions.

2. 0.1 $\frac{g}{L}$ (LC), as an intermediate concentration;

3. 0.2 $\frac{g}{L}$ (HC), as maximum concentration.

Higher concentrations, although were supposed to behave better according to the previous results, could not be tested, because the resulting fluids were to dark to let the Schlieren technique catch streamers images.
Breakdown tests have been implemented following the same procedure shown in fig. 2.4: a LabView software has been written in order to remotely control the function generator and thus the TREK amplifier. Whatever the applied voltage shape, the starting applied value has always been $1\,kV$, the voltage step $150\,V$ and the time duration of each applied step $40\,s$; voltage values, in the case of sine or square wave, are meant to refer to the peak value.
For each type of voltage waveform and polarity, 6 breakdown voltages have been obtained.

2.3.1 DC voltage results, electrical tests

The results about the DC applied voltage are presented in fig. 2.9 for positive and negative polarity. Each value on that plot represents the average breakdown value and the confidence intervals have been obtained through the Tukey honestly significant difference (HSD) formula [41] with 5 % significance level. Such intervals indicate when the difference between two mean values is statistically

significant and they have been calculated as follows:

$$HSD = q_{(1-\alpha),k,N-k}\frac{\hat{\sigma}}{\sqrt{n}} \tag{2.6}$$

where q represents is the $1-\alpha$ percentile from the Studentized range distribution ($1-\alpha$ is the confidence level), k is the number of investigated concentrations (3 in our case), N is the total number of degrees of freedom (18 in our calculations), $\hat{\sigma}$ is the residual standard error, computed from the ANOVA table and n is the total number of tests for each nanofluids ($n = 6$). If the difference between two mean values is bigger than HSD, then it is considered statistically significant.
The reason why we have computed the confidence bounds in the above mentioned way is that, having tested three different nanofluids concentrations, in order to compare the average values it is not possible to use the t−test, which is a suitable statistical test only for two factors comparison [42]. Looking at fig. 2.9, it appears evident that nanofluids have an important and significant effect on the DC breakdown voltage. Again, as in the case of lightning impulse tests, there is an asymmetry between the positive and negative polarity, indicating that the breakdown modes are different and can resemble the previously mentioned ones.
The DC obtained results can be explained in terms of injected space charge, which then acts as homocharge. As already stated in the previous section, nanoparticles act as trapping sites for injected space charge. Thus, when raising voltage, charge carriers start to move from the HV electrode to the LV one until they collide on a nanoparticle surface. Such mechanism is able to reduce the electric field on the HV side and make it difficult to ignite a leader, which is evidently triggered at higher voltages. Fig. 2.10 shows, for the sake of completeness, the Weibull analysis for the DC obtained results, together with the $p = 0.9$ confidence bounds computed with the Monte Carlo pivotal method. Apart from the case of the low concentration nanofluid in positive applied polarity, where three data have been censored because they were suspected to be outliers, the results seem to confirm what it was already clear from fig. 2.9, i.e. the nanofluids exibit a better behavior.
These measurements, as said above, have been carried out on lower concentrations than the impulse breakdown tests; this choice is due to the necessity to deal with transparent samples but prevents us to investigate on the change of behavior at higher concentrations. After $0.5\,\frac{g}{L}$ concentration indeed, previous results highlighted a faster charge transfer of carriers involving nanoparticles; limiting ourselves to $0.2\,\frac{g}{L}$, we did not observe such phenomenon here.

2.3.2 Alternating voltage results, electrical tests

In the case of sinusoidal and square wave voltages, the situation is more puzzling: the differences among the mean values are less evident, if present. It appears anyway quite clear that the behavior of nanofluids in these cases is worse than that of mineral oil; a worsening trend with frequency seems to take place, too. Such considerations are quite evident by giving a look at fig. 2.11, which shows the trends of the average breakdown voltages vs frequency for all the tested fluids; the confidence bounds are computed using equation 2.6.
Again, these results can be explained by considering space charge injection and the consequent trapping due to the nanoparticles presence.

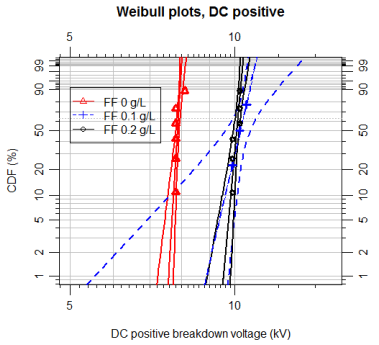

(a) *Weibull analysis for positive polarity.*

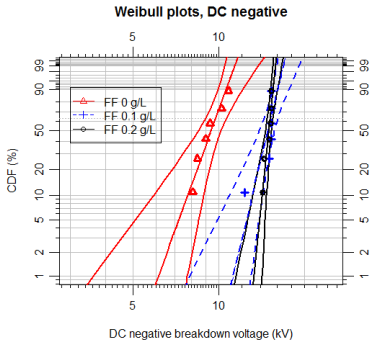

(b) *Weibull analysis for negative polarity.*

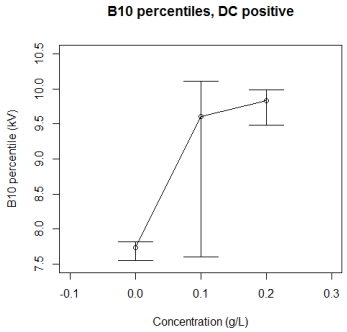

(c) *Weibull B10 for positive polarity.*

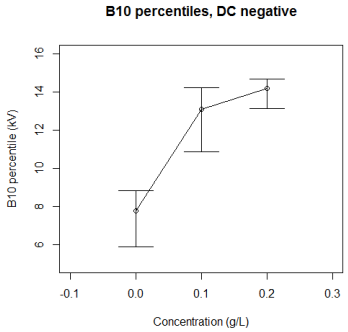

(d) *Weibull B10 for negative polarity.*

Figure 2.10: Weibull charts for DC breakdown data and $B10$ percentiles.

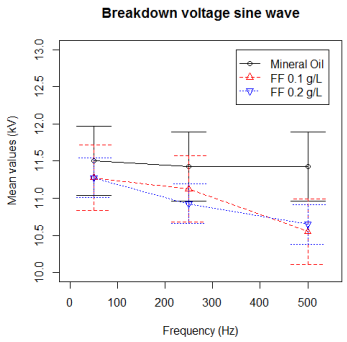

(a) *Breakdown voltages for sine waves.*

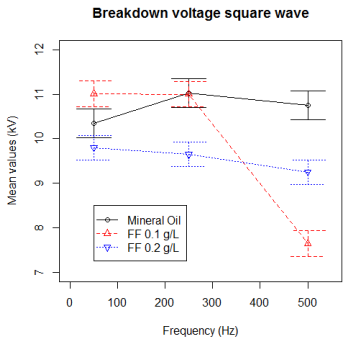

(b) *Breakdown voltages for square waves.*

Figure 2.11: Breakdown results for alternating applied voltages.

While raising voltage, when the space charge injection threshold is reached, charge carriers are injected and then trapped on nanoparticles surfaces as reported for the DC applied voltage in the previous subsection. However, in this

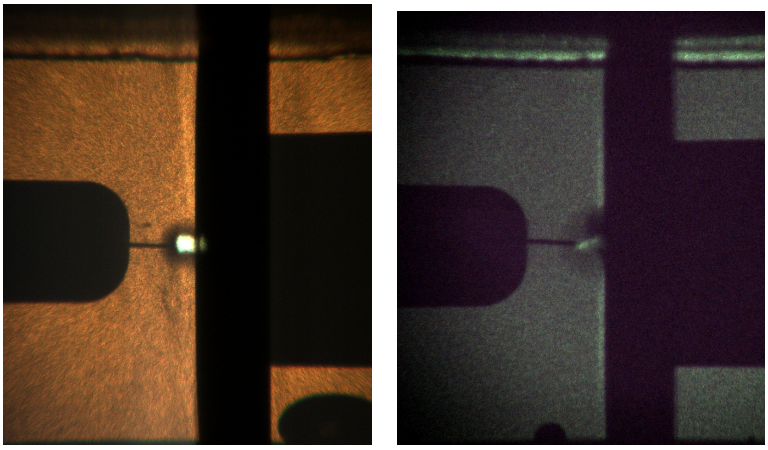

(a) *Breakdown mode for mineral oil.* (b) *Breakdown mode for* $FF\,0.2\,\frac{g}{L}$.

Figure 2.12: Schlieren images of breakdown modes, DC negative voltage, $15\,kV$.

case, voltage polarity reverses every $\Delta t = \frac{1}{f}$, being f the voltage frequency; therefore, at the polarity reversal, the trapped space charge switches from homocharge to heterocharge, increasing in this way the electric field close to the HV electrode [43]. Such phenomenon is able to predict that nanofluids performance worsen at higher concentrations, while the worsening trend with frequency can be explained by considering the nanoparticles detachment time constant. In fact, charge carriers are trapped on nanoparticles surfaces, but they are then detached, after a certain time period, which is determined by the detachment time constant. Higher frequencies mean lower time intervals before the polarity reversal and so less time for the charge carriers to be detached; Measurement results indicate that the detachment constant is of the order of some ms.
Square wave breakdown voltages are lower than sinusoidal ones, as it appears clear from fig. 2.11. Such results can be explained as follows:

- the amount of injected space charge is higher because the lower rise time leads to a higher injected charge for the same voltage peak value;
- the faster polarity reversal does not let trapped charge to detach from nanoparticles and reduce their enhancement field effect.

2.3.3 Schlieren images of the breakdown modes

This subsection presents some acquisitions of the breakdown modes, under both DC and alternating voltage. The aim of such experiments, as already discussed in the previous subsections, was to highlight the different space charge mechanisms which are likely to take place because of the presence of nanoparticles.
The first observation is that the results have been very difficult to analyze, because of the small differences among the nanofluids concentrations; in order to better visualize the differences, we have decided to present only the results regarding mineral oil samples and $FF\,0.2\,\frac{g}{L}$, i.e. the maximum concentration. For DC negative voltage, the results are represented in fig. 2.12. They are relative to a breakdown event which took place at $12\,kV$, i.e. the breakdown inception

for the nanofluid and a higher voltage breakdown for mineral oil, as shown in fig. 2.10. A first look at the two figures reveals a difference in luminescence, which is due to the fact that the two fluids have a different color: mineral oil is yellow, while ferrofluid is dark. Anyway, it is possible to see some small differences in the breakdown region:

- mineral oil leader seems to have a "'kanal"' shape, that is it seems to be filamentary. This can be due to two different reasons:

  1. the aromatic content of the oil is high enough to change the negative streamer propagation mode, as referred by Devins in [12];
  2. the higher voltage at which the breakdown event is captured can be able to ignite a different propagation mode of the streamer, even if it seems difficult that this can happen only at twice the average inception breakdown voltage. For a review about the streamers propagation modes, refer to, for instance, [31], [11], [44], [45], [46].

- nanofluid leader seems to have a different shape, as the dark circle reveals. This circle can be the proof of the trapping tendency of nanoparticles; in [12] the author says indeed that the bushy shape of the negative streamer is due to the charge trapping tendency of aromatics, which is also responsible of its reduced propagation speed [20]. Since nanoparticles seem to have the same behavior, then it is possible that the bushy shape visible from the Schlieren image can be due to that. There is also a second explanation of that dark circle: it is possible that it represents the shock wave originated after the breakdown. Negative streamer propagation speed, as proved by Seagal in [24], are generally faster in conductive nanofluids and so, under the same camera conditions, it is possible that in the mineral oil case we were not able to capture the shock wave, while in the nanofluid case yes. If this was true, the streamer shape should be filamentary, according to the "'two step model"' of Devins [12], but the image resolution and the luminescence difference are not able to clarify this issue at all.

Fig. 2.13 represents, instead, the captured breakdown modes under square wave applied voltage, at $500\,Hz$, i.e. the frequency at which the higher difference seem to arise between the two fluids. Unlike the previous case, where the images were taken at the same voltage value, in this case we decided to consider the situation of breakdown inception ($10.5\,kV$ for mineral oil and $9.5\,kV$ for $FF\,0.2\,\frac{g}{L}$). This picture reveals again a luminescence difference, but it seems to clarify what was happening in the previous image. In fact, looking at the nanofluid breakdown mode, it is quite reasonable to say that the phenomenon is faster and more filamentary than that taking place inside mineral oil.
The explanation of this fact can be found in the switch from homocharge (and its reducing field effect) to heterocharge (and its increasing field effect); the field increase, after the charge injection, is able to explain why the propagation speed is higher and why the leader seems to be more filamentary, i.e. there is no time for it to branch.
It is then possible, after what we have said, that in the DC negative applied voltage case, the nanofluid leader is more filamentary and faster than that propagating inside mineral oil: because of the injected and trapped charge, the strong

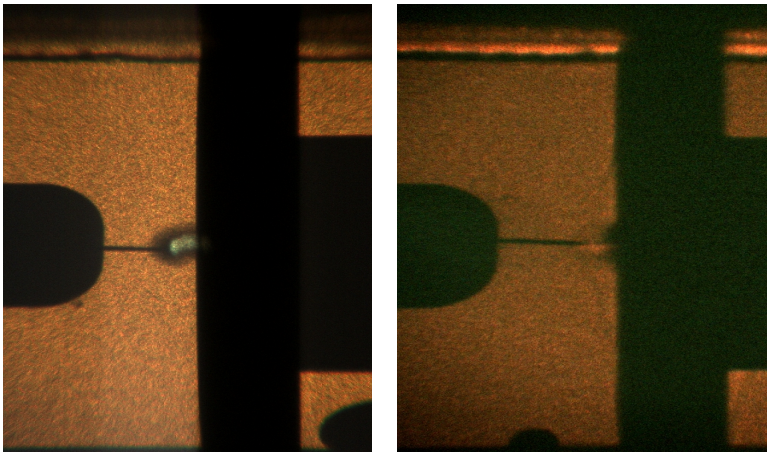

(a) *Breakdown mode for mineral oil.* (b) *Breakdown mode for* $FF\,0.2\,\frac{g}{L}$.

Figure 2.13: Schlieren images of breakdown modes, Square wave applied voltage, $500\,Hz$, breakdown inception.

field reduction at the tip enhances the field increase at the opposite side, favoring the positive polarity propagation mode [12].
Sinusoidal and DC positive results are unfortunately very difficult to analyze because it seems that no differences in the leader propagation modes is present, even if the behavior of the different fluids is quite different from a quantitative point of view, as revealed from the above presented figures. It is possible that this fact is due to the slight differences between the results obtained for mineral oil and $FF\,0.2\,\frac{g}{L}$ under the selected voltage waveforms, which were not easy to detect with the resolution we had on the Schlieren experimental setup.

Chapter 3

Space charge build-up due to nanoparticles

Abstract

The previous chapter has introduced the general phenomena regarding mineral oil-based nanofluids starting from ferrofluid. In particular, it is well accepted that nanoparticles, at least when their concentration is not high, act as electron scavengers, modifying the electric field distribution. The aim of this chapter is to try to analyze the charge build-up phenomenon due to nanoparticles and its consequent effects.

In the previous chapter, in order to explain the experimental results, the charge trapping tendency of nanoparticles has been frequently used. This idea, first introduced in [31], has been able to explain the results obtained by Seagal in [24] and what we have obtained with slower waveforms. In order to understand better the phenomenon, we decided to propose a very simple model trying to depict the situation in a divergent field configuration.
The model we propose is indeed based on the assumption that the electric field distribution is not uniform, with an electrode configuration which resembles the needle to plane one; since the experiments described in the previous chapter have been performed in a divergent field configuration, the results of the following model can be used to give an interpretation to them.
It is well known in literature [47], that under these conditions the field distribution inside one single material is hyperbolic and very difficult to obtain from an analytical point of view, unless we want to estimate the field on the HV tip, which is equal to:

$$E_{tip} = \frac{2V}{rlog(1 + \frac{4d}{r})} \tag{3.1}$$

where V is the applied voltage, r is the needle radius of curvature and d the insulating gap.
In the following, we will need a field formula for the trapped charge estimation, and so we will assume that our field configuration is like a spherical capacitor, like the one shown in fig. 3.1. In this figure, R_1 represents the radius of the inner electrode, representing in our model the radius of curvature of the HV needle,

while R_2 represents the radius of the external conductor, which is related to the insulating gap, d. It follows indeed that $d = R_2 - R_1 \approx R_2$, since $R_2 \gg R_1$. Under this hypothesis, below considering a single material, the electric field can be easily determined from the Laplace equation and the spherical symmetry of the problem:

$$\nabla^2 V = 0 \tag{3.2}$$

$$\frac{1}{r}\frac{\partial}{\partial r}\left(r\frac{\partial V}{\partial r}\right) = 0 \tag{3.3}$$

where the second equation is the development of the first one, considering the polar coordinates and that under spherical symmetry $\frac{\partial}{\partial \Phi}$ and $\frac{\partial}{\partial \theta}$ are equal to 0. Equation 3.3 has to be solved for $r \in [R_1, R_2]$ and so the $\frac{1}{r}$ term can be simplified without any problem because r is always different from 0. In this way, it is possible to state that the electric voltage distribution can be written as:

$$V(r) = \frac{V}{\frac{1}{R_2} - \frac{1}{R_1}}\left(\frac{1}{R_2} - \frac{1}{r}\right) \tag{3.4}$$

while the electric field, being easily $E = -\nabla V$, can be estimated as follows:

$$E(r) \approx \frac{V R_1}{r^2} \tag{3.5}$$

always considering that $R_2 \gg R_1$. The field distribution obtained with formula 3.5 has to be analyzed before being used for successive computations:

- can this formula be applied for nanofluids, where two different materials (oil and nanoparticles, with different permittivities) are mixed?
- it is then necessary to verify if it can be applied in the real case of needle to plane geometry and understand what is the relationship between the real hyperbolic field distribution and the spherical obtained one.

The first question refers to the fact that equation 3.3 is obtained by simplifying the electrical permittivity of the material where voltage is applied; the real equation is in fact:

$$\nabla \cdot (-\epsilon \nabla V) = 0 \tag{3.6}$$

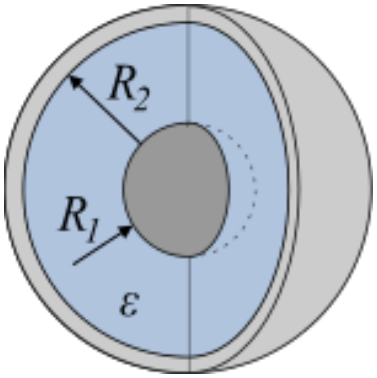

Figure 3.1: Spherical capacitor.

In the hypothesis of a single material with no dependence of the relative permittivity upon the spatial coordinates, ϵ can be simplified, thus obtaining equation 3.3. It is clear then that, generally speaking, it is not possible to use equation 3.3 to estimate the electrical field distribution inside a nanofluid, where ϵ is a function of the position. In that case, the correct equation to solve should be:

$$\nabla \cdot (-\epsilon(\vec{r})\nabla V) = 0 \tag{3.7}$$

where $\vec{r}$ represents the position. $\epsilon(\vec{r})$ is equal to ϵ_{oil} if $\vec{r}$ indicates a point in which the material is mineral oil, while it is equal to $\epsilon_{nanoparticles}$ if $\vec{r}$ is placed on one nanoparticle.
Since the solution of equation 3.7 is impossible to be found from an analytical point of view, it is necessary to understand if it is possible to approximate the real solution by using equation 3.5. In [48] and [49], the authors proved that the global increase of the permittivity switching from mineral oil to mineral oil-based nanofluid is negligible in first approximation and so it is possible to state that $\epsilon(\vec{r}) = \epsilon_{oil} \quad \forall \vec{r}$. This finally authorizes the use of equation 3.5 even for nanofluids, assuming a uniform particles distribution and reasonable concentrations.
The second question, i.e. if the spherical field formula is similar to the hyperbolic one obtained for the same applied voltage and the same electrode geometry, can be solved considering the field value at the needle tip, derived using formulae 3.1 and 3.5, that is:

$$E_{hyp}(R_1) \approx \frac{2V}{R_1 log(1 + \frac{4R_2}{R_1})} \tag{3.8}$$

$$E_{sph}(R_1) \approx \frac{V}{R_1} \tag{3.9}$$

It is obvious that the two field distributions are different, but generally speaking, the spherical one, for the same applied voltage and same geometrical parameters, is bigger than the hyperbolic one, as reported also in some milestone works ([16], [50]). Since, as it will be clear later, we are interested in the region close to the HV needle, for us it is sufficient that the two fields are comparable there. In other words, even if in the reality a certain voltage V is applied and a hyperbolic field is produced, in the model we will use a fictional voltage V_0, which will produce a spherical field which is similar to the real one close to the HV electrode. Such a voltage can be obtained with the following equation:

$$\frac{2V_{applied}}{R_1 log(1 + \frac{4R_2}{R_1})} = \frac{V_0}{R_1} \tag{3.10}$$

$$\frac{2}{log(1 + \frac{4R_2}{R_1})} = \frac{V_0}{V_{applied}} \tag{3.11}$$

By considering a radius of curvature R_1 equal to $1\,\mu m$ and an insulating gap R_2 of $1\,mm$, i.e. the parameter of the experiments described in the previous chapter, the criterion of equation 3.11 states that the ratio between the real applied voltage and the fictional one is 4.2, meaning that in order to obtain the same field we have in the reality, in the model we have to underestimate the applied voltage of a factor equal to 4.2.
We are now able to proceed with the charge build-up model, by formulating the general hypotheses which will be used in the following:

1. spherical geometry: the electric field distributions will be calculated by assuming this particular geometry, with the above mentioned voltage correction;

2. electric charge is injected via a current Dirac pulse of amplitude Q_{tot}. The charging current is therefore assumed to be $i(t) = Q_{tot}\delta(t)$, and so the total injected charge is equal to $Q_{inj} = \int_0^{+\infty} i(t)dt = Q_{tot}$ for the properties of the Dirac $\delta(t)$ function.
This hypothesis means that, as soon as charge is injected, the electric field is reduced to block the injection.

3. nanoparticles are not supposed to be a discrete system, but a continuum, so that the relative permittivity is not a function of spatial coordinates. This means that the stored space charge density on nanoparticles is a continuous function;

4. the linear superposition principle is valid;

5. transient phenomena are neglected, and a steady state space charge trapping expression is used.

The last hypothesis requires the knowledge of a formula, which lets evaluate the amount of charge which is trapped by each nanoparticle. In [31] the author, analyzing the charge trapping tendency of nanoparticles, calculated the saturation stored charge on each nanoparticle as:

$$Q_{sat} = -12\pi\epsilon R_p^2 E_0 \tag{3.12}$$

where ϵ is the permittivity of the host fluid, i.e. the mineral oil, R_p is the mean radius of the nanoparticles and E_0 refers to the electric field before the charge trapping mechanism.
Equation 3.12, after proper modifications, can be used to estimate the space charge density induced by the charge injection from the HV electrode, Q_{tot}, and the trapping behavior of nanoparticles. In fact:

$$\rho(r) = \frac{Q_s(r)}{V_p} \tag{3.13}$$

$$E_0(r) = f(\rho(r)) \tag{3.14}$$

where V_p refers to the volume occupied by the single nanoparticle and $f(\rho(r))$ means that the electric field is a function of the space charge density.
In the following section we will try to find the relation between the space charge density ρ and the electric field.

3.1 Relation between space charge density and electric field

In the previous section, we have found the expression of the electric field generated by the applied voltage, supposing that non space charge was injected. At the end of that section, anyway, we have introduced the charge trapping behavior of nanoparticles, which requires the charge injection from the electrodes;

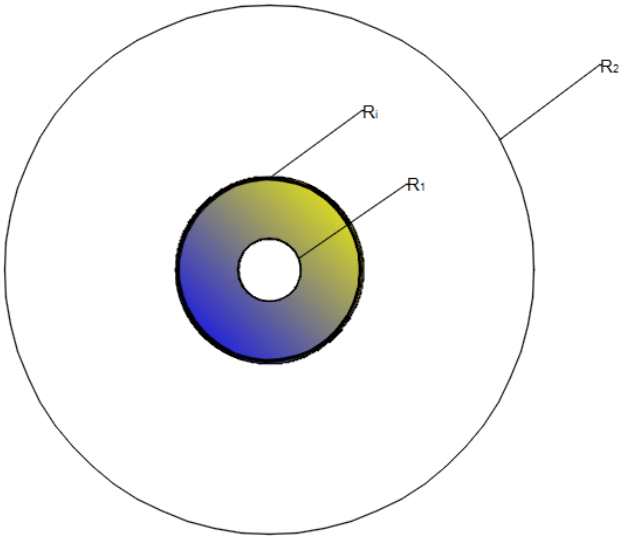

Figure 3.2: Charge trapping scenario at a generic time instant t: volume charge (colored region) and surface charge layer (bold line).

such charge will obviously have an influence on the electric field distribution. The aim of this section is to express the electric field E_0 of equation 3.12 as a function of the stored space charge density, ρ. Let us suppose that, after the injection of Q_{tot}, charge is trapped on each nanoparticle up to the limit defined by equation 3.12. This means that, after a certain time t, the global situation is:

- a certain amount of charge, $Q_{trapped} \leq Q_{tot}$, is already stored on the nanoparticles close to the HV electrode;
- the remaining one, $Q_{tot} - Q_{trapped}$ constitutes a surface charge layer traveling toward the LV electrode until it is completely trapped.

Such situation is shown in fig. 3.2, where the colored section represents the already stored charge, while the remaining one is placed on the surface layer in position R_i and will be trapped in the following instants until it vanishes completely.

The global electric field, according to the linear superposition principle hypothesis, is then related to the following three contributions:

1. the applied voltage;
2. the bulk space charge, which has already been trapped by nanoparticles;
3. the surface space charge which is traveling towards the LV electrode and which has not been trapped yet.

3.1.1 The applied voltage field

The first field contribution, which is only due to the applied voltage, without any charge inside the insulation, can be easily obtained by using equation 3.3,

as we have already discussed. The result is formula 3.5, which is re-called:

$$E_V(r) = \frac{VR_1}{r^2} \tag{3.15}$$

3.1.2 The bulk space charge field

The bulk space charge field can be obtained considering no applied voltage between the two electrodes and neglecting the surface space charge representing the amount of charge not yet stored on the nanoparticles surfaces.
Since we are assuming spherical symmetry, the field expression can be obtained by using the integral form of the gaussian law, i.e.:

$$\iiint_V (\nabla \cdot \mathbf{E})\, \mathrm{d}V = \oiint_{S(V)} \mathbf{E} \cdot \hat{\mathbf{n}}\, \mathrm{d}S \tag{3.16}$$

$$\frac{Q_V}{\epsilon} = \oiint_{S(V)} \mathbf{E} \cdot \hat{\mathbf{n}}\, \mathrm{d}S \tag{3.17}$$

where V indicates the volume enclosed inside the surface S.
Let us suppose to consider a time instant t, where the injected charge Q_{tot} has traveled till the $r = R_i$, and let us suppose we want to calculate the electric field in $r' \leq R_i$; by applying the Gauss Theorem of equation 3.17 to the volume between $r = R_1$ and $r = r'$, it is possible to obtain:

$$E_{bulk}(r') = \frac{1}{r'^2}\left(E_0 R_1^2 + \frac{1}{\epsilon}\int_{R_1}^{r'} \rho(t) t^2 dt\right), \quad r' \leq R_i \tag{3.18}$$

where E_0 represents the field at $r = R_1$ and $\rho(x)$ indicates the unknown function describing the trapped space charge density.
Exactly in the same way, it is possible to derive an expression for the electric field when $r' > R_i$:

$$E_{bulk}(r') = \frac{1}{r'^2}\left(E_0 R_1^2 + \frac{1}{\epsilon}\int_{R_1}^{R_i} \rho(t) t^2 dt\right), \quad r' > R_i \tag{3.19}$$

Before using equations 3.18 and 3.19, it is necessary to find and expression for E_0, which can be obtained remembering that (electric field circulation):

$$V_1 - V_2 = \int_{R_1}^{R_2} E(x) dx \tag{3.20}$$

By applying equation 3.20 to the entire insulating gap and remembering that, in this case $V_1 - V_2 = 0$, the following expression can the obtained:

$$E_0 = \frac{R_2}{R_1(R_2 - R_1)}\left(-\frac{1}{\epsilon}\frac{R_2 - R_i}{R_2 R_i}\int_{R_1}^{R_i} \rho(t) t^2 dt - \int_{R_1}^{R_i} \frac{1}{\epsilon x^2}\int_{R_1}^{x} \rho(t) t^2 dt dx\right) \tag{3.21}$$

3.1.3 The surface charge field

The surface charge field can be obtained considering no applied voltage between the two electrodes and neglecting the bulk charge we have dealt with in the previous subsection. The only term which contributes to create an electric field is the surface charge layer ρ_Σ representing the charge which has not been trapped yet, whose value can be calculated according to the following balance equation:

$$Q_{tot} = 4\pi \left(\rho_\Sigma R_i^2 + \int_{R_1}^{R_i} \rho(t) t^2 dt \right) \tag{3.22}$$

which refers to the usual time instant t, where the space charge has already reached the position $r = R_i$. By using the Gauss theorem of equation 3.17 for the volume between $r = R_1$ and $r = r' < R_i$, it is possible to obtain the following expression:

$$E_{surf}(r') = \frac{E_0 R_1^2}{r'^2}, \quad r' < R_i \tag{3.23}$$

where E_0 represents, as before, the field at $r = R_1$.
In the same way, the field at $r = r' > R_i$ is equal to:

$$E_{surf}(r') = \frac{E_0 R_1^2}{r'^2} + \frac{\rho_\Sigma}{\epsilon}, \quad r' > R_i \tag{3.24}$$

The constant E_0 can be easily obtained by applying the electric field circulation (equation 3.20), which lets us obtain:

$$E_0 = -\frac{\rho_\Sigma R_i \left(R_2 - R_i\right)}{\epsilon R_1 \left(R_2 - R_1\right)} \tag{3.25}$$

The expression for the electric field inside the insulating gap between the two electrodes will simply be $E = E_V + E_{bulk} + E_{surf}$. We are now able to use equation 3.12 to find the expression of ρ. The first term of equation 3.12 can be re-written in terms of ρ by remembering that $\rho \frac{4}{3}\pi R_p^3 = Q$, where R_p is the nanoparticles mean radius, while the second one requires the knowledge of the electric field which is generated by a charge distribution between $r = R_1$ and $r = r'$, i.e.:

$$\rho(r') \frac{4}{3}\pi R_p^3 = 12\pi\epsilon R_p^2 \left(E_{charge\, till\, r'}\right) \tag{3.26}$$

The electric field of equation 3.26 can be determined with the expressions found in the previous sections and, after some calculations, it is possible to obtain the following charge density equation:

$$\rho(r') = \frac{9\epsilon}{R_p} \left(\frac{V R_1}{r'^2} + \frac{Q_{tot} R_2 (r' - R_1)}{4\pi\epsilon r'^3 (R_2 - R_1)} - \frac{R_2}{\epsilon r'^2 (R_2 - R_1)} \int_{R_1}^{r'} \rho(t) t (t - R_1) dt \right) \tag{3.27}$$

which is an equation of the type:

$$\rho(x) = f(x) + \int_{R_1}^{x} g(x,t)\rho(t)dt \tag{3.28}$$

Parameter	Symbol	Value [Unit]
Nanoparticles radius	R_p	10 [nm]
Applied Voltage	V	2 [kV]
HV electrode radius of curvature	R_1	1 $[\mu m]$
LV electrode coordinate	R_2	1 $[mm]$
Total injected charge	Q_{tot}	100 [pC]
Oil permittivity	ϵ	19.5 $[\frac{pF}{m}]$

Table 3.1: Values of the parameters appearing in equation 3.27.

i.e. a second kind volterra integral equation, which depends on the parameter Q_{tot}. In [51], the author reports all the studies about the Volterra integral equations and refers that, in the case of the second kind equation, a procedure to find the analytical solution exists and leads to the following result:

$$\rho(x) = f(x) + \int_{R_1}^{x} \Gamma(x,s) f(s) ds \tag{3.29}$$

where $\Gamma(x,s)$ is called the resolvent kernel of equation 3.28 and is determined by an iterative procedure. It is possible indeed to prove that $\Gamma(x,s) = \sum_{i=1}^{+\infty} k_i(t,s)$, where:

$$k_1(t,s) = g(t,s); \tag{3.30}$$

$$k_2(t,s) = \int_{s}^{t} g(t,\tau) g(\tau,s) d\tau \tag{3.31}$$

$$k_i(t,s) = \int_{s}^{t} g(t,\tau) k_{i-1}(\tau,s) d\tau \tag{3.32}$$

For the purposes of this thesis, we do not want to solve equation 3.27 in an analytical way, but we simply propose a numerical scheme, which is derived from [51]. Let us suppose that we know the solution, for a given integration step h, at points $r_i = ih$, $i = 0, 1, 2, n-1$. An approximate value for $\rho(rn)$ can be obtained by replacing the integral on the right side of equation 3.27 with a numerical integration rule using the values of the integrand at r_i, $i = 0, 1, n$ and solving the resulting equation for $\rho(rn)$. Since $\rho(r0) = f(r0)$, the approximate solution can be computed in this step-by-step fashion.
Before solving equation 3.27 with this numerical procedure, it is anyway necessary to define the value of all its parameters, which are defined in table 3.1.

In table 3.1, the only parameter which has to be explained is $Q_{tot} = 100\,pC$. Usually, charge is injected from HV needles because of the partial discharges (PDs) or streamers presence; in the following, we will present some results about PDs activity inside nanofluids and we will show that $Q = 100\,pC$ represents the order of magnitude of the worst case in terms of charge injection before PDs start to be ignited. This means that our choice for the simulation has been intended to consider the worst case. After such clarification, it is possible to present the results of the simulation, which are reproduced in figure 3.3. This picture shows the solution of the above mentioned Volterra equation for $r \in [R_1, 5R_1]$ for the sake of clarity in the final representation. In fact, it is reasonable that the trapped charge is placed only in a narrow region close to the HV electrode

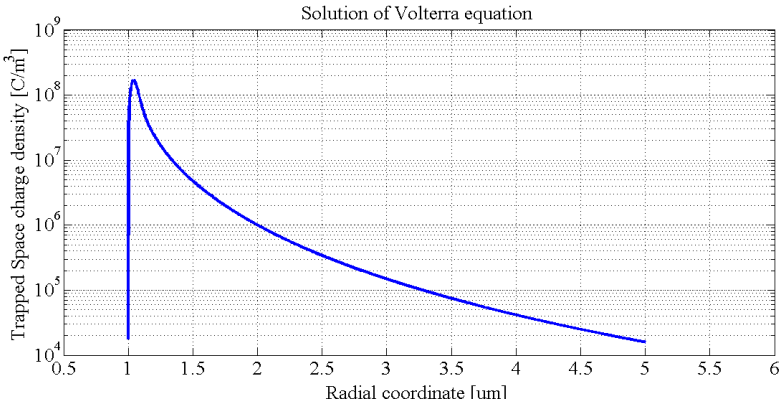

Figure 3.3: Results of the equation 3.27.

from which it is injected. In this chapter we are not interested in the value of the space charge density which results from the solution of the equation, but it is noteworthy that the trend is not monotonous, but it presents a clear peak very close to the HV needle. Such a peak, being constituted of homocharge, and remembering that it is a low mobility charge peak, is the responsible of the phenomena which have been discussed in the previous chapter. Under DC voltage, such a charge build-up is able to hinder the nanofluid breakdown voltage, by reducing the field on the HV side, increasing in this way the voltage which is necessary to ignite a leader and thus a discharge, while under alternating voltage, the low mobility of such a layer is dangerous at the polarity reversal when it reverses into heterocharge, thus increasing field values when voltages are still low.

The presence of the above mentioned peak can also reveal that, for nanofluids, the injection mechanism can be a real pulsed-like phenomenon as we have supposed, because the charge build-up is able to reduce the field below the injection threshold. A new injection pulse can be activated only when the complete charge is depleted or shifted towards the lower voltage electrode. This interpretation of the results of equation 3.27 will be used to understand the polarization currents measurements which will be conducted on nanofluids, which should reveal such a pulsed injection behavior.

Chapter 4

AC Breakdown voltages and Partial Discharge measurements

Abstract

The previous chapter has been a sort of break in the presentation of the measurement results about nanofluids, but it has been necessary in order to understand their behavior. With this chapter, we continue dealing with breakdown results description under sinusoidal AC voltages and we introduce partial discharges (PDs) measurements, carried out in order to compare the inception voltages both for nanofluids and mineral oils.

4.1 AC breakdown voltage

In this section we present the sinusoidal AC breakdown voltage results obtained on our performed nanofluids, under quasi-uniform conditions. These measurements, unlike the ones obtained in the previous chapters, are more subjected to the samples manufacturing process (contaminants and moisture for instance), and therefore more attention to avoid sample contamination has been paid.
Four different fluid samples have been prepared, according to the procedure described previously:

- Mineral Oil, used as benchmark, and hereafter labeled as MO;
- 0.1 $\frac{g}{L}$ ferrofluid-based nanofluid, hereafter labeled as FF0.1;
- 0.2 $\frac{g}{L}$ ferrofluid-based nanofluid, hereafter labeled as FF0.2;
- 0.5 $\frac{g}{L}$ ferrofluid-based nanofluid, hereafter labeled as FF0.1.

No other concentrations have been considered, because preliminary tests revealed that the "'optimum"' concentration for impulse breakdown tests was

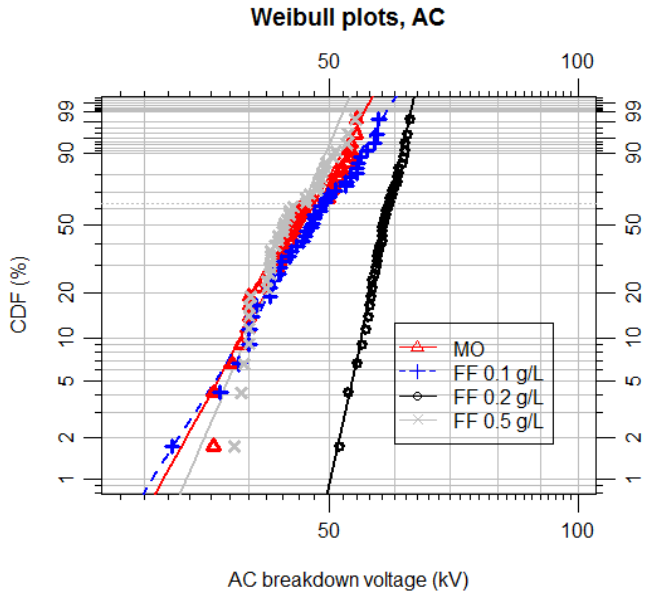

Figure 4.1: Weibull plot for AC breakdown voltages.

0.5 $\frac{g}{L}$. The breakdown voltage (BDV) of the samples has been measured using an automated test kit with maximum test voltage of 75 kV, 60 Hz (Baur DPA 75C). Four sets of measurements, each consisting of 10 tests, were carried out to reduce confidence bounds amplitude and thus to achieve a large statistical significance. The adopted test procedure is specified in the IEC 60156 standard [52]. The electrode cell was modified to operate with a low quantity of NF, 50 ml. The cell contains two stainless steel semi-spherical electrodes having a body diameter of 7.8 mm, a tip radius of 4 mm and spaced 2.5 mm. For the same fluid, the BDV were, on average, lower than those observed using a standard cell [53]. The reason why the obtained results are lower than the ones which can be found on literature is anyway explained in [53], where the author refers to the so-called "'dimensional"' effect regarding the electrode surfaces: the bigger the active electrode surfaces, the lower the obtained breakdown voltages, because of the higher probability to find local asperities (hot spots) where streamers can occur leading to the complete discharge. Anyway, since in this work we have conducted a comparative study, the dimensional effect is not a problem. The results have been elaborated by using the 2-parameter Weibull model, which has already been introduced in equation 2.1; the final plot comparing the different concentrations is reported in fig. 4.1. Differently from the breakdown tests under lightning impulse voltages, for AC the best concentration seems to be 0.2 $\frac{g}{L}$. Beta values, revealing the physical mechanism behind the failure of the investigated system ([36]), are quite similar for the MO, FF0.1 and FF0.5, but it is higher for FF0.2; this sort of determinism indicates that, probably, the addition of nanoparticles in that selected concentration creates the maximum benefit to the base insulating fluid.
Fig. 4.1 does not report any confidence bounds for the sake of clarity; a data-set

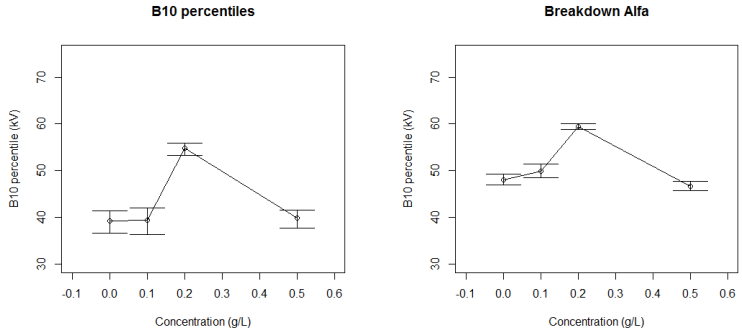

(a) *B10 values of the breakdown voltages vs nanofluid concentration.*

(b) *Weibull alpha vs nanofluid concentration.*

Figure 4.2: Comparison of the AC breakdown voltage percentiles and relative confidence bounds.

composed of 40 tests should be anyway able to reduce the statistical uncertainty, but they are anyway necessary to correctly compute a comparison test. As in the previous chapters, it is not possible to perform a normal t-test, because it is designed for the comparison of just two variables[1]. For our purposes, we can just say that the differences among the different nanofluids concentrations are significant if the different confidence bounds do not overlap; we have therefore computed the latter by using the Monte Carlo pivotal method (confidence level $\sigma = 0.9$), indicating that the significance of the tests is equal to $\alpha = 1 - \sigma = 0.1$ or, considering the Bonferroni correction, $\alpha_{corrected} = m\,(1 - \sigma) = 0.4$.
Fig. 4.2 shows the comparison between the B10 ([35]) values of the breakdown voltages (left) and Weibull alpha (right) versus the nanofluids concentrations. This figure further clarifies what it was visible from the full Weibull charts, i.e. FF0.2 represents the best nanofluid concentration regarding AC breakdown voltages, whatever the statistical significance is equal to. The other concentrations seem to behave in the same way, suggesting that nanoparticles do not have any particular influence unless they are added in the "'correct"' amount.
The interpretation of these results is quite complicated, because we have found, as already remarked, an "'optimum"' nanofluid concentration which differs from what it has been found for impulse breakdown tests. Again anyway, it seems there are two contrasting phenomena, one prevailing at lower concentrations, which generally improves the performace of the insulating fluid, and the other one which instead tends to reduce the withstand capabilities and which starts to dominate after a certain concentration. It is possible, and generally speaking reasonable, that the two mentioned phenomena are the same which have been claimed in the previous chapters, i.e.:

- charge injection and trapping, according to the model which has been introduced and discussed in the previous chapter. This allows to think that the injected charge reduces the field close to the HV electrode, tending to increase the necessary voltage for the breakdown inception. One

[1] Actually, it is possible to use the normal t-test for more than two variables by using, for instance, the Bonferroni correction of the significance ([54]).

of the postulated breakdown mechanism for industrial-grade oils is that suspended polar particles are attracted towards microscopic protrusion at the electrodes through dielectrophoretic forces. If a partial bridge is formed between the electrodes, this can become the site at which breakdown takes place ([55]). Since the dielectrophoretic forces are linked to the square value of the electric field, a voltage reduction can slow down such failure mode;

- fast charge transfer phenomena, which tend to deteriorate the performance of the insulating fluid transforming the latter in a conducting fluid. When the nanoparticles distance gets too small, secondary charge emission is able to "'bypass"' the trapping behavior of nanoparticles and increase the global conductivity. In this way, the nanofluid first loses its better properties, and then it even worsens at higher concentrations.

4.2 Partial Discharge Inception Voltages

This section reports the results about the partial discharge (PD) measurements performed on nanoluids. For general information about partial discharges, the reader can refer, for example, to [56] or [57].
PD features have been investigated, as usual, using a divergent field configuration, just to highlight high field effects at reduced voltage; point/plane electrode configuration has been hence adopted. Tungsten steel needles ($1\,\mu m$ radius of curvature and $0.5\,mm$ diameter) have been manufactured by Fine Science Tools GmbH; gap spacing was $20\,mm$. Since PDs are fast pulses events, they prefer to circulate inside capacitive branches, as for instance the insulating sample itself. For this reason, a coupling capacitor is usually needed for PD measurements ([57]), but it tends to reduce the signal sensitivity, increasing the path the pulse has to travel before being measured. In order to improve the sensitivity and thus increase the measurement bandwidth, some researchers ([58], [59]), have started to use the sample itself as coupling capacitor, by designing the LV electrode with a guard ring. For PD detection, the measurement impedance ($50\,\Omega$) was connected between the low voltage electrode and the guard ring. Fig. 4.3 shows the cell which has been used during the experiments. As it is possible to see, in this particular case, the coupling capacitor is not represented by the sample itself but, in order to minimize the amount of nanofluid to be used, a filler ring with a high permittivity fluid (natural ester FR_3, described, for instance, in [60]) has been used.
PDs have been measured under different voltage conditions:

- $50\,Hz$ sinusoidal voltage;
- DC, both positive and negative.

The AC test setup consisted of a 220 V/30 kV transformer and a capacitive divider (used only to measure the applied voltage, as the coupling capacitor is not necessary as we have said). PD signals were recorded by a Techimp PDCheck detector. For testing under DC voltages, a Fug - HCN 35-35000 bipolar 35 kV DC source was used. The entire test setup was placed in a shielded cabinet to reduce the effect of the external noise and thus increase the signal to noise ratio. The sensitivity of the system was better than $1\,pC$ and tested with a TechImp

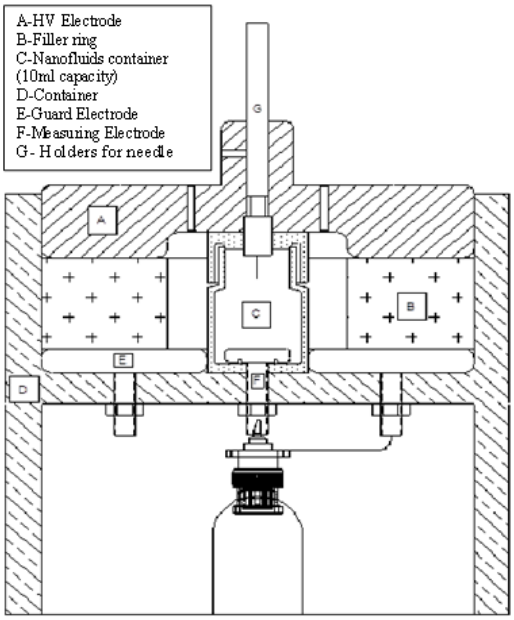

Figure 4.3: Nanofluid cell for PD detection

calibrator; anyway, since the test cell capacitance is very low, one should expect calibration errors ([57]). To overcome this problem, the PD pulse DC component has been estimated as the median of the 20 lowest harmonics of the PD current spectrum. Partial discharge inception voltage (PDIV) was measured starting with an initial voltage of 2 kV; the voltage was raised in steps of 1 kV, each lasting 5 minutes, till the occurrence of the first PD pulses. Measurements were repeated to get 5 PDIV values. By further increasing the voltage, PD magnitudes increase, but the pulse waveform does not change. However, above a given threshold, the pulse tends to spread in the time domain transferring more charge, as shown in Figure 4.4 ([61], [62]). This suggests the development of more intense streamers. In order to study this behavior, the applied voltage was raised above PDIV till a substantial change in the PD pulse shape could be observed. Since for short gaps (as the one used in these experiments), when streamers are observed, breakdown follows after increasing the applied voltage only slightly, tests were stopped when pulses as the one shown in Figure 4.4 (on the right) were first observed.

The results of the PDIV measurements have been modeled considering the 2-parameters Weibull distribution of equation 2.1 and the corresponding B10 values (and relative confidence bounds, computed with the Monte Carlo pivotal method with 90% confidence level) have been summarized in fig. 4.5.

Such results correlate the applied voltage to the electric field, which has been computed considering the Mason's formula, which has been introduced in the previous chapter in equation 3.1. A rapid look at the results indicate that, under AC conditions, the PDIV values are higher than the DC obtained ones (both for positive and negative polarity); furthermore under DC, the negative

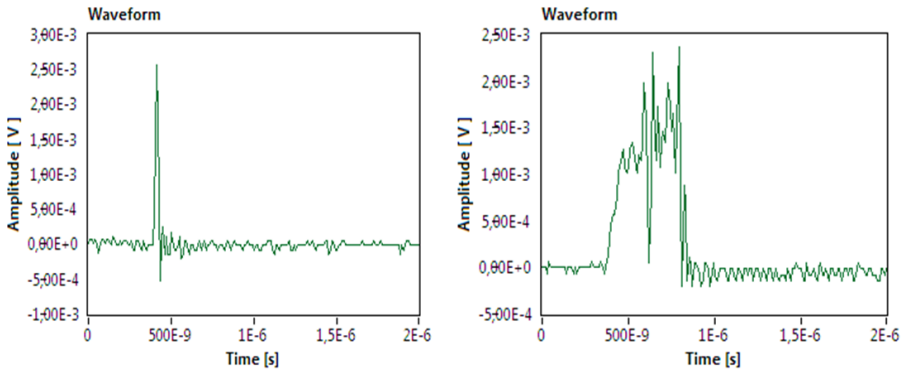

Figure 4.4: Example of the difference between a PD (left, V=14 kV) and a streamer (right, V=26 kV); acquisitions performed with the TechImp PD Check system. Applied voltage: DC positive.

polarity results are lower than the corresponding ones obtained under positive polarity. The difference between AC and DC conditions can be interpreted in a difference between the electrical parameters of the nanofluids, in particular:

- under AC conditions, the electric field is permittivity dependent;
- under DC conditions, the electric field depends on the conductivities.

Since both the permittivity and the conductivity of magnetite nanoparticles are higher than the corresponding values for mineral oil, it is quite clear that the base oil is subjected to a larger electrical stress both in AC and DC, which tends

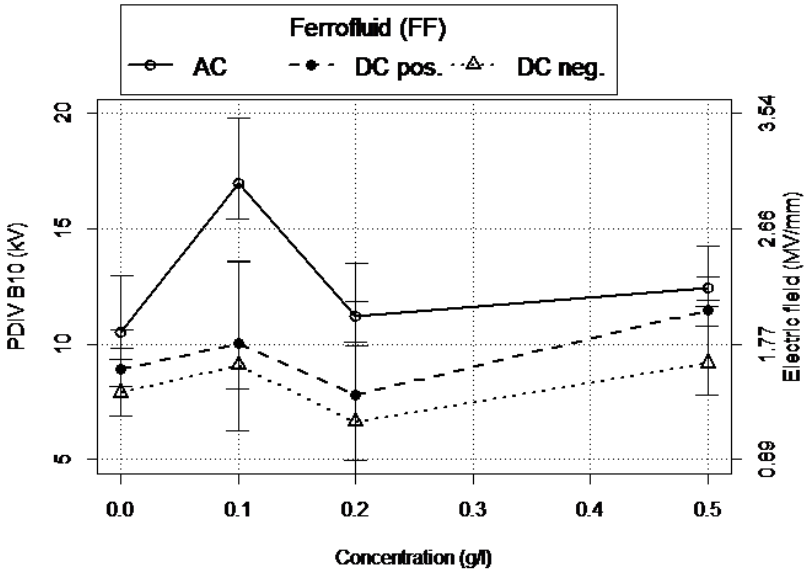

Figure 4.5: PDIV (B10) for nanofluids depending on the concentrations.

to increase the local field close to the HV needle in the presence of nanoparticles. Moreover, as the conductivity mismatch is much higher than the permittivity one, it is reasonable that PDIV values are lower for DC applied voltages.
Apart from the differences between AC and DC applied voltages, which can be explained in terms of the different parameters determining the local electric field, it is surprising that, once more, the "'optimum"' concentration nanofluid is different from the previously determined one. Summarizing, we have three different best concentrations:

1. 0.5 $\frac{g}{L}$, for lightning impulse breakdown tests;
2. 0.2 $\frac{g}{L}$, for AC breakdown tests;
3. 0.1 $\frac{g}{L}$, for PDIV tests.

The reason why the "'optimum"' concentration changes with the performed test is not easy to understand; it is for sure connected to the different mechanisms a particular test highlights, but it is anyway very difficult to define a global theory trying to predict the best concentration for a certain test. For lightning impulse breakdown tests, we have said that a key parameter can be represented by the attachment constant increase due to the presence of nanoparticles, and this can be obtained with very high concentrations, until the distance between nanoparticles starts to ignite fast charge transfer phenomena.
For AC breakdown tests the same considerations should be done, but we have to say that in this case moisture plays a significant role [63]. The moisture trapping behavior of the surfactant-nanoparticles system is able to create a water shell around the nanoparticles themselves; this would ease secondary charge transfer reducing the concentration at which they take place. Furthermore, if in the previously reported results, the test setup was able to highlight the streamers propagation issues, AC breakdown tests are designed to be done in uniform field configurations, where the streamers inception mechanism dominates. It is possible, as Devins said in [12], that in case of inception, a lower attachment constant is needed to slow down electrons, differently from the case in which they are already accelerated and "'hotter"'.
The setup of PDIV tests is designed to highlight discharge inception under non uniform fields; as in the previous case, inceptions are optimized by low concentrations. It is anyway interesting to notice that, under DC applied voltage, it is not sure that the best concentration is 0.1 $\frac{g}{L}$, as the trend seems to increase after the maximum tested concentration.
As for the interpretation of the other measurements, the charge build-up model can help to understand the trend we have obtained. At low voltages, when the charge is injected from the HV needle, the field can be estimated thanks to the Mason's formula; this is generally true, according to what we have said in the previous chapter, but at a molecular level the field is enhanced in the oil because of the permittivity (or conductivity, in DC) mismatch between oil and nanoparticles. The enhancement lets the PDIV be lower than in the case of fresh oil, but this cannot be proved because it would require very high values of the measurement sensitivity. The injected charge is then trapped by the nanoparticles surfaces according to the general model which has been presented in the previous chapter, leading to a field reduction which hinders the previous field enhancement. It is clear now that, the higher the concentration, the higher

the trapped charge ($Q_{tot} = 12\pi\epsilon E N_p R_p^2$, being N_p the number of nanoparticles); this charge is then moved towards the lower voltage electrode, until the polarity reversal transforms it into heterocharge. The latter, as already said, increases the field close to the HV needle, leading to a higher discharge probability. Higher concentrations do not only increase the trapped charge, but they also increase the fluid conductivity and the charge transfer ratio, which tends to reduce the heterocharge effect. A sort of balance between these two phenomena is claimed to explain the obtained results.
To investigate the behavior at voltages higher than PDIV, the voltage was raised above PDIV till the transition from fast to slow streamers; the maximum discharge magnitude and the repetition rate at the different voltage levels was recorded. Given the low repetition rate of PD in oil, the results are somehow erratic.

The results of such experiments have been summarized in fig. 4.6 and compared with the mineral oil, which acts as a benchmark as usual.
Starting from the results under AC applied voltage, it is clear that the maximum investigated concentration has the worst behavior, since the PD induced charge diverges at moderately low voltages, meaning that at such voltages the first streamers are incepted. The other cases are quite similar, in the sense that $0.2\,\frac{g}{L}$ behaves in the same way as mineral oil, while $0.1\,\frac{g}{L}$ shows a lower charge until the streamer inception voltage, which seems to take place at the same voltage of the base fluid.
The trend under DC applied voltage is less clear. Fig. 4.5 reveals that the improvement at the best concentrations is less marked than in AC, and this, as already said, is due to the fact that magnetite nanoparticles are conductive and lead to an increase of the electric field in the oil. The strange thing is that the concentration which seems to behave better in this case is $0.2\,\frac{g}{L}$, because it shows a lower charge until $25\,kV$, while the best concentration has a sudden worsening at $17\,kV$, even if it is possible that there may have been some errors due to the reduced PD rate under DC voltages. Apart from this behavior, the higher concentration still continues to have a lower PD to streamer transition, revealing that above $0.2\,\frac{g}{L}$ the fluid is too conductive. A comparison with the AC case shows that the streamer injection voltage takes place at lower voltages, confirming the role of conductivity in the determination of the electric field which leads to the Fowler-Nordheim injection current, which is here re-called:

$$j_c = \frac{e^3 E^2}{8\pi h \Phi t^2\left(\frac{\Delta\Phi}{\Phi}\right)} e^{-\frac{8\pi\sqrt{2m}\Phi^{\frac{2}{3}}}{3heE^2} v\left(\frac{\Delta\Phi}{\Phi}\right)} \tag{4.1}$$

where:

- e represents the elementary charge;
- E represents the electric field;
- h represents the Planck constant;
- Φ represents the work function of the metal inside the nanofluid;
- m represents the mass of the electron;
- t^2 and v represent two experimental functions. According to [31], $v(y) = 0.95 - y^2$ and $t^2(y) = 1.1$.

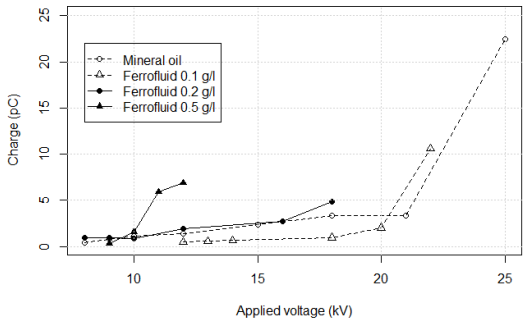

(a) *Trend of PD magnitude vs applied voltage in AC.*

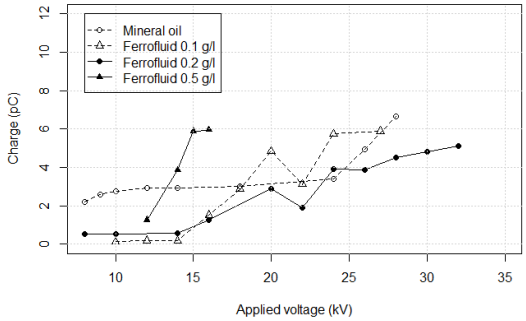

(b) *Trend of PD magnitude vs applied voltage in DC positive polarity.*

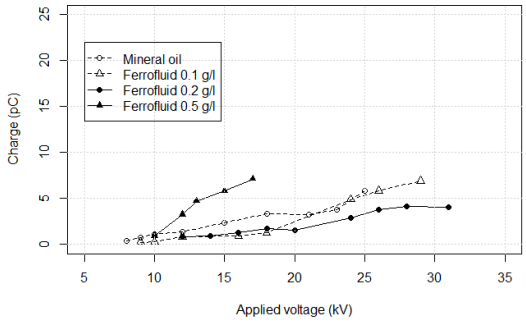

(c) *Trend of PD magnitude vs applied voltage in DC negative polarity.*

Figure 4.6: Comparison of the PD magnitudes vs applied voltage in the different polarities.

Equation 4.1 indicates a strong dependence of j_c (and thus the injected charge) from the electric field; the higher the field, the higher the injected current, or,

equivalently, the higher the conductivity, the higher the injected current.
DC negative voltage confirms the considerations which have been made for DC positive. A first observation directly comes from figure 4.5, where DC negative results are the lowest which have been measured; this is due to two different reason:

1. the first reason is that the electric field is higher than the case of AC applied voltage, and the same of DC positive applied voltage because of the dependence upon the conductivity;

2. the second reason is that electron injection is generally easier than hole injection or, alternatively, electron injection is easier than field ionization [17]. This explains why DC negative results are different from the positive ones.

The relation between nanofluid concentration and voltage is the same also in this last case: the streamer inception voltage is lower if the concentration gets higher ($0.5\,\frac{g}{L}$ is still the worst fluid, because its transition voltage takes place at $10\,kV$), while the other two concentrations behave better than mineral oil; as in the previous case, $0.2\,\frac{g}{L}$ seems to behave better than the optimum concentration in terms of PDIV.

Figure 4.7 compares the PD repetition rates with the applied voltages in the different configurations. Repetition rates, as known from the general PD theory ([59]-[64]), are connected to charge depletion issues from the region where PDs take place: higher repetition rates mean higher conductivities while lower ones are connected to a more intense trapping behavior of the insulating material under test.
The measured trend for AC[2] partially supports this statement, because the $0.5\,\frac{g}{L}$ is the one which tends to explode at low voltages, even if $0.2\,\frac{g}{L}$ showed the highest rates. $0.1\,\frac{g}{L}$ nanofluid is in this case the best fluid without any doubt (at least until $17.5\,kV$), and this suggests that at this concentration, the conductivity increase is able to limit the homocharge-heterocharge switch.
Under DC applied voltage, repetition rates of nanofluids are always lower than mineral oil and the best concentration fluid is $0.2\,\frac{g}{L}$. Since in DC there is no heterocharge switch, because there is no polarity reversal, this behavior is surely connected to the trapping tendency of nanoparticles, which contrasts with the conductivity increase (and thus the repetition rate increase, as explained in [64]).

The results presented in this section and the previous one are not clear and somehow contrasting, but it is anyway noteworthy that three different mechanisms have to be investigated to gain more experience on nanofluids behavior:

- charge injection properties: it is necessary to understand the mechanisms of injection involving nanofluids. Are they similar to that of the base fluid or not?

- nanofluid conductivity: what is the relation between nanoparticles concentration and the conduction mechanisms?

[2] In AC applied voltage, the PD repetition rates are measured in pulses per voltage cycle.

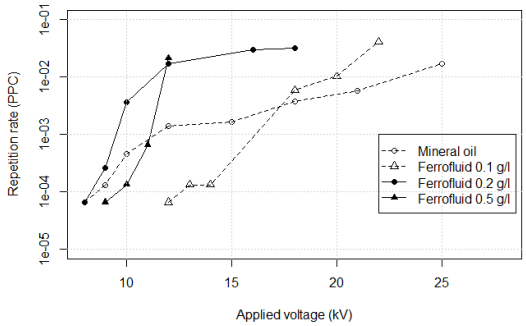

(a) *Trend of PD repetition rate vs applied voltage in AC.*

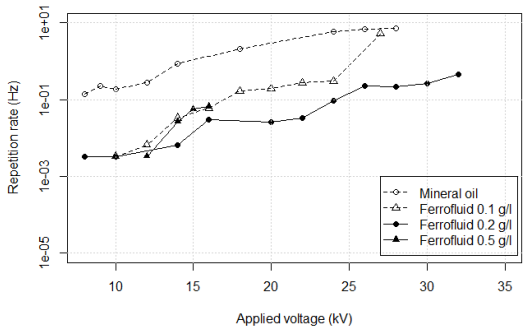

(b) *Trend of PD repetition rate vs applied voltage in DC positive polarity.*

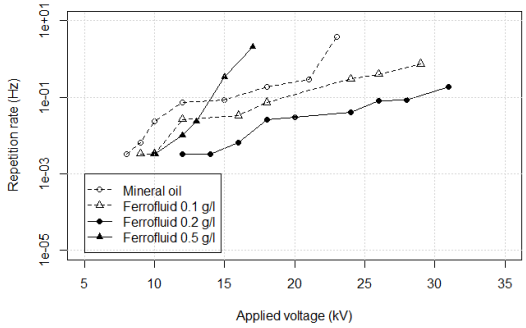

(c) *Trend of PD repetition rate vs applied voltage in DC negative polarity.*

Figure 4.7: Comparison of the PD repetition rates vs applied voltage in the different polarities.

- nanofluid dielectric spectroscopy: do nanoparticles introduce particular mechanisms related to the electrical permittivity?

The following chapters will try to give an answer to the postulated questions by presenting some models and experimental evidence.

Chapter 5

Electrical field model

Abstract

As stated at the end of the previous chapter, we have three different questions to answer. This short chapter presents a simple semi-empirical model trying to predict the field variation due to the nanoparticles presence. First, a simple model is derived, considering the only geometrical effect of spherical nanoparticles, while in the second part of the chapter a sort of generalization is done considering also the contribution of surfactants and the space charge which is induced by nanoparticles.

5.1 First elementary model

The aim of this section is to introduce a geometrical model trying to determine the electric field which is created in a nanofluid. In chapter 3 we have dealt with such a problem, neglecting the discrete nature of nanofluids and thus avoiding to treat the local enhancement of the field due to the nanoparticles. Here we would like to overcome the latter hypothesis, and we propose a model starting from the following hyphoteses:

1. nanoparticles are supposed to be perfectly spherical;
2. the mean free path between nanoparticles is $\gg$ than the nanoparticles radius;
3. the ratio between the conductivity of magnetite nanoparticles and mineral oil is $\neq \infty$;
4. the enhancement effect is confined in a region which is proportional to the nanoparticles radius;
5. we neglect the presence of surfactant particles.

The second and third hypotheses mean that nanoparticles do not interact amoung each other and it is like there is only one of them. Such situation is depicted

in figure 5.1. Let us suppose to apply a constant voltage V and suppose to consider a steady state situation; the electrical field can be determined thanks to the following equations:

$$\int_a^b E(x)dx = V(a) - V(b) \tag{5.1}$$

$$div_\Sigma \vec{j} = 0 \tag{5.2}$$

$$\vec{j} = \sigma E \tag{5.3}$$

By applying these equations to fig. 5.1, we easily obtain the solving equations:

$$E_1 (d_1 + d_2) + 2E_3 d_3 + E_4 d_4 = V \tag{5.4}$$

$$\sigma_3 E_3 - \sigma_4 E_{4n} = 0 \tag{5.5}$$

$$E_{4n} = E_4 sin(\theta) \tag{5.6}$$

In the case of AC applied voltage, the solving equations are the same, with the only difference that $div_\Sigma \vec{D} = 0$, and hence $\epsilon_3 E_3 - \epsilon_4 E_{4n} = 0$. This means that, by applying AC, we only have to change the conductivity with the permittivity. The solution of the group equations 5.4-5.6 is:

$$E_1 = \frac{V}{d} \tag{5.7}$$

$$E_4 = \frac{d_3 + R}{R + d_3 \frac{\sigma_4}{\sigma_3}} E_1 \tag{5.8}$$

$$E_3 = \frac{\sigma_4}{\sigma_3} E_4 sin(\theta) \tag{5.9}$$

The solved equations show the dependence from d_3. In order to give a final formula we need to express d_3 as a function of the other geometrical parameters. In particular, the adopted procedure is semi-empirical, because the value of d_3 has been determined by comparisons with finite element simulations. Following this approach, we have found that:

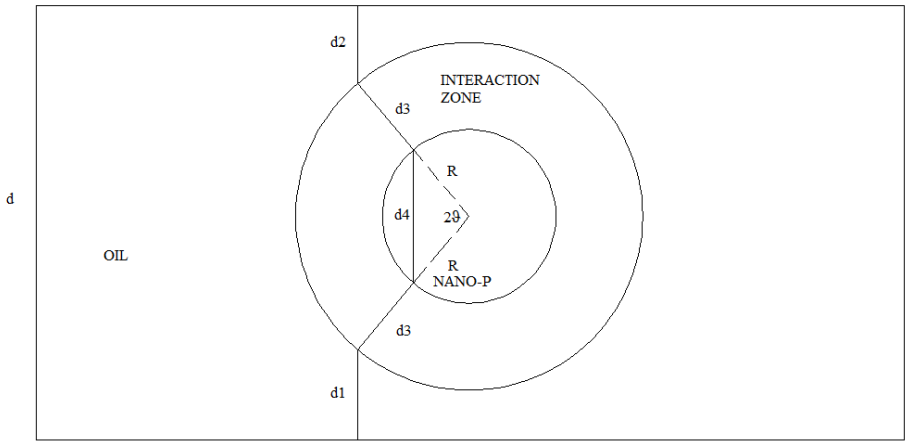

Figure 5.1: Representation of the modeled scenario.

- d_3 is equal to R in the case of a two dimensional computation;
- d_3 is equal to $\frac{R}{2}$ in the case of three dimensional computations.

In order to test the goodness of the obtained formula, we compare the analytical result with the one obtained with a finite element simulation in two dimensions; the latter is presented in figure 5.2. Such simulation is obtained considering the following parameters:

1. $d = 1\,m$ and $V = 1\,V$, i.e. the applied electric field is equal to $1\,\frac{V}{m}$;
2. $\sigma_3 = 1\,\frac{S}{m}$ and $\sigma_4 = 1000\,\frac{S}{m}$.

Fig. 5.2 shows a maximum electric field of $2.06\,\frac{V}{m}$, while the obtained formula lets us estimate a value of $2.0\,\frac{V}{m}$, with a very small prevision error (less than 3%).
For a reason which will be clear in the following (in particular in chapter 7), it is necessary to evaluate the field between two nanoparticles which are closer than $2R$ in the case of a bi-dimensional situation. Figure 5.3 shows the model of the situation we would like to study. Two nanoparticles of radius R are supposed to be at a distance $x < 2R$ and we would like to calculate the different field values, supposing to know the background field.
Let us suppose the insulating gap, where the voltage V is applied, is equal to $d + 4R$, being d a geometrical variable. Using the labels of figure 5.3, it is possible to write the following equations:

$$4RE_p + 2RE_0 + xE_i + \frac{V}{d+8R}(2R + d - x) = V \tag{5.10}$$

$$E_p\sigma_p = E_0\sigma_o \tag{5.11}$$

$$E_p\sigma_p = E_i\sigma_o \tag{5.12}$$

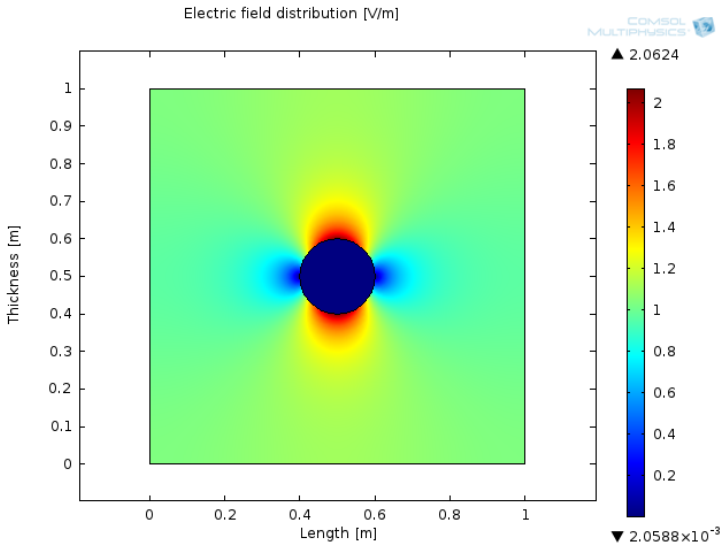

Figure 5.2: Field simulation example.

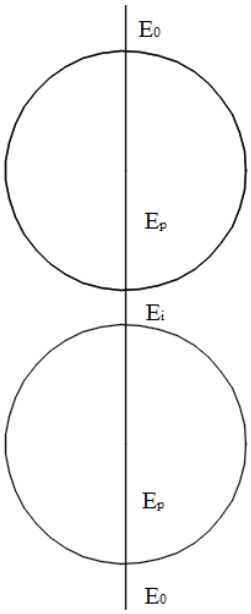

Figure 5.3: Schematic representation of the situation.

After some calculations, it is possible to derive the following expression for the internal field (assumed to be uniform):

$$E_i = \frac{V}{d+8R}\frac{6R+x}{x+2R+4R\frac{\sigma_o}{\sigma_p}} \tag{5.13}$$

which can be written in an easier way remembering that $E_{background} = \frac{V}{d+8R}$:

$$E_i = E_{background}\frac{6R+x}{x+2R+4R\frac{\sigma_o}{\sigma_p}} \tag{5.14}$$

Equation 5.14, remembering that $\frac{\sigma_o}{\sigma_p} < 1$ in the case of magnetite nanoparticles, reveals that the field between the two nanoparticles is always higher that the background one, with a limit of 3, when the distance x gets to 0.

5.2 Improved model

In this section we want to improve the above introduced model, in order to take into account the presence of surfactant particles which, as we have already said in previous chapters, are able to keep nanoparticles kept out.
The surfactant which Magnacol has used to manufacture Ferrofluid is oleic acid, presented in figure 2.1. As we said, it is characterized by a hydrophilic tip, attracting water molucules and thus creating a water shell around. The thickness of such a water shell can be estimated by a simple analysis considering the starting moisture of the base mineral oil. Let us suppose to consider a spherical nanoparticle of radius R_p and we want to determine the external radius of the

water shell, x. Moreover, let m be the moisture level of mineral oil (typically in the $5 - 30\,ppm$ range); it follows that:

$$\frac{4}{3}\pi \left(x - R_p\right)^3 N_p \left[1\,L\right] = m \tag{5.15}$$

where $N_p\left[1\,L\right]$ represents the number of nanoparticles which are present in $1\,L$ nanofluid.
Considering a nanofluid of concentration $c\left[\frac{g}{L}\right]$, the following relation can be written:

$$c\left[\frac{g}{L}\right] = 1000\frac{\frac{4}{3}\pi R_p^3 N_p\left[1\,L\right]\rho\left[\frac{kg}{m^3}\right]}{\left[1\,L\right]} \tag{5.16}$$

Equation 5.16 can be used to determine $N_p\left[1\,L\right]$, which in turn can be inserted inside equation 5.15 to estimate the thickness of the water shell. The result is:

$$x = R_p + \sqrt[3]{\frac{1000 m R_p^3 \rho\left[\frac{kg}{m^3}\right]}{c\left[\frac{g}{L}\right]}} \tag{5.17}$$

Equation 5.17, and in particular $x - R_p$, is represented in figure 5.4 for different moisture levels.

The improvement of the field model consists in the analysis of the contribution the water shell can have on the electric field distribution and the introduction of a region, which is know in literature with the name "'interphase"', which consists in a transition region between the water shell and the host fluid ([65]-[66]-[67]-[68]). The model we propose here is represented in figure 5.5 and starts from these considerations:

- since magnetite nanoparticles and water have a very similar permittivity, we suppose to consider an ideal nanoparticle with radius $R = R_p + WS_t$, where R_p is the mean radius of magnetite nanoparticles and WS_t represents the thickness of the water shell obtained with the above written equations (this region is labeled with the number "'2"' in figure 5.5;

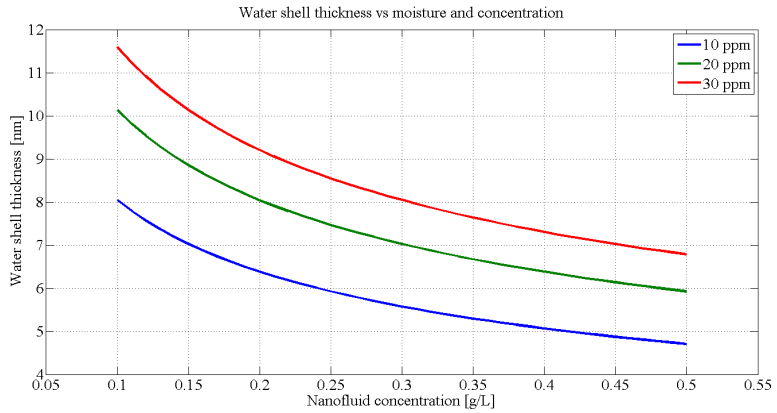

Figure 5.4: Water shell external coordinate vs concentration.

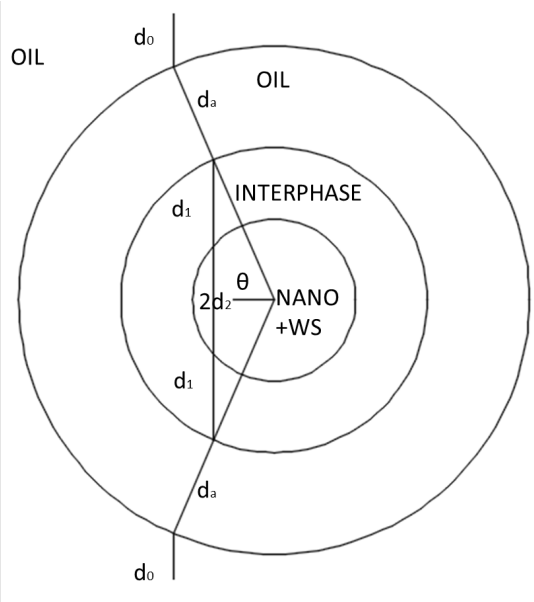

Figure 5.5: Improved model general scheme.

- we consider the interphase thickness t_1 (region "'1"' in figure 5.5) equal to the nanoparticles radius R_p;

- we consider also a region labeled as "'a"', where we suppose the field variations are confined. Such a region has a thickness which is equal to R if we consider a two dimensional case, while $\frac{R}{2}$ if we switch to a three dimensional case, as in the previous model.

In figure 5.5 there is the indication of the field line we consider to simplify the problem; we suppose indeed that the field lines are aligned with those inside the "'equivalent"' nanoparticle, even if this is not generally true.
Simple geometrical considerations allow to state the following things:

1. $d_0 + 2d_a sin(\theta) + 2d_1 + 2d_2 = d$, where d is an auxiliary thickness where the voltage V is applied;

2. $d_2 = \sqrt{R^2 - (t_1 + R)^2 cos^2(\theta)}$;

3. $d_1 = (t_1 + R)sin(\theta) - \sqrt{R^2 - (t_1 + R)^2 cos^2(\theta)}$.

Starting from these results, it is possible to write the same equations of the previous section:

$$E_0 d_0 + 2d_a E_a sin(\theta) + 2E_1 d_1 + 2E_2 d_2 = V \tag{5.18}$$

$$\epsilon_2 E_2 = \epsilon_1 E_1 \tag{5.19}$$

$$\epsilon_a E_a = \epsilon_1 E_1 sin(\theta) \tag{5.20}$$

Parameter	Symbol	Value [Unit]
Nanoparticle+WS radius	R	0.05 [m]
Interphase thickness	t_1	0.05 [m]
Inter-oil region	d_a	0.1 [m]
Oil Permittivity	ϵ_a	2
Interphase relative permittivity	ϵ_1	4
Particle relative permittivity	ϵ_2	8
Background field	E_b	0.33 $[\frac{V}{m}]$

Table 5.1: Values of the parameters of the simulation of figure 5.6.

After some calculations, it is possible to obtain the following expressions:

$$E_2 = E_b \frac{d_1 + d_2 + d_a sin(\theta)}{d_2 + d_1 \frac{\epsilon_2}{\epsilon_1} + d_a \frac{\epsilon_2}{\epsilon_a}} \tag{5.21}$$

$$E_1 = \frac{\epsilon_2}{\epsilon_1} E_2 \tag{5.22}$$

$$E_a = \frac{\epsilon_2}{\epsilon_a} E_2 sin(\theta) \tag{5.23}$$

where $E_b = \frac{V}{d}$ refers to the background field. These equations have been again compared with finite element simulations to verify their correctness; the Comsol simulation result is shown in figure 5.6, with the parameters of table 5.1. The derived equations are able to estimate the maximum and minimum field as follows:

- maximum field, predicted value: 0.48 $\frac{V}{m}$, obtained value: 0.47 $\frac{V}{m}$;
- minimum field, predicted value: 0.12 $\frac{V}{m}$, obtained value: 0.14 $\frac{V}{m}$.

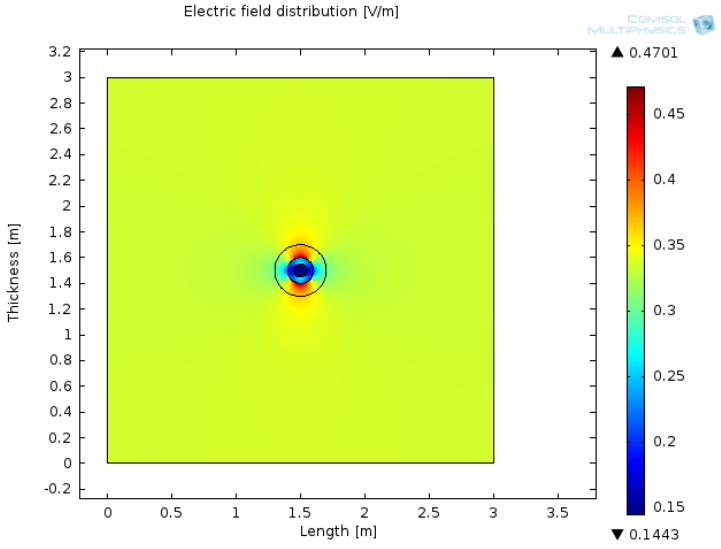

Figure 5.6: Finite element analysis of the improved model.

Apart from the comparison between the obtained formula and the finite element simulation result, where the parameters have been randomly chosen, it is necessary to spend few words about the relative permittivity of the interphase region. According to the "'Lewis"' nanocomposites model ([65]), "'the intensity I_α of a material property α does not change abruptly but gradually over the course of several nanometers. Each atom or molecule in this interfacial area will interact with its surroundings via short- and long-range forces."' (after [69]). This means that the permittivity ϵ_1 differs from that of mineral oil and it is not uniform as we have supposed. For the sake of simplicity, we neglect this fact and simply consider $\epsilon_1 = \frac{\epsilon_a+\epsilon_2}{2}$, i.e. the average value between mineral oil and the nanoparticle-water shell corona around.

There is a last model which considers all the phenomena induced by nanoparticles. We have said in the previous chapters that nanoparticles bahave as charge traps when voltage is applied; this induces charge to create a layer around the nanoparticles, which in turn is able to attract opposite polarity particles. In other words, if nanoparticles are able to attract electrons on their surfaces, electrons are then able to attract positive ions which form a counterion layer and force them to move only along precise trajectories. This particular phenomenon has been firstly studied by Schwarz in [70] for micrometric colloidal solutions, but the described mechanism is likely to interest also nanoparticles-based colloidal solutions.

5.3 Theory of electrons and counterions interactions

This section recalls the theory presented in [70] about the interaction between fixed charges which are trapped on particles surfaces and the counterions which are attracted. Schwarz considered a fluid of complex conductivity $\Sigma_a = \sigma_a + j\omega\epsilon_a$, while particles are supposed to have a mean radius R and complex conductivity $\Sigma_i = \sigma_i + j\omega\epsilon_i$. The sphere is electrically charged and surrounded by counterions of electric charge e_0 and mechanical mobility u[1], which can be moved only along the particles surface, but not perpendicular to it; in other words, the counterions motion is assumed to be tangentially. It is then clear that the counterions density is a function of the electric field, in particular:

$$\sigma(E) = \sigma_0 + \sigma(\bar{E}) \tag{5.24}$$

where σ_0 is the constant value representing the counterions density when no electric field is applied and $\bar{\sigma}$ is the variation due to the electric field. The induced ions current density is made of two contributions:

$$j_e = e_0\sigma\mu E \tag{5.25}$$

$$j_d = -\frac{ukT}{R}\frac{\partial\sigma}{\partial\theta} \tag{5.26}$$

which are, respectively, the electric field and the diffusion contribution. In the previous equations, μ refers to the ions mobility, k is the Boltzmann constant and θ is the angular coordinate which has been introduced because of the

[1] The mechanical mobility is defined as the velocity per unit force, i.e. $u = \frac{v}{F} = \frac{v}{qE} = \frac{u_{el}}{q}$, where u_{el} refers to the electrical mobility.

spherical symmetry of the problem. The equation which allows to determine the counterions density is:

$$\frac{\partial \sigma}{\partial t} - div(j_e + j_d) = 0 \tag{5.27}$$

i.e. the continuity equation which has to be coupled with the Laplace equation:

$$\nabla^2 \Psi_a = 0 (r > R) \tag{5.28}$$

$$\nabla^2 \Psi_i = 0 (r < R) \tag{5.29}$$

with the following boundary conditions:

$$\lim_{r \to R} \Psi_a = \lim_{r \to R} \Psi_i = \Psi_s \tag{5.30}$$

$$\Psi_a \longrightarrow -E_r cos(\theta)\, for\, r \longrightarrow +\infty \tag{5.31}$$

$$\lim_{r \to 0} \Psi_i \neq \infty \tag{5.32}$$

$$\Sigma_a \frac{\partial \Psi_a}{\partial r} - \Sigma_i \frac{\partial \Psi_i}{\partial r} = -i\omega e_0 \bar{\sigma} \tag{5.33}$$

These solving equations can be solved with standard methods, as for instance by representing the unknown variables by means of Legendre polynomials $P_n(cos\theta)$. In this way, it is possible to find that:

$$\sigma = \sigma_0 - \frac{1}{1 + i\omega\tau} \frac{e_0 \sigma_0}{kT} \Psi_s \tag{5.34}$$

where $\tau = \frac{R^2}{2ukT}$ represents a relaxation of the change in the counterion density, which depends, not surprisingly, on the ions mobility: the higher the mobility, the higher the relaxation frequency.
After some calculations, the electric potential can be determined as:

$$\Psi_a = -E_r cos\theta + \frac{\bar{K_i} - K_a}{\bar{K_i} + 2K_a} R^3 E \frac{cos\theta}{r^2} \quad (r \geq R) \tag{5.35}$$

$$\Psi_i = -\frac{3K_a}{2K_a + \bar{K_i}} E_r cos\theta \quad (r \leq R) \tag{5.36}$$

where $\bar{K_i} = K_i + i\omega\epsilon_0 \frac{2\epsilon_s^\star}{R}$ and $\epsilon_s^\star = \frac{1}{1+i\omega\tau} \frac{e_0^2 \sigma_0 u \tau}{\epsilon_0}$.
Equations (5.35) and (5.36) are very important because they let formulate the following equivalence principle: *The dielectric behavior of a sphere with the counterion layer is identical with that of a sphere without such a layer but with apparent dielectric constant:*

$$\bar{\epsilon_i} = \epsilon_i + \frac{1}{1 + i\omega\tau} \frac{e_0^2 \sigma_0 R}{\epsilon_0 kT} \tag{5.37}$$

Equation (5.37) will let us use the model formulated in the first section of this chapter to take into account the space charge effect on the electric field distribution, without further complicating the analytical procedure.

Chapter 6

Injection at electrodes

Abstract

This chapter contains a study aimed at analyzing the injection of charge carriers in ferrofluid-based nanofluids. Conductivity tests in divergent field conditions are described and discussed to compare the different mechanisms with respect to mineral oil. Long tests have been realized too, in order to highlight the stability of nanofluids under divergent fields. Nanofluids will reveal to be unstable under DC applied voltages; a simple model to interpret this phenomenon will be proposed.

This chapter will introduce some results about conductivity tests at different regimes. Such tests have been proposed for simple liquids in [17] or [50], but nobody has ever performed them on mineral oils, because of the complexity of the chemical structure which characterizes them [17]. Recently, Butcher et alia ([71]) have made conductivity measurements on mineral oils under divergent field configurations and different voltage levels. Usually, when performing such tests, three conduction regimes can be seen:

- Ohmic regime, for relatively low voltages, where current and voltages are linearly correlated, i.e. it is possible to assume a voltage-current relation of the type $I = \frac{V}{R}$, where R stands for the resistance of the insulating fluid;
- Fowler-Nordheim regime, for intermediate voltages, where the following relation correlates current and applied voltage ([72]):

$$I = KV^2 e^{-\frac{B}{V}} \tag{6.1}$$

  where K and B are constants; in particular:

$$B = \frac{3\chi d\epsilon}{2\Delta d} \tag{6.2}$$

  where χ is the electron affinity barrier, Δd the barrier thickness (assumed to be few nanometers), d is the gap width and ϵ represents the electrical permittivity;

- space charge saturation regime (SCLC), for high voltages. Halpern and Gomer in [50] have studied such regime, approximating the geometry with a simpler model and found the following voltage-current relation:

$$I = \frac{3\alpha}{8}\frac{\mu\epsilon}{d}V_{app}^2 \tag{6.3}$$

  where $\alpha \approx 0.6\pi$ represents the emission solid angle and μ is the charge carriers mobility.

The values of voltages which are needed to enter a well precise regime depend on the geometry of the used cell, because the key parameter is, as always, the electric field. Figure 6.1 shows an example of a voltage-current plot highlighting the three above mentioned regimes. It refers to mineral oil as insulating sample, $d = 10\,mm$ gap, needle to plane electrode configuration and different voltage polarities (open symbols: negative, closed symbols: positive). As it is possible to see from the axes labels, the plot represents $ln\left(\frac{I}{V^2}\right)$ vs $\frac{1}{V}$ and so, if the voltage is high enough to ignite the Fowler-Nordheim regime, a linear trend is expected, as revealed from equation (6.1): for such a reason, the plot represented in fig. 6.1 is know in literature as "'Fowler-Nordheim"' plot. The three regimes are clearly visible in this picture:

1. for low voltages ($V \leq 4\,kV$), the regime is ohmic;
2. for intermediate voltages ($4 \leq V \leq 10\,kV$) the trend is linear and the Fowler-Nordheim regime dominates this voltage interval;
3. for higher voltages a saturation effect is visible, highlighting the last regime, which is the SCLC, from which the mobility of the carriers can be outlined.

Measuring the slope of the voltage-current plot in the Fowler-Nordheim regime, it is possible to estimate the parameters which define the constant B of equation

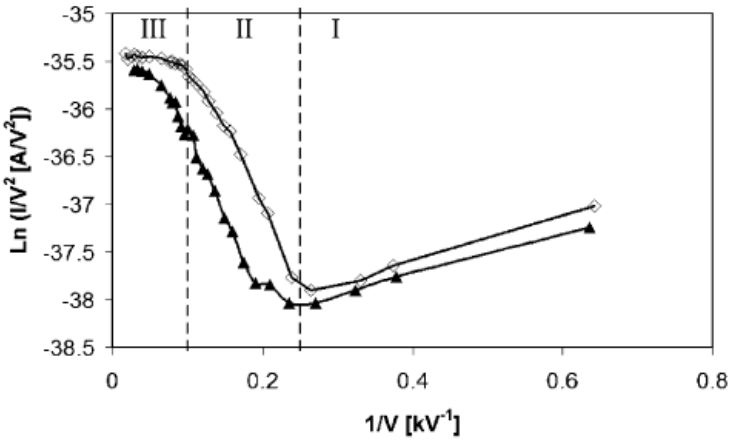

Figure 6.1: Example of a Fowler-Nordheim plot for mineral oil (after [71]). Open symbols: negative polarity; filled symbols: positive polarity.

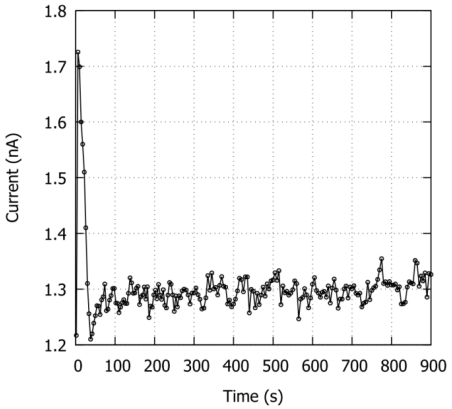

Figure 6.2: Example of the recorded current ($V = +8.5\,kV$, mineral oil).

(6.2), in particular the electron affinity barrier. Comparing the positive and negative trends of figure 6.1, the following considerations can be done:

- the ohmic region seems to be different, and this is documented also in [17], where the author refers to the different mobility of positive and negative ions, since the conduction in fluids is due to the ion motion;
- the Fowler-Nordheim injection threshold is higher for positive polarity, because, as known in literature, electron emission is easier than field ionization (i.e. hole injection).

The tests described in this chapter have been performed on samples of the same nature of the ones defined in the previous chapters, but only one concentration has been tested; $0.2\,\frac{g}{L}$ nanofluid has indeed been considered because it has proved to be one of the best concentration regarding injection phenomena.
The divergent field conditions have been realized with a needle to plane electrode configuration; a tungsten steel needle ($1\,\mu m$ radius tip and $0.5\,mm$ diameter) manufactured by Fine Science Tools GmbH was used as the high voltage electrode. The ground electrode was a brass plane with pseudo-Rogowsky; gap spacing was $20\,mm$.
The voltage source was either a Spelmann DC Generator PCM50P120 for positive polarity, or a PCM50N120 for negative polarity; DC current has been recorded with a Keithley 388 electrometer.
For each specimen, voltage has been raised from a lower value ($4\,kV$) to a higher value (from 11 to $13\,kV$), by steps of $500\,V$. Both positive and negative polarities are considered; to avoid the full breakdown of the oil (or nanofluid) gap, the maximum voltage level was lower using positive polarity, because positive streamers are considered the most dangerous events leading to breakdown ([12]).
A first question to be answered, before starting with the tests, is the time interval which is needed to reach the steady state; this is an important issue, because it is necessary to understand when voltage has to be raised. The theory suggests that the transient current is dominated by the time constant $\tau = \frac{\epsilon}{\sigma}$, with obvious meaning of the symbols; in the case of oil, the time constant is of the order of tens of seconds. Figure 6.2 confirms that the transient behavior is very short and that the steady state condition is reached after one hundred seconds. As

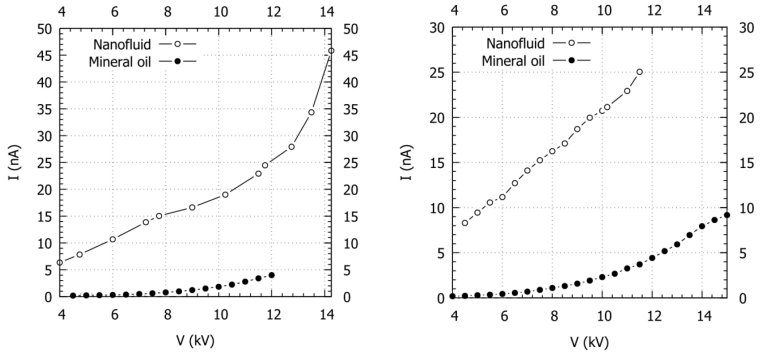

(a) $I - V$ *trend comparison for positive voltage.*

(b) $I - V$ *trend comparison for negative voltage.*

Figure 6.3: Comparison of the $I - V$ trends for the investigated samples.

final current, we have considered the median value of the last recorded 200 s. A global overview of the obtained results highlights the conductivity increase due to the presence of nanoparticles. Figure 6.3 shows this aspect and anticipates that:

- the nanofluid conductivity is more or less one order of magnitude higher than that of mineral oil;
- for nanofluid, the $I - V$ trend has a linear shape till higher voltages.

The second consideration allows us to state that, before analyzing better the obtained currents, nanofluids have a higher injection voltage compared to mineral oil; mineral oil trends indeed start to deviate from the linear shape at lower voltages. From figure 6.3, it is not definitely clear if the non-linear trend refers only to the Fowler-Nordheim regime or also to the SCLC one, as it may seem from the slope reduction of the last few points; in order to understand better the issue, the Fowler-Nordheim plot is needed and represented in figure 6.4. This figure highlights the different regimes and, as expected, in the case of negative polarity, there is the transition between the Fowler-Nordheim to the SCLC one; unfortunately, this was not visible for positive polarity as the tests were stopped at lower voltages to prevent streamer inception. As outlined earlier, the following considerations can be done for our investigated mineral oil:

1. the ohmic conduction is different in the case of positive and negative polarity, because of the different mobilities of positive and negative ions, as reported in some milestone works ([4],[17]);
2. the injection threshold voltage is different, in the sense that electrons are more easily injected than holes;
3. the slopes of the linear lines are different, indicating that the affinities are different in the case of positive and negative charges. In particular, positive polarity slope is higher, indicating a higher energy required to inject, which is in agreement with the necessity of higher electric fields;

4. unlike figure 6.1, where the separation between the ohmic and injection regime is quite marked, in our case it seems to be rather blurred, suggesting that an intermediate phenomenon may take place, as for instance the Schottky injection, which usually starts at a lower voltage than the Fowler-Nordheim one. For more details about the difference between the two types of injections, the reader can refer to several works, as for instance [4],[17] or [31];

5. a Schottky injection process may be possible, because the calculated energy barriers are, for positive and negative voltage, $0.09\,eV$ and $0.22\,eV$, i.e. not so higher than $10kT$ at room temperature.

The case of $0.2\,\frac{g}{L}$ nanofluid is shown in figure 6.5, where the Fowler-Nordheim plot is reported. As supposed when looking at figure 6.3, nanofluid provide results different from mineral oil. In particular, the injection threshold voltage is higher than that of mineral oil.
The plot of figure 6.5 does not reveal a problem that had to be solved to arrive to it. The negative charging current, above a certain voltage value, showed a very strange behavior, which is reported in figure 6.6. Such behavior was likely to take place only when the negative polarity was considered; similar effects were not observed on the positive polarity. We might expect to observe them at higher voltages, however the inception of streamers in oil, at such high voltages, might hinder the observation, destroy the electrometer used for the measurements, or change the order of the nanoparticles in the fluid.
The pulsed-like mechanism represented in figure 6.6 does never reach a steady state value within reasonable time intervals, indicating that this is not a phenomenon connected with the electrical properties of the nanofluid, like in the case of mineral oil. Before trying to entering the details of such phenomenon, we have to say that the "'steady state current"' reported in figure 6.5 is equivalent to the minimum value of the recorded trend in a window of $10000\,s$ maximum. This choice does not take into account the real intrinsic steady state current because, as we will see in the following, the minimum current is influenced by

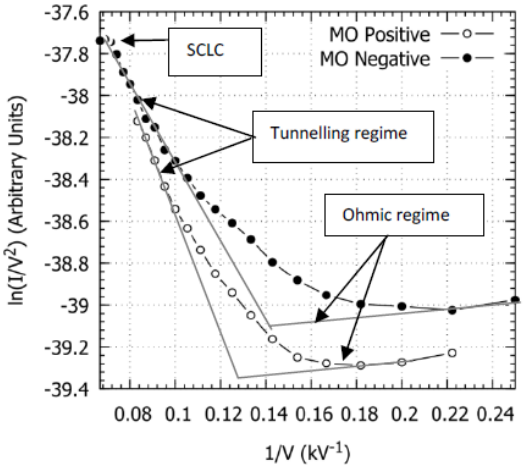

Figure 6.4: Fowler-Nordheim plot for mineral oil.

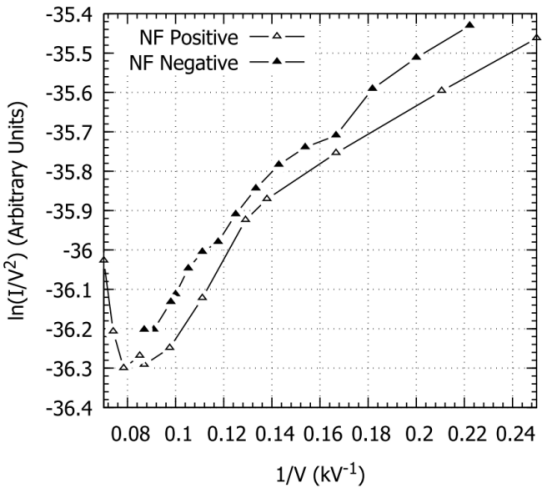

Figure 6.5: Fowler-Nordheim plot for the investigated nanofluid.

a sort of space charge like mechanism. Therefore, comparing the FN plots obtained earlier in this chaper for positive and negative polarities should be done in a very cautious way.
If we think to the scenario close to the HV electrode, the needle is in contact with oil both in the case of mineral oil sample and in the case of the nanofluid; it is then difficult to think that there is a change of electron affinity switching from the base fluid to the nanoparticles-based one. It is possible, on the contrary, that the electric field changes the equivalent barrier charges have to overcome

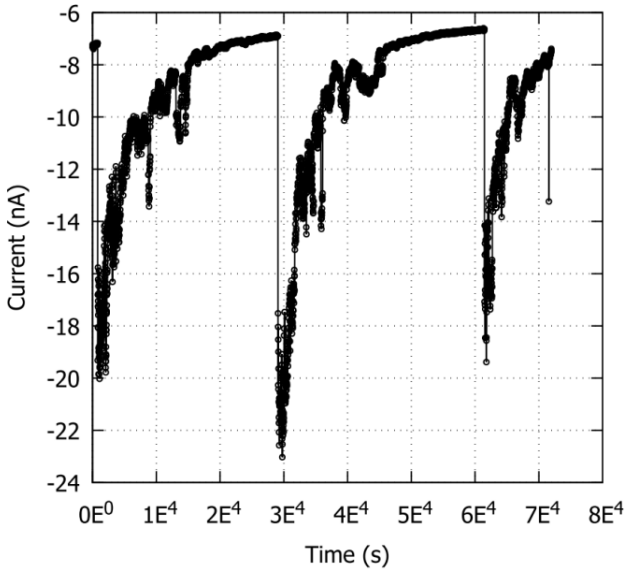

Figure 6.6: Example of recorded conduction current for nanofluid ($V = -8.5\,kV$).

in order to be injected inside the investigated fluid. Taking the case of mineral oil as reference, we have already shown in the previous chapters how low concentration nanofluids act as electron traps, causing a reduction of the electric field close to the region where they are injected (homocharge effect). This phenomenon, again, can be the cause of the behavior observed for nanofluids, because:

1. first, an enlargement of the linear regime can be explained by a field reduction, i.e. at the same voltages, the highest electric field is lower than the one inside mineral oil;

2. second, the pulsed-like polarization currents can find their explanation in the change of mobility due to the charge trapping on nanoparticles surfaces.

The last consideration arises from the fact that, the shape of the conduction current is like the one of figure 6.6 only when the applied polarity is negative and the voltage is above a certain threshold (in the case of our experiment, this threshold was about $-8.5\,kV$). Since nanoparticles are more conductive than mineral oil, the electric field distribution is higher inside the latter, causing an injection at lower voltages; such charge is then trapped by the nanoparticles surfaces in a negligible time interval [31] and reduces the field causing the apparent better behavior observed in figure 6.5. At higher voltages, i.e. for $V > 8.5\,kV$ (negative polarity), the electric field is anyway so high to let charge injection take place; this injection brings a current increase due to the increase of charge carriers [17]. At this point, the injection is inhibited again, but the electric field causes a charge shift towards the low voltage electrode; such movement takes place according to the mobility of the carriers, which is equal to the mobility of the nanoparticles because charges are trapped on their surfaces. As charges moves towards the LV electrode, the current reduces because carriers leave the high field region, till re-injection takes place again when the field on the HV tip restores to the starting value.
If this phenomenon is really likely to take place, after several pulses we should find traces of nanoparticles on the low voltage electrode. Figure 6.7 represents the LV electrode after one months testing. In the picture, a clear nanoparticles

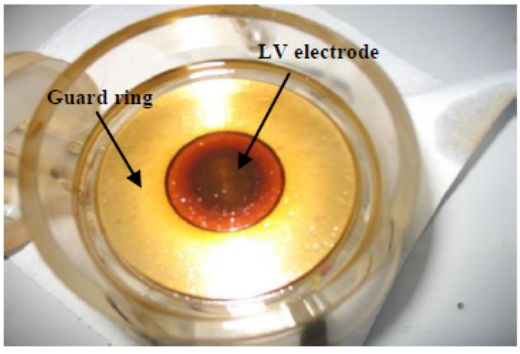

Figure 6.7: LV electrode after one month testing. Note that the guard ring is not affected by the phenomenon.

(a) *HV needle before the conduction test.*

(b) *HV needle after the conduction test.*

Figure 6.8: Optic microscope pictures of the HV needle before and after the test.

aggregation is evident in a circle inside a rounded brass region. The latter is the guard ring allowing the bulk conduction current measurement and so it is not affected by the phenomenon, which is likely to take place only on the measuring LV electrode in the middle.
A real interesting thing which has been observed after the same time interval is that a nanoparticles aggregation has been observed on the HV electrode, too: this is clearly visible in figure 6.8. Such aggregation cannot be justified by the considerations which have been made previously, and it will be explained with a simple model in the following section. Instead, we would like now to verify if the pulsed-like mechanism of figure 6.6 is really linked to the charge trapping behavior of low concentration nanofluid.
The way to verify it consists in the comparison of the recorded conduction current under negative polarity of a low concentration nanofluid and a high concentration one, that is:

- 0.2 $\frac{g}{L}$ nanofluid, as the low concentration one;
- 1.0 $\frac{g}{L}$ nanofluid, as the high concentration one.

The experimental setup and the preparing procedure of the fluids is the same described above. The only thing which changes in the two fluids is the mean distance among nanoparticles which can be estimated considering, in first approximation, the theory of gases presented, for example, in [73].
Let us suppose that the nanoparticles distribution is uniform, as it should be thanks to the presence of the surfactants which prevents the agglomeration due to Wan der Waals forces; neglecting the electron dimensions (which are more than one order of magnitude lower than the nanoparticles dimensions), the mean free path among nanoparticles can be written as:

$$\lambda = \frac{1}{N\pi R^2} \tag{6.4}$$

where N represents the mean number of nanoparticles per unit volume and R their average radius. The nanoparticles density inside the fluid can be expressed in terms of the nanoparticles concentration c and their density ρ, thus obtaining the following expression for the mean free path λ:

$$\lambda = \frac{k}{c} \tag{6.5}$$

Sample	Mean free path among nanoparticles	[Unit]
$0.2\,\frac{g}{L}$	1040.0	$[nm]$
$1.0\,\frac{g}{L}$	210.0	$[nm]$

Table 6.1: Mean distance among nanoparticles inside the two investigated fluids.

where k is a constant which depends on the nanoparticles type and their concentration x inside the blending fluid:

$$k = \frac{\rho R}{750x} \tag{6.6}$$

Considering the macroscopic density of the magnetite ($5.2\,\frac{g}{cm^3}$), the ferrofluid concentration (50%) and the mean radius of the nanoparticles ($15\,nm$), it is possible to obtain the values of the mean free paths shown in table 6.1. Figure 6.9 compares the conduction currents for the two investigated fluids at three representative voltages.
For the lowest concentration, the recorded current at the lowest voltage shows the transient current before the steady state, but apart from a noisy behavior, no particular phenomena seem to take place. The subfigures at higher voltages are completely different because of the presence of slow current peaks of similar amplitude and time duration, as previously reported in figure 6.6. The peak amplitude is of about $10 - 15\,nA$, while the time duration is of about $30000\,s$. Excluding the current peaks, the current value is of the same order of magnitude in both cases (about $6 - 7\,nA$). The observed peaks disappear after one month of testing, when visual inspection revealed the separation between the host mineral oil and the nanoparticles and aggregation phenomena on both electrodes.
The figures relative to the highest concentration nanofluid do not show similar peaks, but present the same noisy behavior. The same aggregation phenomena interest this concentration, too. This apparent incongruity can be explained considering that different nanofluid concentrations mean different conduction mechanisms, as already pointed out in the previous chapters.
At low concentrations, nanoparticles act as trapping sites for charges, thus tending to reduce their apparent mobility. Charge is therefore likely to alter the injection mechanisms as explained before, when dealing with the Fowler-Nordheim plot of the $0.2\,\frac{g}{L}$ nanofluid. Higher concentrations force nanoparticles to be closer allowing the inception of faster charge transfer mechanisms involving nanoparticles themselves.
To understand the two different behavior, it is useful to consider the distribution of free paths between the nanoparticles. The theory of the random walk [74] indeed states that, in the case of uniformly distributed particles distribution, the path distribution λ between nanoparticles is of exponential type:

$$f(\lambda) = \frac{1}{\bar{\lambda}} e^{-\frac{\lambda}{\bar{\lambda}}} \tag{6.7}$$

where f indicates the probability density function and $\bar{\lambda}$ refers to the mean free path which has been calculated, in the case of our investigated concentrations, in table 6.1. Whatever the mean free path, the probability theory states that the probability to find a path which is smaller than $\bar{\lambda}$ is equal to $\int_0^{\bar{\lambda}} f(\lambda) d\lambda = 1 - \frac{1}{e}$.

This means that particles are very close in the case of the higher concentration nanofluid, allowing tunneling charge transfer to take place; in such case the homocharge effect due to the charge trapping phenomenon is not likely to take place, and charge does not affect the electric field distribution. This is in agreement with the results presented in figure 6.9, where no current peaks appear.
Trapping phenomena, as already stated before, are not likely to explain the nanoparticles aggregation close to the HV needle; it is possible they explain the aggregation at the lower voltage electrode (figure 6.7), but it is necessary to admit the existence of another force acting on nanoparticles to explain figure 6.8.
Let us analyze which forces act on the single nanoparticle inside the host fluid; they are summarized in figure 6.10.

As the picture says, the nanoparticle is supposed to be negatively charged, and so the coulombic force is the one explaining the aggregation on the lower

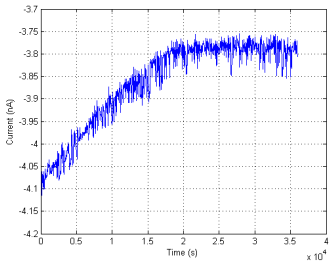

(a) *Applied voltage:* $4\,kV$ *(*$0.2\,\frac{g}{L}$*).*

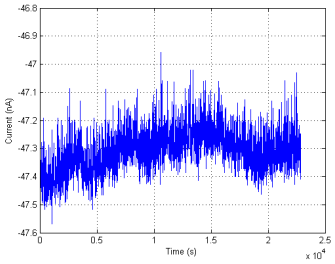

(b) *Applied voltage:* $4\,kV$ *(*$1.0\,\frac{g}{L}$*).*

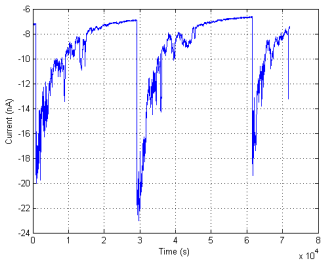

(c) *Applied voltage:* $8.5\,kV$ *(*$0.2\,\frac{g}{L}$*).*

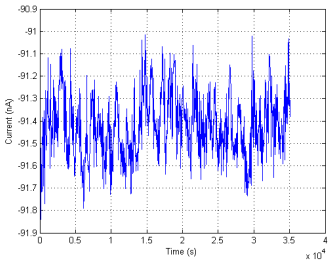

(d) *Applied voltage:* $8.5\,kV$ *(*$1.0\,\frac{g}{L}$*).*

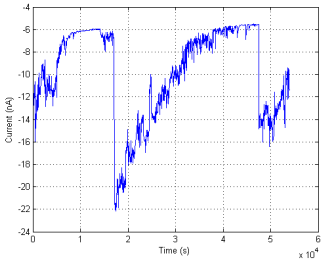

(e) *Applied voltage:* $11\,kV$ *(*$0.2\,\frac{g}{L}$*).*

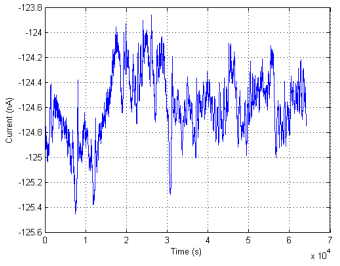

(f) *Applied voltage:* $11\,kV$ *(*$1.0\,\frac{g}{L}$*).*

Figure 6.9: Comparison of the recorded conduction currents of the two investigated fluids at three representative voltages.

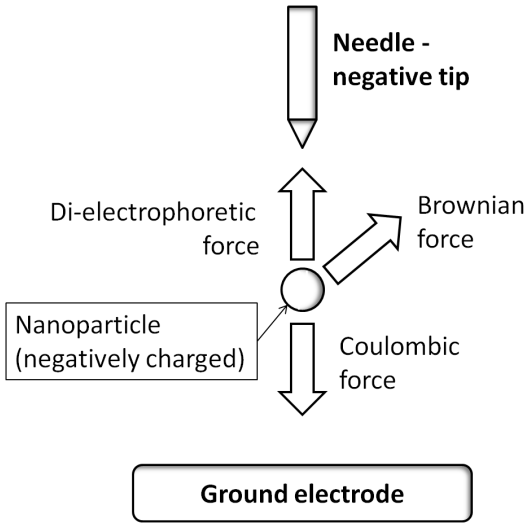

Figure 6.10: Schematic representation of the forces acting on the single nanoparticle inside the host fluid.

voltage electrode of figure 6.7. The Brownian force describes the interaction between nanoparticles and the structure of the host fluid and for this reason has a random orientation; it is then difficult to think that they are responsible of a net movement. When dealing with such interactions in simulations, the following expression is generally used to model it:

$$F_B = \zeta \sqrt{\frac{12\pi k_b \mu T R_p}{\Delta t}} \tag{6.8}$$

where ζ is a normally distributed parameter, k_b is the Boltzmann constant, μ is the dynamic viscosity of the fluid , T the absolute temperature of the fluid, R_p the mean radius of the nanoparticle and Δt is the simulation time step.
The di-electrophoretic force is connected to the permittivity mismatch between the nanoparticle and the host fluid and exists only when the electric field is not uniform [75]:

$$F_{DEP} = 2\pi R_p^3 \epsilon_0 \epsilon_f Re \left(\frac{\epsilon_p - \epsilon_f}{\epsilon_p + 2\epsilon_f} \right) \nabla^2 E \tag{6.9}$$

where ϵ_f is the relative permittivity of the host fluid and ϵ_p is the relative permittivity of the nanoparticles. It is clear by looking equation 6.9 that the di-electrophoretic force is present only when $\epsilon_p - \epsilon_f \neq 0$ and the field second derivatives are different from 0. As picture 6.10 reveals, di-electrophoretic forces are directed towards the HV electrode, thus justifying the agglomeration of nanoparticles there. Anyway, in order agglomeration to take place, it is necessary that the resultant of the forces close to the HV needle is upward directed, or, in other words, that di-electrophoretic forces are more intense than coulombic ones. Before continuing, for the sake of completeness, it is necessary to mention also a frictional force, which acts on nanoparticles when they start to move. The Stoke's law can be used to evaluate this force, because of the low

Parameter	Value	[Unit]
c_0	0.4	$[\frac{g}{L}]$
n	10	[-]
μ	5	[cSt]
ρ_p	5.5	$[\frac{g}{L}]$
R_p	10	[nm]
R_t	1	$[\mu m]$
R	1	[mm]
ϵ_f	2.2	[-]
ϵ_p	80	[-]
T	300	[K]

Table 6.2: Parameters used in the Comsol simulation for the study of the nanoparticles behavior.

Reynolds numbers:

$$F_v = -\frac{18\mu}{\rho_p D_p^2} v^2 \tag{6.10}$$

where ρ_p refers to the particles density, $D_p = 2R_p$ is their diameter and v their speed. Viscous forces will be neglected in the following, but their effect is a slowing down of the macroscopic shifts.
A key point is now to understand whether di-electrophoretic forces are higher than coulombic ones close to the HV needle. This is the necessary condition for the agglomeration to take place. We will do it with a finite element simulation and by using the expressions we have presented above with some simplistic assumptions to estimate the electric field.
Simulations have been performed using Comsol simulation toolkit, and considering the following model:

$$\begin{cases} \nabla \cdot (-\epsilon \nabla V) = \rho \\ \sum_i F_{j,i} = \frac{d(m_p v_j)}{dt} \quad j = 1...N \end{cases} \tag{6.11}$$

where N is equal to the number of nanoparticles, v_j is the velocity of the $j-th$ particle, m_p its mass and the sum operator refers to all the forces which have been mentioned before; it is then evident from the set of equations 6.11 that the general approach consists in the consideration of the single particle behavior.
The above introduced model requires the knowledge of the charge the nanoparticles trap on their surfaces, which can be determined considering the charge dynamics after the injection from the needle. For the sake of simplicity, considering that the trap equations are nonlinear and the time constant of the charging transient is very small [31], the charge dynamics is neglected and the trapped charge is supposed to be the same for all the nanoparticles. In particular, we have supposed that the number of stored electrons on each nanoparticle is 10, which is a reasonable number considering the considerations presented in [31].
Table 6.2 summarizes all the parameters which are of interest for the above mentioned simulation, in particular:

- c_0 represents the nanofluid concentration;

- n is the number of electrons which have been stored on the nanoparticles surfaces;
- μ represents the kinematic viscosity of the base fluid, and it has been chosen close to that of naphtenic mineral oils [4];
- ρ_p is the mean density of the nanoparticles;
- R_p, R_t and R represent, respectively, the mean radius of nanoparticles, of the needle tip and the gap distance.

Preliminary simulations revealed that, changing the applied voltage, different phenomena were likely to happen:

1. Starting from $0\,kV$ to a voltage level which was approximately $-2\,kV$, Brownian forces were the dominating ones, for simulation times of the order of tens of hours;
2. A further raise in the applied voltage caused the increase of both the dielectrophoretic force and the electrical one, resulting in a change of the nanoparticles distribution.

In order to show the results of such simulations and highlight the nanoparticles movement, we present the time variation of the nanoparticles distribution density, considering different values of applied voltage. Figure 6.11 shows two time varying distributions revealing the nanoparticles behavior. In particular, the x-axis represents the distance from the center of the high voltage electrode, while the y-axis is the nanoparticles distribution density between the HV electrode and the corresponding value on the x-axis; the time axis is indicated by the color. In the case of low applied voltage, it is quite clear that no global charge shifts toward the HV electrode are likely to happen. The proof of such statement is the absence of a significant time variation of the number of nanoparticles at a certain x value; a noisy trend appears in the case of a large number of simulated nanoparticles because of the Brownian forces which have a random distribution. Differently, if the applied voltage is $-2\,kV$ there is a clear time effect on the nanoparticles distribution, revealing that coulombic and di-electrophoretic forces are not compensating. More in detail, it seems that there are two global movements:

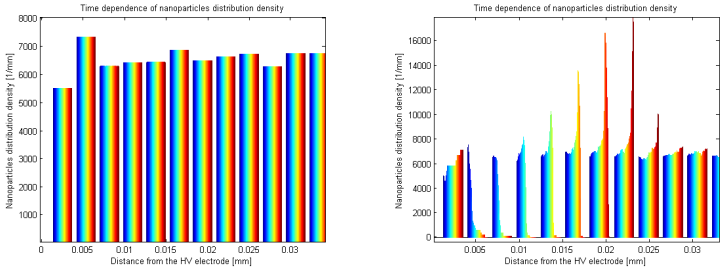

(a) $V = -0.2\,kV$. (b) $V = -2\,kV$.

Figure 6.11: Comparison between different Comsol simulations. The time color axis ranges from $1\,s$ (dark blue) to $30\,min$ (red)).

1. The first one, which is driven by the di-electrophoretic forces, towards the HV electrode;

2. A second one, towards the LV electrode, which can be driven only by the electric field and which takes place far from the needle.

The obvious result of such a combination is that, even if the average concentration is always the same (c_0), because the number of nanoparticles inside the fluid does not change, there are regions in which the concentration is higher and a central region in which it is lower.
The above discussed method, although it contains a simplification in the number of trapped electrons, is able to depict the time scale which is needed to activate the nanofluid instability, i.e. some days, but it does not allow us to catch all the parameters having influence on the investigated phenomenon. From the above introduced simulation result, it is not clear if the predominance of the di-electrophoretic force upon the coulombic one is geometry dependent or not and if some other parameters are likely to interfere with this phenomenon. A simple analytical model is therefore presented in the following sections aiming to give an answer to all these questions.

6.1 Simplified Model

In Chapter 3, we have already shown the way to evaluate the electric field distribution assuming that the needle to plane geometry can be represented by two concentric spheres[1]. The nanoparticles concentration will obviously be time and position dependent, because of the action of the di-electrophoretic and coulombic forces, so we can state that $c = c(r,t)$. It is possible to express the concentration in the following way:

$$c(r,t) = c_0 + \Delta c(r,t) \tag{6.12}$$

where c_0 is the "'nominal"' particles concentration; simple considerations allow us to state that $\Delta_c(r,t)$ has a mean value equal to 0:

$$\frac{1}{V}\int_{R_t}^{R} c(r,t)r^2 dr = c_0 = c_0 + \frac{1}{V}\int_{R_t}^{R} \Delta c(r,t)r^2 dr \tag{6.13}$$

where V represents here the volume and not the applied voltage, which will indicated in the following with the symbol V_0. For small time instants, it is possible to suppose that $|\Delta c(r,t)| \ll c_0$, which obviously fails at longer times because otherwise it will contrast with the observation that nanoparticles can aggregate.
Equation 3.5 showed that:

$$E(r) = \frac{V_0 R_t}{r^2} \tag{6.14}$$

supposing that $R \gg R_t$. Knowing the electric field distribution, we are able to give the expression of all the forces acting on the nanoparticles at the time

[1] This hypothesis leads to an overestimation of the field, but in Chapter 3 we have determined the scale factor to consider the same electric field close to the HV region.

(t=0) the voltage is applied, which will cause their movement and the consequent concentration variation. The equation which can allow us to analyze the nanoparticles concentration is the well-known continuity equation:

$$\frac{\partial c}{\partial t} + \nabla \cdot j = 0 \tag{6.15}$$

where c is the nanoparticles concentration and j represents the nanoparticles concentration flux. Considering the spherical simmetry of the problem, equation 6.15 can be simplified as follows:

$$\frac{\partial c}{\partial t} + \frac{1}{r^2}\frac{\partial (r^2 j_r)}{\partial r} = 0 \tag{6.16}$$

where j_r represents the radial component of the flux. In order to solve equation 6.16, it is necessary to express j_r, which, for the sake of simplicity, depends on:

- a di-electrophoretic term, $j_{diel} = -\mu_{np} c F_D$, where μ_{np} is the nanoparticle mechanical mobility;
- an electric term, $j_{el} = \mu_{np} cenE$, where n is the number of stored electrons on the nanoparticle surface and e is the elementary charge;
- a diffusive term, which takes into account the nanoparticle motion due to diffusion, $j_{diff} = -\mu_{np} k_b T \frac{\partial c}{\partial r}$, where k_b is the Boltzmann constant.

For the sake of simplicity, we decided to neglect the following terms:

1. Gravitational and Brownian forces: we suppose that they are of lesser importance;
2. Drag forces, because, as we have already anticipated in the previous section, their effect is only a delay of the results.

The problem described by equations 6.14 and 6.16 is not physically true, because of several simplifications:

- some forces have been neglected, but this is a minor issue;
- the electric field is considered to be non influenced by the nanoparticles movement. The latter results in a change of concentration, as described in equation 6.12, which, in turn, has an influence on the relative permittivity of the fluid. Generally speaking, the following relation holds:

  $$\epsilon = \epsilon(c) = \epsilon(r, t) \tag{6.17}$$

  which told us that the electric field is a time dependent variable, which is determined by solving the Poisson equation:

  $$\nabla \cdot (-\epsilon(c) \nabla V) = \rho \tag{6.18}$$

  where ϵ cannot be simplified because of its dependence on the radial coordinate and ρ represents the injected charge which is then stored on the nanoparticles surfaces: this charge can indeed have an influence on the electric field.

The complete set of equation of the "'rigorous"' solution should be, finally:

$$\begin{cases} \nabla \cdot (-\epsilon(c)\nabla V) = \rho \\ \frac{\partial c}{\partial t} + \nabla \cdot j = 0 \\ F(\rho, c, V) = 0 \end{cases} \tag{6.19}$$

where the last equation allows to determine the charge distribution according to the nanoparticles re-distribution. A possible equation to be used is the one presented in the previous chapter, i.e. equation 3.27.
For the moment, let us consider the simplified problem consisting in the single equation 6.16, assuming constant field and stored charge. Considering the terms which define the radial component of the nanoparticles flux j_r, equation 6.16, can be written as:

$$\frac{\partial c}{\partial t} - k_3 \frac{\partial^2 c}{\partial r^2} + \frac{\partial c}{\partial r}\left(-\frac{2k_3}{r} + \frac{k_2}{r^2} - \frac{k_1}{r^5}\right) + \frac{3k_1 c}{r^6} = 0 \tag{6.20}$$

where the parameters k_1, k_2 and k_3 are defined as follows:

$$k_1 = 8\mu_{np}\pi R_p^3 \epsilon_0 \epsilon_f \frac{\epsilon_p - \epsilon_f}{\epsilon_p + 2\epsilon_f} V_0^2 R_t^2 \tag{6.21}$$

$$k_2 = n\mu_{np} V e R_t \tag{6.22}$$

$$k_3 = \mu_{np} k_b T \tag{6.23}$$

Equation 6.20 has to be defined within a radial coordinate range, which is $[R_t, R]$, while the time interval ranges from $0\,s$ to t_0, which is a positive, finite time instant. Since the domain where equation 6.20 is defined is not R^2, we need to define some boundary conditions, which are of the following type:

$$c(r, 0) = c_0 \tag{6.24}$$

$$j_r(R, t) = 0 \tag{6.25}$$

$$\frac{1}{V}\int_{R_t}^{R} c(r, t) 4\pi r^2 dr = c_0 \tag{6.26}$$

where (6.24) represents the initial solution, (6.25) indicates that there is no particles flux outside the domain and the last condition ((6.26)) is an equivalent way to state that the particles number is a constant quantity. From a mathematical point of view, the two boundary conditions (6.25) and (6.26) define a mixed Neumann-Dirichlet problem.
For the sake of simplicity, without loosing generality, we have preferred to solve an equivalent problem, with easier Dirichlet boundary conditions:

$$c(r, 0) = c_0 \tag{6.27}$$

$$c(R, t) = c_0 \tag{6.28}$$

$$\frac{1}{V}\int_{R_t}^{R} c(r, t) 4\pi r^2 dr = c_0 \tag{6.29}$$

i.e., we have transformed (6.25) in a Dirichlet boundary condition. Figure 6.8 shows that this condition is not definitely true, because we have observed aggregation on the LV electrode, where $r = R$. Since we have empirically observed

Parameter	Value	[Unit]
c_0	0.4	$[\frac{g}{L}]$
n	10	[-]
μ_{np}	10^7	$[\frac{m^2}{Js}]$
R_p	10	[nm]
R_t	1	$[\mu m]$
R	1	[mm]
ϵ_f	2.2	[-]
ϵ_p	80	[-]
T	300	[K]

Table 6.3: Parameters used in the Matlab simulation for the study of the nanoparticles behavior.

that aggregation on the ground electrode occurs at times much longer than aggregation on the needle tip, we solve the model for a time window in which the concentration on the LV electrode can be considered fixed, i.e. t_0 has been chosen in the order of seconds. The defined problem is then a linear problem with non-constant coefficients, which has been solved with a Crank-Nicolson scheme [76], which has been proposed to solve parabolic equations of the following type:

$$\frac{\partial f}{\partial t} = m_1 \frac{\partial^2 f}{\partial r^2} + m_2 \frac{\partial f}{\partial r} + m_3 f \tag{6.30}$$

After meshing the radial domain in N points, the second member of equation 6.30 has to be discretized and evaluated in a precise time instant. In fact:

$$\frac{f_i^{(t+1)} - f_i^t}{\Delta t} = F(f_{i+1}, f_i, \Delta r, t_?) \tag{6.31}$$

where the $t_?$ on the second member means that the function F can be computed in every time instant between t_i and t_{i+1}. Crank-Nicolson solution scheme can be obtained by computing F in the time instant $t + \frac{1}{2}$, using the following linear interpolation:

$$F(f_{i+1}, f_i, \Delta r, t + \frac{1}{2}) = \frac{F(f_{i+1}, f_i, \Delta r, t) + F(f_{i+1}, f_i, \Delta r, t+1)}{2} \tag{6.32}$$

Simulation parameters have been chosen according to the FEM analysis performed in the previous section and summarized in table 6.3.
By varying the three parameters k_1, k_2 and k_3, the ratio between the considered forces (and then the resulting macroscopic phenomenon) changes. In particular, once fixed the geometrical parameters and simply varying the voltage values, we obtain the two different set of trends shown in fig. 6.12, where each line represents the radial dependence of the concentration at one time instant and shows a double tendency. Fig. 6.12 (b) refers to $V_0 = -2\,kV$ and reveals that the particles which are closest to the high voltage needle move upward (i.e. the di-electrophoretic force is upward directed). A region with a low concentration of nanoparticles grows up, forcing a diffusion controlled movement. Far from the needle, where the di-electrophoretic force is negligible, the electric one

should prevail. However, at short times such effect is not visible, because far from the needle the electric field tends to 0, thus requiring major times for the nanoparticles to shift.
A simple reduction of the applied voltage can cause a completely different scenario. Figure 6.12 (a) shows indeed that, in the case of $-200\,V$ as theoretical applied voltage, the nanoparticles concentration is completely different from the previous picture. In this case, because of the reduced voltage level, the di-electrophoretic forces do not prevail upon the electric ones and thus the nanoparticles movement is downward directed.
Apart from the discussion and interpretation of the results of the model, which again are obtained for different particular configurations, the different behavior of nanoparticle concentration can be easily predicted with a simple observation. Under the assumptions of this model, the aggregation phenomenon at the high voltage needle takes place if the following condition holds:

$$F_D > enE \tag{6.33}$$

where F_D represents the di-electrophoretic force. If we substitute the expressions of the di-electrophoretic force and the electric field in inequality 6.33, we obtain the following condition for the di-electrophoretic force to prevail:

$$r < \sqrt[3]{\frac{8\pi R_p^3 \epsilon_0 \epsilon_f (\epsilon_p - \epsilon_f) V_0 R_t}{(\epsilon_p + 2\epsilon_f) en}} = r_{critic} \tag{6.34}$$

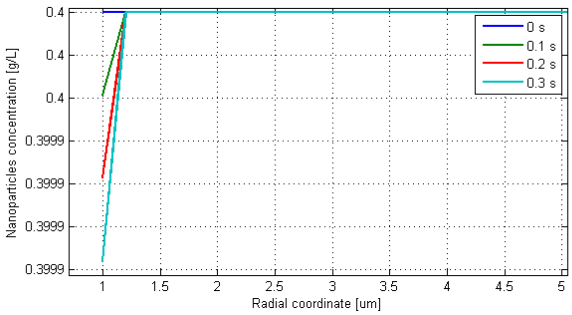

(a) $V = -0.2\,kV$.

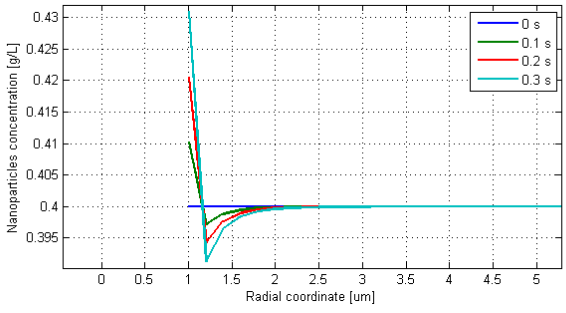

(b) $V = -2\,kV$.

Figure 6.12: Comparison between different Matlab simulations. Each line represents the nanoparticles concentration distribution at different time instants.

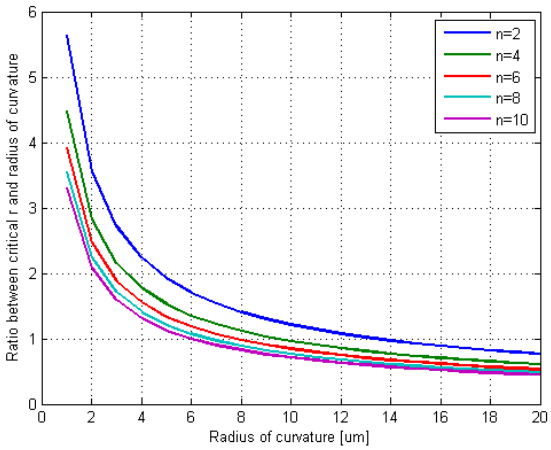

Figure 6.13: Ratio between r_{critic} and R_t vs R_t (parameters of table 6.3).

The r_{critic} value, defined in equation 6.34, represents the radial coordinate below which the di-electrophoretic force prevails over the electric one and is dependent, among the other factors, on the tip radius R_t. Obviously, in order to have a real aggregation phenomenon, equation 6.34 has to be coupled with the following relation:

$$r_{critic} > R_t \tag{6.35}$$

Even if expression 6.34 has been obtained by neglecting some important contributions and by making some simplifying assumptions, it can help us to explain why in our experiments the same voltage level sometimes allowed aggregation to occur and why in other cases not. Applying the same voltage level to tips which have a random distribution of the radius of curvature, it is possible that in some cases r_{critic} is higher than R_t and in other cases it is lower, i.e. r_{critic} has a random behavior as the parameter from which it depends.
Figure 6.13 shows, for different values of the parameter n, the dependence of r_{critic} upon the needle tip radius; in particular it is interesting to notice that, although r_{critic} increases with R_t, after a certain point it becomes lower than it. This confirms that di-electrophoretic contribution can be appreciated only in the case of very sharp needle electrodes. The simplified model we have discussed is then able to predict the particle agglomeration which takes place at negative DC voltage, i.e. when electron injection takes place.
The aggregation phenomenon has been outlined even in the case of DC positive applied voltage; in that case, anyway, no nanoparticles aggregation has been seen on the ground electrode. If we think to the forces represented in fig. 6.10, we can easily make some considerations:

- the coulombic force acts on the nanoparticles because they are electrically charged, because of the charge injection phenomenon;
- under DC negative applied voltage, electrons are really injected from the HV needle and charge nanoparticles;
- under DC positive applied voltage, we may assume that positive holes are

injected from the HV tip, but actually electrons are extracted from the insulation gap.

The last consideration allows us to neglect the coulombic effect, which is responsible of the aggregation of the LV side, while the di-electrophoretic term cannot be neglected, because it is linked to the permittivity mismatch and the non-uniformity of the electric field but not to the field polarity. An obvious consequence of these phenomena is that the aggregation on the HV needle is faster than the case of negative polarity, where the coulombic forces slow it down; this result seems to have a correspondence with the physical reality.
A question which is not easy to answer is what can happen if the applied voltage is time dependent, in particular sinusoidal. A first answer, which is influenced by the fact that under AC space charge is not problem, is that nothing happens because there is no net space charge injection and this answer seems to be in agreement with the experimental results which showed no particles agglomeration at $V_0 = 7\,kV_{rms}$. Under DC, we have found that $V_0 = 8.5 - 9\,kV$ is the minimum voltage required for the aggregation to take place; remembering the considerations made in the previous chapters (see in particular equation 3.11), the equivalent voltage to be used in the model is $V_0 = 2\,kV$, as considered in our simulations. The selected AC voltage has been chosen in order to consider the same applied peak value, because the same square root value would have triggered partial discharges, as shown in chapter 4.
A more careful analysis of the problem shows that, even under AC applied voltage, di-electrophoretic forces have a mean value different from 0, as the following Fourier decomposition reveals:

$$F_D \propto V(t)^2 = V_0^2 sin^2(\omega t) = \frac{V_0^2}{2} - V_0^2 cos(2\omega t) \tag{6.36}$$

ans thus, after considering the average operator:

$$\langle F_D \rangle \propto \frac{V_0^2}{2} = V_{rms}^2 \tag{6.37}$$

It is then clearer from this equation why we have not observed any aggregation phenomenon under AC:

- both coulombic and di-electrophoretic forces have a pulsating behavior, but di-electroforetic forces have an average values which is different from 0 and is proportional to the square of the root mean square of the applied voltage;
- in order for aggregation to occur, it is necessary that the di-electrophoretic force overcomes a certain value, and this happens when DC voltage is above $8.5\,kV$. Equation 6.37 shows that, under AC, the inception voltage for aggregation is $8.5\,kV_{rms}$, i.e. far above what we have used for our experiments.

One of the weakest points of the presented model is the constancy of the parameter n, i.e. the number of electrons on the nanoparticles surfaces, on the whole domain. This hypothesis leads to an error in the estimate of the nanoparticles distribution, especially in the region where the electric forces prevail over the di-electrophoretic ones. In this region indeed, one should expect an increase of

the nanoparticles concentration compared to the nominal value, but this is not visible by looking at fig. 6.12. By analyzing the values of the concentration more in details, it is possible to conclude that the described behavior takes place, but it is not visible because it is distributed in the whole region where $r > r_{critic}$. It is more reasonable instead to suppose that the nanoparticles concentration increases only in a region close to r_{critic}, at least for time instants which are in the order of seconds. Obviously, if we consider a non-uniform charge distribution on the nanoparticles, the model can become too complicated. Thus, in the next section we would like to understand if a more complex model leads to a significant change of the results.

6.2 Improved model

Before starting to improve the previous model, few words have to be spent about the nature of the parameter n. As already said, it is a consequence of the charge injection taking place from the HV electrode and the nanoparticles trapping behavior. This charge trapping tendency is able to reduce the electric field at the needle tip, inhibiting the injection itself. We assume then that the charge injection process is a pulse like mechanism, i.e. each time it consists in a pulse of magnitude Q_{tot}. The time between two consecutive injection pulses is the time needed to deplete the region close to the HV needle. For the following simulations, we assume $Q_{tot} = 1\,pC$ as the PD injected charge was found to be at least one order of magnitude higher [77]. Lower charge values can obviously be injected too, but as the nanoparticles movement driving force is represented by the charge, $Q_{tot} = 1\,pC$ represents the worst case. In chapter 3 we have presented a simple model to estimate the charge distribution on the nanoparticles at the end of the charging transient, starting from the expression found by Sullivan in [31]:

$$Q_s = -12\pi\epsilon R_p^2 E_0 \tag{6.38}$$

where Q_s indicated the global charge accumulating on the single nanoparticle. The result of the investigation presented in chapter 3 led us to the formulation of equation 3.27, which is represented in figure 6.14 in the case of $Q_{tot} = 1\,pC$. The result of equation 3.27, shown in figure 6.14, will be used in the following in place of the uniform constant parameter n; this will produce a more reliable simulation result, even if it will be considered, as done before, a constant term. Since the number of stored electrons is now a variable, we need to slightly modify equation 6.20 to take this effect into account; the final equation to be solved is the following one:

$$\frac{\partial c}{\partial t} - k_3\frac{\partial^2 c}{\partial r^2} + \frac{\partial c}{\partial r}\left(-\frac{2k_3}{r} + \frac{k_2}{r^2} - \frac{k_1}{r^5}\right) + c\left(\frac{3k_1}{r^6} + \frac{k_2}{nr^2}\frac{\partial n}{\partial r}\right) = 0 \tag{6.39}$$

where k_1, k_2 and k_3 have the same definition of the previous case.
In order to obtain a more refined solution close to the needle, where the solution is expected to change with the fastest rate, we have decided to solve equation 6.39 with a Galerkin finite element method with initial and boundary conditions expressed in (6.27), (6.28), (6.29) and thus using a non uniform mesh. Using the same parameters of table 6.3, and choosing for Q_{tot} a value of $1\,pC$, we have obtained the results shown in figure 6.15, where we have considered different

voltage levels. Like the profiles which have been shown in the previous section, the voltage effect is still evident here and no upward movement is observed at the lowest voltage level. Moreover, as we expected from the nanoparticles conservation, the reduction of the concentration close to the needle is compensated

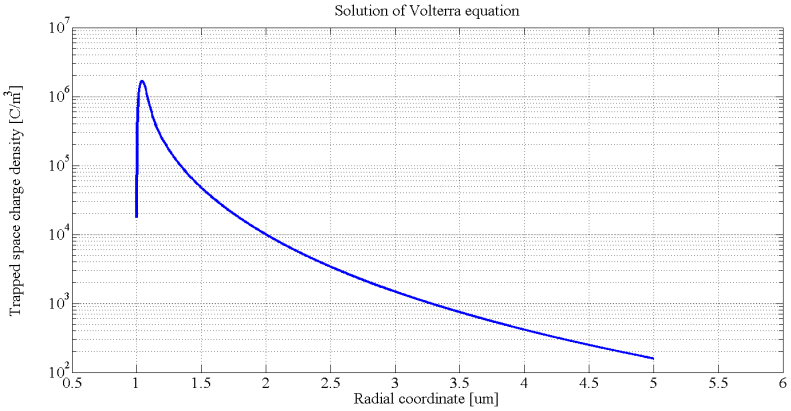

Figure 6.14: Charge distribution after injection from the HV needle ($Q_{tot} = 1\,pC$).

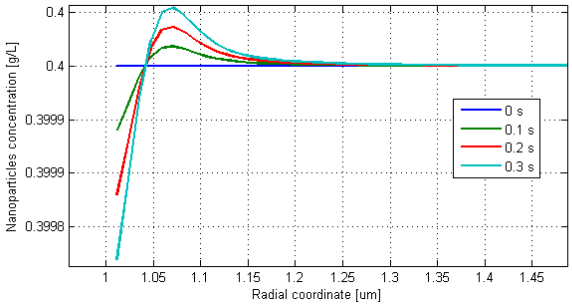

(a) $V = -0.2\,kV$.

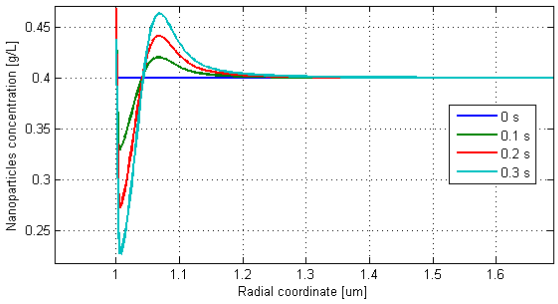

(b) $V = -2\,kV$.

Figure 6.15: Comparison between different Matlab simulations. Each line represents the nanoparticles concentration distribution at different time instants. The results have been obtained using the improved model.

by an increase immediately after. A more reasonable nanoparticles distribution is obtained even in figure 6.15-b, where the effect of the coulombic forces is likely to be evident. Unfortunately, no time effect is present, because we do not update the $n(r)$ variable at each simulation step, reducing in this way the maximum time instant t_0 at which we have to stop the simulation. As we are not able to obtain an easy analytical expression for the charge density ρ and thus for the number of charge carriers stored on the nanoparticles surfaces, $n(r)$, for this case we cannot find a criterion able to understand when the di-electrophoretic forces are stronger than the electrical ones, but from the simulations we have found that, for the particular investigated geometry, the critical voltage is of the same order of magnitude as the one found with the simplified model. Since the results of this model are quite in agreement with the ones obtained with the simpler one, the higher complexity does not justify its use.
The output of the presented models highlight the weakness of nanofluids towards charge injection. First experimental evidence has shown that the tunneling regime is somehow shifted towards higher voltages compared to the typical ones found for mineral oil, but the stability when it is triggered is evidently lower. This has been demonstrated and verified for DC applied voltages of both polarity, and only demonstrated for AC voltages and does not depend upon the nanofluid concentration. It is true indeed that higher concentration nanofluids do not suffer of the problem of charge trapping, but we have demonstrated that the non stable phenomenon which has been investigated in this chapter is connected only to the presence of nanoparticles and the degree of non uniformity of the electrical field. Higher concentration nanofluid, not presenting the coulombic repulsion effect, are likely to behave worse than lower concentration fluids, confirming that the latter are the only ones which could be used for insulating purposes.

Chapter 7

Dielectric properties of mineral oil-based nanofluids

Abstract

We have said in previous chapters that the positive results obtained for nanofluids could be due to either the effect nanoparticles may have on the electric field or other mechanisms like charge trapping or transport. In this chapter we explore the dielectric and conduction properties of nanofluids trying to understand more deeply their interactions with the base mineral oil.

7.1 Nanofluid electrical permittivity

In chapter 5, we have presented different models which could evaluate the electric field inside a nanofluid considering different aspects which determined a higher (or lower) analytical complexity of the final derived formulas. Looking at all of them, it is evident how the nanoparticles electrical permittivity plays a key role, influencing the electrical permittivity of the whole nanofluid.
Different models to predict the permittivity have been proposed recently ([48]-[49]), but none of them considered the "'interphase"' role or, in equivalent terms, the gradual charge of permittivity moving from the nanoparticle, ϵ_p, to the host fluid, ϵ_f[1].
For this reason, and to better understand the microscopic interaction between nanoparticles and host fluids, we have devoted our attention to the dielectric properties of nanofluids.
At the beginning of our considerations, we re-call the first results obtained in

[1]To be precise, the "'interphase"' region existence has been postulated for solid nanocomposites. We assume therefore that such a region exist for nanofluids, too.

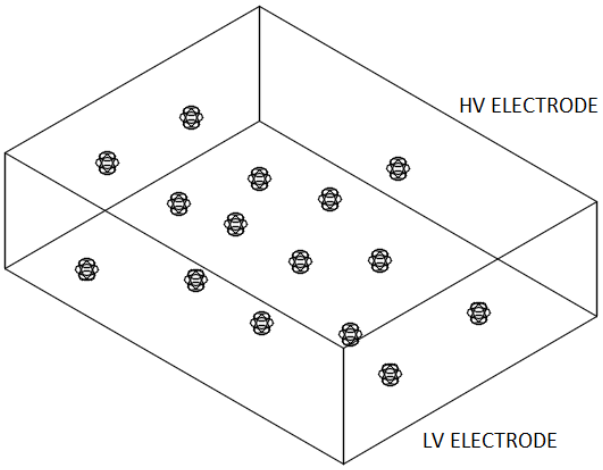

Figure 7.1: Plane-plane configuration of a nanofluid: the dots represent the nanoparticles.

chapter 5, for a general $3-D$ plane-plane electrode configuration scenario:

$$E_1 = \frac{V}{d} \tag{7.1}$$

$$E_4 = \frac{d_3 + R}{R + d_3 \frac{\sigma_4}{\sigma_3}} E_1 \tag{7.2}$$

$$E_3 = \frac{\sigma_4}{\sigma_3} E_4 sin(\theta) \tag{7.3}$$

where E_1 represents the background field, E_4 the field inside the nanoparticle and E_3 the "'connecting"' field around the nanoparticle (refer to figure 5.1 for a better understanding). The above equations depend on the parameter d_3, which has been defined equal to $\frac{R}{2}$ (the nanoparticle radius), for the sake of simplicity and according to a FEM simulation.
The electrical permittivity, as remarked in [4], does depend only on the material and not on the geometry which is used to its estimation; such statement allows then the use of a simple plane to plane configuration for our following purposes. The latter configuration does not ignite any di-electrophoretic phenomenon, either. Figure 7.1 represents the situation we would like to use for our simplified permittivity model. We suppose to apply a voltage value V_0between two parallel surfaces of the external parallelepiped representing the cell where the nanofluid is placed, and we write a simple energy balance, i.e.:

$$\frac{1}{2} C V_0^2 = \iiint_V \frac{1}{2} \epsilon E^2 dV \tag{7.4}$$

where the first term represents the electrostatic energy stored by the global capacitor of capacitance C, while the second term represents the sum of the energies of the subsystems composing the capacitor. The system represented in figure 7.1 is indeed composed of three different sub-components:

- host mineral oil, far from the nanoparticles;

- mineral oil, around the nanoparticles;
- nanoparticles.

Each of these sub-components is exposed to a different field value, when the voltage value V_0 is applied:

1. E_1 is the field which is applied to the host mineral oil;
2. E_4 is the field inside the single nanoparticle;
3. E_3 is the field in the region around nanoparticles of thickness $d_3 = \frac{R}{2}$.

Each sub-component is characterized even by a different electrical permittivity, which is obvious for the host mineral oil and the single nanoparticle, but it is less obvious for the remaining region, where we suppose that the permittivity is the average between that of mineral oil and that of moisture/nanoparticle (they are similar):

$$\epsilon_{f\,around} = \frac{\epsilon_f + \epsilon_p}{2} \tag{7.5}$$

For the sake of clarity, the field equations presented in chapter 5 have been determined supposing that $\epsilon_{f_{around}} = \epsilon_f$ (at least in the first part of the chapter). In this chapter, we have decided to use those simple field equations, but supposing that the permittivity does not change abruptly from nanoparticles to the host mineral oil; in the following, we will try to give the general correct model, showing that the complexity it adds is not required because of the slight change of the permittivity it produces.
The additive property of integrals allows us to make the following simplification:

$$\iiint_V \frac{1}{2}\epsilon E^2 dV = \iiint_{V_{oil}} \frac{1}{2}\epsilon_f E_1^2 dV + \iiint_{V_{np}} \frac{1}{2}\epsilon_p E_4^2 dV + \iiint_{V_{oil\,around}} \frac{1}{2}\epsilon_{f\,around} E_3^2 dV \tag{7.6}$$

while the first term of equation 7.4 can be writted as:

$$\frac{1}{2}CV_0^2 = \frac{1}{2}\epsilon_{nanofluid}\frac{S}{d}V_0^2 \tag{7.7}$$

because, in the plane-plane configuration, $C = \frac{S\epsilon}{d}$, where S represents the electrode surface and d the thickness.
If we use the expressions of the field which have been re-called before and calculate the three integrals of equation 7.6, the energy balance 7.4 allows us to determine an expression for the relative permittivity of a nanofluid[2]:

$$\epsilon_{nf} = \frac{d}{S}\left\{\epsilon_p \frac{c}{\rho_p}\frac{9\epsilon_{oil}^2}{d^2(2\epsilon_{oil}+\epsilon_p)^2} + \epsilon_{oil}\frac{1}{d^2}\left(Sd - \frac{27c}{8\rho_p}\right) + \epsilon_{int}\frac{9\epsilon_p^2 N_p R_p^3}{d^2(2\epsilon_{oil}+\epsilon_p)^2}\frac{19\pi^2}{24}\right\} \tag{7.8}$$

where ϵ_{int} represents the permittivity which we have derived by equation 7.5 and N_p is the number of nanoparticles inside the volume $V = Sd$. By making simple considerations, it is possible to find the following relation:

$$N_p = \frac{3cSd}{4\pi R_p^3 \rho_p} \tag{7.9}$$

[2]The presented formula is valid for every insulating system in which there is an addition of spherical particles.

Material	Permittivity
Mineral Oil	2.2
Moisture	81.0
Nanoparticles	80.0

Table 7.1: Relative permittivities far from the frequency interval where space charge phenomena are likely to take place (data taken from [31].

Formula 7.8 is obviously valid in the frequency interval far from that in which space charge phenomena are likely to take place, i.e., when the basic permittivities are defined by table 7.1.

Equation 7.8 has been represented, for different nanofluid concentrations, in figure 7.2. The model which has been developed clearly shows that the permittivity increase due to the presence of nanoparticles is not very high even in the case of high permittivity nanoparticles, like magnetite particles. In [49], the authors underline that, in the case of nanoparticles, the simple Maxwell composition rule is not sufficient to justify the small increase of permittivity; in our case, we have supposed that the moisture trapping behavior of nanoparticles and the inter-phase existence can be enough to explain the permittivity mismatch between the experimental value and the Maxwell predicted value.
It is then necessary to perform some experimental measurements to verify if our hypothesis is correct or not.
Mineral oil and mineral oil-based nanofluids have been prepared in the same way as already described in previous chapters and tested with a Alpha Beta Novocontrol Dielectric Analyzer. In order to measure the dielectric properties of the fluids, an ad-hoc cell has been built according to the $IEC\,60247:2004$ standard, and which is represented in figure 7.3. As it is possible to see from this picture, it is a vertical cylindrical capacitor with some devices aimed at reducing the stray effects and ensure that the measured capacitance is equal to the one defined by the theory:

$$C = \frac{2\pi\epsilon_0\epsilon_r L}{log\left(\frac{R_2}{R_1}\right)} \tag{7.10}$$

where L is the length of the active part of the cell, R_2 is the external radius and R_1 the internal one. The Alpha Beta Analyzer, after applying $3\,V_{rms}$ to the cell, performs a frequency span between two selected frequencies, which in

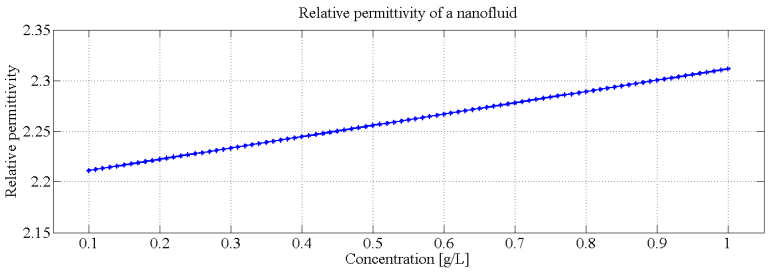

Figure 7.2: Relative permittivity from the model of equation 7.8.

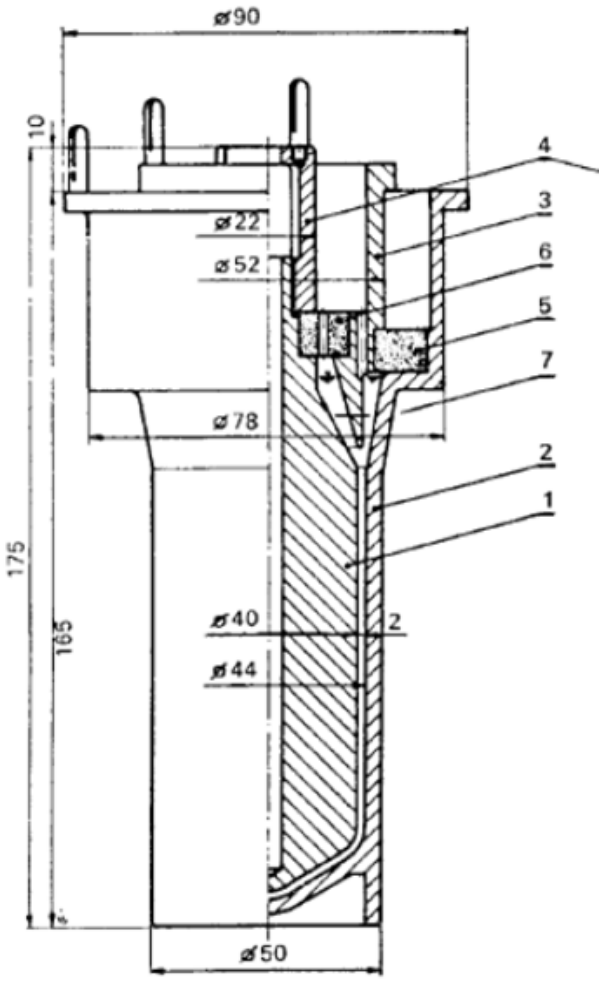

Figure 7.3: Schematic representation of the used cell

our case have been $1\,mHz$ and $100\,kHz$, measuring the impedance between its two terminals, i.e. the quantity $Z_p = \frac{1}{\omega C}$. Knowing at this point the geometrical capacitance of the cell, C_0, it is possible to derive the real and imaginary parts of the relative permittivity vs the frequency. An example of the above mentioned trends for mineral oil are presented in figure 7.4, which refers to a generic frequency span performed at 40 degrees.

Such acquisition shows that minearal oil relative permittivity is quite constant in a wide frequency range, apart from low values, as already known in literature because of space charge related phenomena [4]. These phenomena are likely to create electrical layers in the proximity of the electrodes and thus have the ultimate effect to increase the relative permittivity; in the following, we will not focus on such frequency spectrum, because we have not the possibility to further investigate on such space charge phenomena.

Mineral oil relative permittivity usually ranges between 2.1 and 2.5, depending

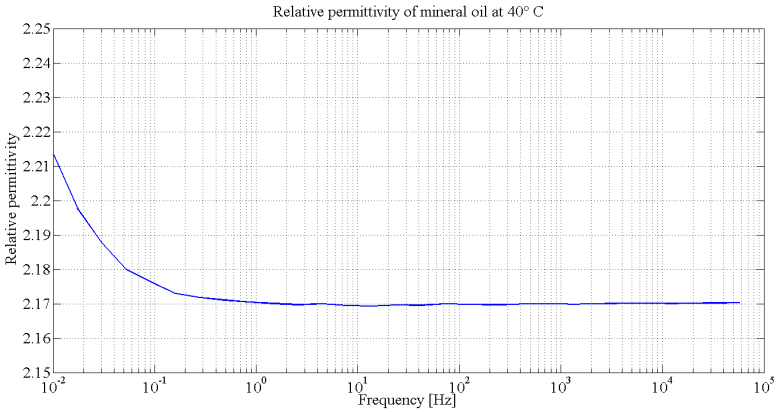

(a) *Real part of the permittivity.*

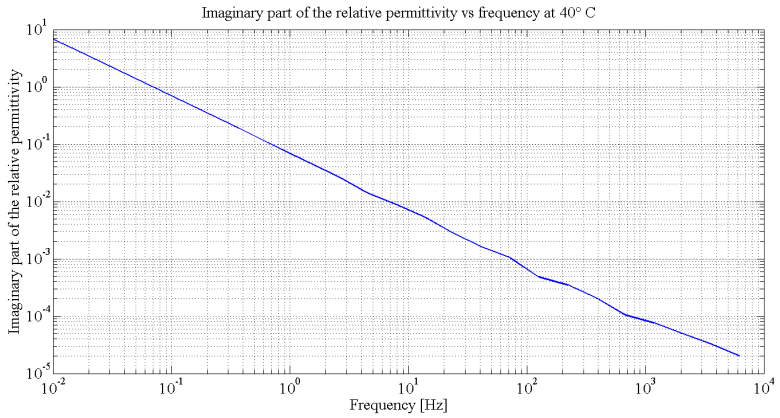

(b) *Imaginary part of the permittivity.*

Figure 7.4: Example of a capacitance acquisitions vs frequency performed with the Alpha Beta Analyzer: real and imaginary part of the relative permittivity. Measurements performed at 40 degrees.

on several factors, such as the aromatic content or antioxidant additives [4]; our mineral oil shows a permittivity close to 2.17 at 40 degrees, but considering the temperature effect, we may assume that at room temperature its real value is 2.2. A quantity which is usually less easy to understand is the imaginary part of the permittivity, ϵ'', which seems to be proportional to $\frac{1}{\omega}$, being ω the angular frequency; this is confirmed in several works, like for instance [4] and [17], where the AC conductivity, $\sigma_{AC} = \sigma_{DC} + \omega\epsilon''$ is calculated and shown to be constant in a wide frequency range. Obviously, if the AC conductivity is constant, it follows that $\epsilon'' \propto \frac{1}{\omega}$.
An example of the measured AC conductivity is presented in figure 7.5, which always refers to 40 degrees; it is possible to verify from this picture that the AC conductivity is constant in a large range of frequencies and equal to $4 \cdot 10^{-12} \frac{S}{m}$, which is in agreement with some other results relative to the same oil [78]. Another important parameter, which is usually considered by the technicians trying to give a quantitative measure of the dielectric losses of the insulation

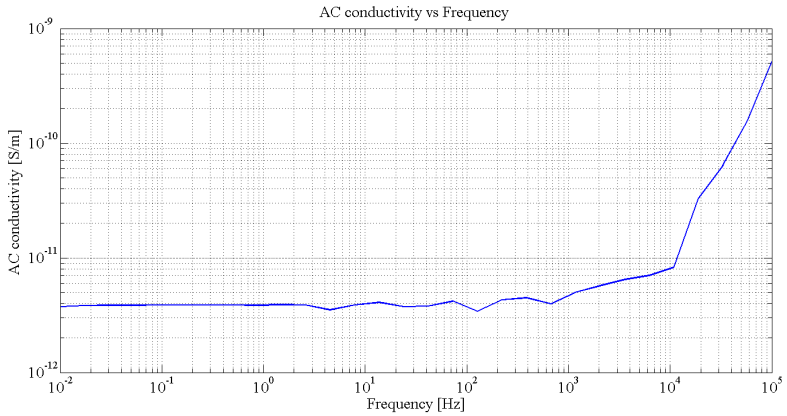

Figure 7.5: Example of the AC conductivity obtained for mineral oil.

material, is the loss tangent, $tan\delta$, which is calculated as follows:

$$tan\delta = \frac{\sigma_{AC}}{\omega\epsilon'} \tag{7.11}$$

which reveals that, in the case of oils, where both the real part of the permittivity and the AC conductivity are quite constant, is proportional to $\frac{1}{\omega}$. Usually, and this is the case for our measurements, mineral oils are characterized by a $tan\delta$ equal to 10^{-3} at $50\,Hz$ and room temperature (the results are not reported here for the sake of brevity).
The permittivity measurements have been performed on different nanofluids, which have been prepared according to the already meantioned procedures; the following concentrations have been considered:

- mineral oil, i.e. $0\ \frac{g}{L}$ nanofluid concentration, as benchmark;
- $0.1\ \frac{g}{L}$ nanofluid concentration;
- $0.2\ \frac{g}{L}$ nanofluid concentration;
- $0.5\ \frac{g}{L}$ nanofluid concentration;
- $1.0\ \frac{g}{L}$ nanofluid concentration.

These concentrations are similar to all the ones testes throughout this thesis, because for different reasons have proved to be the best in terms of insulating purposes, especially the lower ones. In the following, we would like to show if the model of equation 7.8 is able to predict the obtained results; moreover, for the sake of completeness, we will also presents a representative acquisition result, i.e. the one which is relative to $0.2\ \frac{g}{L}$ concentration, because such concentration has been the one showing the best properties in more situations.
Figure 7.6 has been obtained by comparing the model of equation 7.8 with the $50\,Hz$ obtained measurements. The figure shows an interesting thing, that is, the obtained data are fitted in a good way till the concentration $0.5\ \frac{g}{L}$; after such concentration, it is evident that the model predicts always higher permittivities than the measured ones. In order to understand why the model fails to

predict all the obtained data, it is necessary to remember that it is obtained using the field expressions calculated in chapter 5, where the distance between nanoparticles is always higher than $2R$, being R the nanoparticles radius. It is then clear that, the model prediction linearly raises with the concentration, while a saturation effect is expected when the distances among the nanoparticles reduce, as it is possible to see from figure 7.6. It is anyway quite difficult to understand why such saturation starts at intermediate concentrations, which, after all, are still so small in terms of mean free path between nanoparticles; possible other phenomena are likely to take place.
Apart from such problems at higher concentrations, the good quality of the predictions at low concentrations suggests that "'interphase"' issues are likely to explain the nanoparticles effect on the dielectric properties of mineral oil based nanofluid. It is therefore unnecessary to obtain a more refined permittivity model, taking into account:

- the more precise electrical field model, obtained in the second section of chapter 5;
- the different distribution of the paths between nanoparticles to try to catch the saturation effect.

At the end of chapter 5, we have re-called the theory of the electrical double layer for colloidal solutions [70], according to which counterions are attracted by charged particles and forced to move only on tangential directions. This phenomenon is particularly important, because it is the proof that nanoparticles are able to attract charges, as postulated by O'Sullivan in [31], and furthermore are able to attract free charges which are able then to determine non stable behaviors, like the one shown in the previous chapter.
A way to detect if electrical double layers exists on the nanoparticles of the nanofluids tested in this thesis consists in analyzing the trend of the imaginary part of the relative permittivity; if a loss peak does appear at intermediate-upper frequencies, this can be explained only in terms of counterions-relaxation issues, according to definition of τ in formula 5.34.

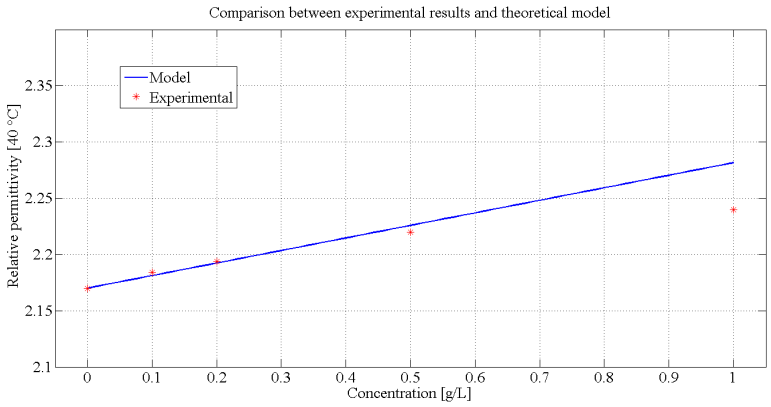

Figure 7.6: Comparison between the permittivity model and the measured values.

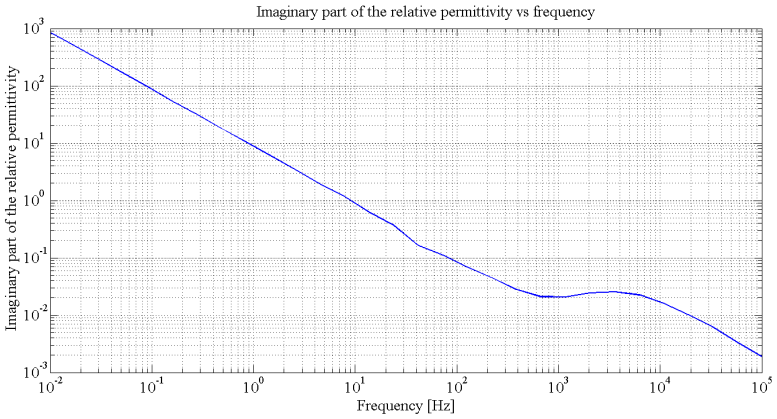

Figure 7.7: Imaginary part of the relative permittivity for 0.2 $\frac{g}{L}$ nanofluid.

Figure 7.7 shows for 0.2 $\frac{g}{L}$ nanofluid the imaginary part of the relative permittivity at 40 degrees and a clear loss peak is visible in the frequency range between $1\,kHz$ and $100\,kHz$. As suggested by the theory, the relaxation frequency is related to the dimensions of the counterions, their relative mechanical mobility and the temperature. We are not interested here to understand the origin of such counterions, which are probably linked to the ions residuals inside the nanofluids, but just to underline that such phenomenon can be the basis of other mechanisms, as a net movement of nanoparticles, as reported in [70], or, especially for higher concentrations, charge transfers between nanoparticles.
The presence of the "'Schwarz"' peak in the imaginary part of the relative permittivity is not the only difference when dealing with nanofluids. Comparing figures 7.7 and 7.4b it is evident that the losses inside nanofluids are higher at least two order of magnitude than those inside mineral oil: this result is worlds apart than what said by Bartnikas in [4], where a good insulator is supposed to show reduced losses whatever its final application. Nanofluids are, on the contrary, highly lossy insulators, because:

1. they are obtained starting from commercial products, which cannot be purified and which are, for this reason, highly contaminated;

2. they introduce field variations from a microscopical point of view, which are likely to be able to dissociate ions, creating a higher charge availability;

3. the counterions related mechanisms are likely to produce electrical losses [70];

4. nanoparticles act as polar particles [48], and polar fluids are characterized by higher losses than non polar ones ([4], [17]).

In this section we have analyzed the dielectric properties of nanofluid, trying to understand with a very simple model where do they come from. We have understood, comparing the obtained results with the prediction, that a key parameter is the "'interphase" region around nanoparticles. The nanoparticles presence also justifies the formation of an electrical double layer, which is claimed to be the main responsible of the non-stable mechanisms regarding nanofluids.

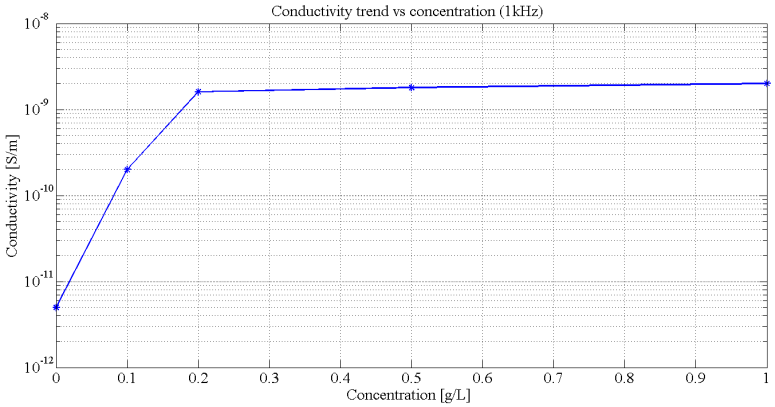

Figure 7.8: Electrical conductivity vs nanofluid concentration.

7.2 Electrical conductivity of nanofluids

In this section we will deal with conductivity issues. The electrical conductivity can be obtained from a measure of the loss tangent, using the following formula:

$$\sigma_{AC} = \omega \epsilon' tan\delta \tag{7.12}$$

Since in the case of insulating fluids, as already remarked in the previous section, the electrical conductivity is quite constant over a large range of frequencies, we can use, as reference, the values obtained for a particular frequency, for instance $1\,kHz$. Figure 7.8 shows the conductivities of the investigated nanofluids at 40 degrees, revealing an already observed behavior, that is, the conductivity increase reaches a saturation plateau at the concentration level which provides the optimum dielectric properties ($0.2\,\frac{g}{l}$). It is therefore evident that something happens at those particular concentrations.
The aim of such section is to try to understand the reason of such behavior, by proposing again a simple model. Before starting, it is necessary to remember, because it will be our starting hypothesis, that the testing voltage is $3\,V_{rms}$, i.e., a very low voltage, which, considering the geometry of the cell, generates a very low field, unable to ionize any species of the fluid, neither to cause charge injection. In other terms, nanoparticles are supposed to be free of charges, but free charges can be present inside the nanofluid for other reasons, as for instance contamination.
We would like to study the conduction process of a charge carrier between two nanoparticles, by calculating the tunneling probability, using a very simple approach. Let us suppose to consider the situation of figure 7.9, where a particle with global energy E is traveling towards a potential wall of amplitude U and thickness x; the classical theory states that the particle is able to overcome the potential barrier if and only if $E > U$.

The Schrodinger equation [79], on the contrary, admits the possibility for the particle to overcome such a barrier, by defining a transmission probability, which can be expressed in the following way, in the case of a simple barrier, like the one shown in figure 7.9:

$$p = e^{-2x\sqrt{\frac{8\pi^2 m(U-E)}{h^2}}} \tag{7.13}$$

where e is the Napier number, x the barrier thickness, m the particle mass and h the Planck constant.
If we think now to the nanoparticles system, and the relative electric field they create, when a voltage value is applied, a charge carrier "'sees"' a potential barrier between two nanoparticles because of the electrical field enhancement. A tunneling probability, p, can be thus derived, by using for instance equation 7.13; in the case of the nanoparticles distribution, nevertheless, the potential wall thickness x is not constant, but follows an exponential law, according to what we have already said in previous chapters, when the theory of random walk has been quoted [74]:

$$f(x) = \frac{1}{\lambda_m} e^{-\frac{x}{\lambda_m}} \tag{7.14}$$

where f represents the probability density function, x the random variable and λ_m the mean free path, which has already been the subject of our discussion.
The non-constancy of the barrier thickness does not create anyway a problem, because we will calculate in the following an average tunneling probability, which is defined as:

$$\langle p \rangle = \frac{\int_0^{+\infty} p(x) \frac{1}{\lambda_m} e^{-\frac{x}{\lambda_m}} dx}{\int_0^{+\infty} \frac{1}{\lambda_m} e^{-\frac{x}{\lambda_m}} dx} \tag{7.15}$$

In order to correctly compute the second term of equation 7.15, it is necessary to estimate the barrier which defines the single tunneling probability, $U - E$. We suppose in the following that such barrier is due to the electric field between two consecutive nanoparticles[3], which can be of two different types, according to the distance between them, as shown in figure 7.10.

This picture shows what has been already determined in chapter 5, where the electrical field distribution has been derived, considering the case that the distance between nanoparticles was bigger than $2R$ (case (a)), and the case in which the distance was lower (case (b)). In both cases, the obtained distributions are an approximation of the real electrical field distribution, but we have shown that the level of accuracy is quite good. For the sake of clearness, in figure 7.10, the dashed lines refer to the background field, while the continuous ones refer to the actual field value.

[3]In other words, we suppose that $E = 0$.

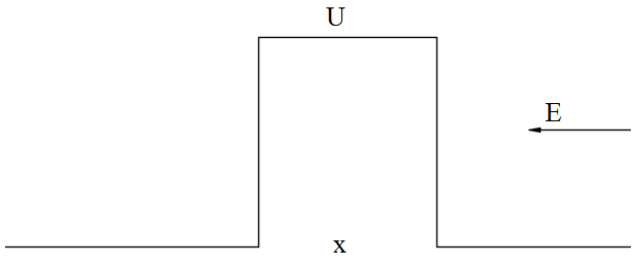

Figure 7.9: Generical situation where a particle with energy E has to overcome a potential wall U.

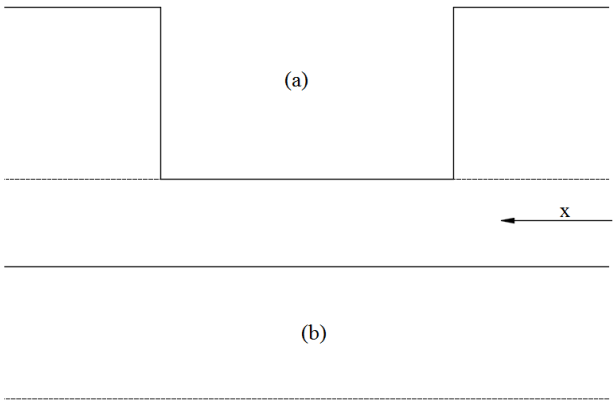

Figure 7.10: Electric field distribution between two consecutive nanoparticles (dashed lines refer to the background field). Case a: distance between nanoparticles bigger than $2R_p$; case b: distance lower than $2R_p$, being R_p the nanoparticles radius.

In order to estimate the barrier height U, the following relation has been considered:

$$U = \int_0^x E dx \tag{7.16}$$

where E represents the electric field distribution represented in figure 7.10. Equation 7.15 has been computed for different values of the concentration and unitary background field; unfortunately, being the potential barrier inside a non linear quantity, an analytical solution has not been possible to determine. The results of the above mentioned calculations are shown in figure 7.11.

The figure shows that the tunneling probability, although the investigated concentrations, as we have said, are not too high, increases rapidly, because of the contribution of the small paths between nanoparticles, which have the maximum probability, according to equation 7.14.
The probability theory states that, if a random event has a probability equal to p, the mean time between two consecutive observation of the event is $\Delta t = \frac{1}{p}$; it follows that the probability represents a measure of the mean frequency of the tunnel event. This perspective allows us to express the global nanofluid

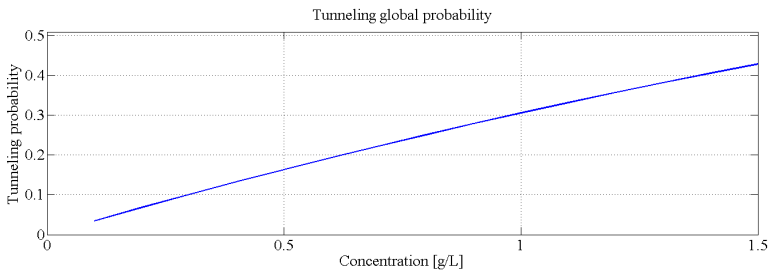

Figure 7.11: Tunneling global probability vs concentration.

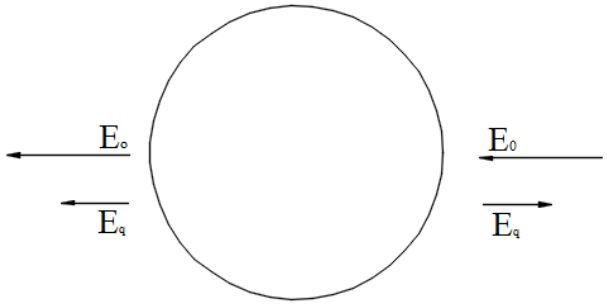

Figure 7.12: Simple diagram representing the fields acting close to the nanoparticle.

conductivity as follows:

$$\sigma_{AC} = \langle p \rangle \, \sigma_0 + \sigma_{oil} \tag{7.17}$$

where σ_0 represents the ferrofluid concentration, i.e., the AC conductivity of a fluid in which the tunneling probability is equal to 1. Equation 7.17 cannot be directly applied to our measures of figure 7.8, because we have no measures of the ferrofluid conductivity, but a qualitative agreement can be found, because of the fast saturation of $\langle p \rangle$, suggesting that the the investigated phenomenon may be the cause of the observed results even if strong simplifications have been used.

A confusing issue, when thinking to the results of figure 7.11, is that the higher the electric field, the lower the tunneling probability; this is contrasting with our idea that the electric field helps the injection, but it is correct because in our calculations we have supposed that the electric field due to the applied voltage represents the barrier to overcome. The electric field is able to help nanoparticles only in the case of trapped charge. In this way, when a charge carrier has to move from one nanoparticle to the following one, the electric field created by the trapped charge is likely to reduce the barrier the moving charge has to overcome, as it is familiar from the Schottky or Fowler-Nordheim injection.

The trapped charge does create an electrical field distribution which can be approximated by the Coulomb law:

$$E_q = \frac{q}{4\pi\epsilon r^2} \tag{7.18}$$

while the potential gap between two nanoparticles at distance x is equal to:

$$U = \int_R^{R+x} E_q dr = \frac{qx}{4\pi\epsilon R(R+x)} \tag{7.19}$$

Figure 7.12 shows how the electric field due to the charge presence acts; it is clear indeed that, on one side, it overlaps with the background field, further inhibiting the tunneling, but from the other side the charge field is opposed thus reducing the tunneling barrier: this effect is likely to increase the probability of equation 7.13. Unfortunately, we have not the possibility to test such considerations, because our Alpha-Beta analyzer has not the possibility to apply more

than $3\,V_{rms}$. High voltage DC conductivity measurements will be the only way to verify the correctness of our hypotheses system and will be performed in the following.

Conclusions

Our target, at the beginning of this thesis, has been the study of the main properties characterizing mineral oil-based nanofluids aimed to understand if they could be considered as good alternatives for mineral oil for insulation purposes. At the end of the work, our first answer is surely positive, i.e., nanofluids have proved to behave better than mineral oil, especially in the case of alternating voltages and when the concentrations were not too high to ignite secondary phenomena, like tunneling conduction or anything else. We have seen indeed that AC breakdown voltage, maybe thanks to the surfactant help, is much higher than that of the benchmark oil, and the same conclusion can be drawn for impulse voltages, where the asymmetry between the positive and negative voltage is somehow reduced favoring the dielectric strength.
DC results, on the other hand, highlight that the situation is not so easy to dismiss; they have in fact introduced the problem of space charge trapping, a problem which was already known in literature [31], but whose implications had not been explored yet. The developed model has let us to finally prove the tendency of the nanoparticles to create, with low concentrations, a charge peak characterized by a low mobility, which is likely to undermine the stability of the fluid, especially in the case of non uniform fields, as largely investigated in chapter 6. This is an important results, which proves that although at the beginning the performance of the fluid can be optimal, as shown in chapter 2, after some days the intrinsic nanofluid instability can become manifest, causing deleterious results for the whole application where they are installed. From this perspective, it is difficult to think that the research about nanofluids can find an immediate application. Big manufacturers need stable and repetitive results and the situation concerning nanofluids is, at the moment, quite confused, because a lot of research groups are interested in the single results, immediately after the manufacture process. The previous statement and the results of this thesis should have proved that, when dealing with nanofluids, the situation is in continuous evolution, showing the uselessness of all the studies about the outstanding properties they have. The latter have been necessary in a first stage, when we needed to learn if the nanoparticles technology could be of help in the case of liquid insulation.
The problems arose in this thesis and in the world, where some ferrofluid-based transformers have been installed showing the same aggregation phenomena which have been studied in this thesis, allow us to think that the research efforts have to be shifted towards insulated nanoparticles-based nanofluids, like for instance SiO_2 or TiO_2, which have been proved to behave as good as conductive nanoparticles [80],[77], [81].
The immediate consequence of such tendency will be, as obvious, the loss of the

huge increase in the thermal exchange properties presented by the nanofluid, which, in a certain sense, has been one of the reason which has driven a lot of people to start studying them. If we remain anyway linked to the idea of the nanofluid starting from mineral oil, after all we are not scared of the thermal exchange properties, because they would not change too much after the insertion of low concentration nanoparticles. The little increase in the viscosity [86], [87] does not represent a problem, either.
All these issues, on the contrary, can represent a criticality if the nanofluids will be performed starting from vegetable derived fluids or synthetic esters, which are known to be less conductive because more viscous in general. In these thesis we have not dealt with such kinds of fluids, which are now on fair because of their "'green"' behavior; their performance have proved to be comparable with that of mineral oil, regarding the inception phenomena, but the resistance to the streamer and leader propagation in such fluids is lower than that in mineral oil [7], [35]. For such a reason, vegetable fluids are still nowadays used in low-medium voltage applications rather than high voltage ones. The more and more insistent requests for environmental free insulation liquids, however, will carry researchers to focus on these kind of fluids as starting point for the nanofluids manufacture; it is indeed more interesting to improve the properties of these class of fluids, rather then the optimal properties of mineral oil, which has the problem of the toxicity and the disposal.
[82], [83] [84] and [85] are only few examples of the results of the researchers' work on this subject; we believe that in the future the list will be more populated and we hope some manufacturers will risk the final application, too.

Bibliography

[1] Goetter, R. W., *Innovations in unsaturated polyester resins for electrical insulation*, Electrical Manufacturing and Coil Winding Expo 2010-2013, pp. 119-121.

[2] Arief, Y.Z., Ismail, M.I., Makmud, M.Z.H., Adzis, Z., Muhamad, N.A., *Partial discharge characteristics of natural rubber blends with inorganic nanofiller as electrical insulating material*, Applied Mechanics and Materials 284-287, pp. 188-192.

[3] Akmal, M.J.-N., Afendi, M.P.-M., Asiah, M.-N., Addawiyah, Z.-R., Faizal, K.-N., *Effects of SiO2 and TiO2 nanofillers on conductivity level of LLDPE-NR nanocomposite HV insulator*, Applied Mechanics and Materials 284-287, pp. 305-309.

[4] Bartnikas, R., *Electrical insulating liquids (Engineering Dielectrics)*, R. Bartnikas Editor, sponsored by ASTM Committee D9, Vol. 3, 1994.

[5] Feil, D.L.P., Silva, P.R., Bernardon, D.P., Sperandio, M., Medeiros, L.H., *Development of an efficient distribution transformer using amorphous core and vegetable insulating oil*, Electric Power Systems Research 144, pp. 268-279.

[6] Hrkac, M., Papageorgiou, P., Kosmoglou, I., Miatto, G., *BIOTEMP transformer technology for innovative compact substation*, IET Conference Publications 2010 (572 CP).

[7] Liu Q., Wang Z. D., *Streamer Characteristic and Breakdown in Synthetic and Natural Ester Transformer Liquids under Standard Lightning Impulse Voltage*, IEEE Transactions on Dielectrics and Electrical Insulation Vol. 18, No. 1; February 2011.

[8] Yang, L., Du, K., *A comprehensive review on heat transfer characteristics of TiO2 nanofluids*, International Journal of Heat and Mass Transfer 108, pp. 11-31.

[9] Sridhara, V., Satapathy, L.N., *Effect of Nanoparticles on Thermal Properties Enhancement in Different Oils-A Review*, Critical Reviews in Solid State and Materials Sciences 40 (6), pp. 399-424, 2015.

[10] Lipscomb, T.G., *Electrical Insulating Oils*, ASTM STP 998, American Society for Testing and Materials, Philadelphia, 1988, pp. 5-24.

[11] Par Wedin, *Electrical Breakdown in Dielectric Liquids, a Short Overview*, IEEE Electrical Insulation Magazine, November/December Vol. 30, No. 6, 2014.

[12] Devins J. C., Rzad S. J., and Schwabe R. J., *Breakdown and prebreakdown phenomena in liquids*, Journal of Applied Physics, 52, 4531 (1981); DOI: 10.1063/1.329327.

[13] Chadband W. G., *On variations in the propagation of positive discharges between transformer oil and silicone fluids*, J. Phys. D: Appl. Phys., vol.13, no. 7, pp. 12991307, 1980.

[14] Denat A., Gosse J. P., and B. Gosse, *Electrical conduction of purified cyclohexane in a divergent electric field*, IEEE Trans. Electr. Insul., vol.23, no. 4, pp. 545554, 1988

[15] Ingebrigtsen S., Lundgaard L. E., and strand P. O., *Effects of additives on prebreakdown phenomena in liquid cyclohexane: I. Streamer initiation*, J. Phys. D: Appl. Phys., vol. 40, no. 17, pp. 5161516, 2007.

[16] Halpern B. and R. Gomer, *Field Ionization in Liquids*, J. Chem. Phys. 51,1048 (1969).

[17] Schidt W., *Liquid state electronics of insulating fluids*, CRC Press, 1997.

[18] Dumitrescu L., Lesaint O., Bonifaci N., Denat A. and P. Notingher, *Study of streamer inception in cyclohexane with a sensitive charge measurement technique under impulse voltage*, J. Electrostat., vol. 53, no. 2, pp. 135146, 2001.

[19] Ingebrigtsen S., *The influence of chemical composition on streamer initiation and propagation in dielectric liquids*, PhD dissertation, Dept. Chemistry, Norwegian Univ. Sci. Technol., Trondheim, 2008.

[20] Chadband W. G. and Wright G. T. *A pre-breakdown phenomenon in the liquid dielectric hexane*, Brit. J. Appl. Phys. 16, 305 (1965).

[21] Murray D.W., McDonald J.M., White A.M., and Wright P.G., *Proceedings of World Petroleum Congress*, Vol. 11, No. 4, 1983, pp. 447-457.

[22] Wilson A. C. M., *Insulating Liquids: Their Uses, Manufacture, and Properties*, Peter Peregrinus Publication, Stevenage, UK, 1980.

[23] Hobson C. D. and Pohl W., *Modern Petroleum Technology* Wiley, New York, 1973.

[24] Seagal V. et al, *AC (60Hz) and Impulse Breakdown Streangth of a Colloidal Fluid Based on Transformer Oil and Magnetite Nanoparticles*, IEEE Int. Symp. on Electrical Insulation, Arlington, Virginia, USA, June $7-10$, 1998.

[25] Ibrahim K. et alia, *Realization of Partial Discharge Signals in Transformer Oils Utilizing Advanced Computational Techniques*, IEEE Transactions on Dielectrics and Electrical Insulation Vol. 19, No. 6; December 2012.

[26] Cleary G. P., Judd M. D., *UHF and current pulse measurements of partial discharge activity in mineral oil*, IEE Proceedings - Science, Measurement and Technology, Volume: 153, Issue 2, 9 March 2006.

[27] Bianco V., Manca O., Nardini S., Vafai K., *Heat Transfer Enhancement with Nanofluids*, Taylor&Francis Publisher, 2015.

[28] Das S. K., Choi S. U., Wenhua Y., Pradeep T., *Nanofluids: Science and Technology*, Wiley-Interscience Publisher, 2007.

[29] Segal V. and Raj K., *An investigation of Power Transformer Cooling with Magnetic Fluid*, Indian Journal of Engineering and Material Sciences, 1998.

[30] US Patent N. 3215572 A, *Low viscosity magnetic fluid obtained by the colloidal suspension of magnetic particles*, filed Oct 9, 1963.

[31] Sullivan F. M. O., *A Model for the Initiation and propagation of Electrical Streamers in transformer oil and Transformer based nanofluids*, Ph.D degree thesis, Massachusetts Institute of Technology, USA, 2007.

[32] Hiroyuki Ohshima, *Electrical Phenomena at Interfaces and Biointerfaces*, John Wiley & Sons, Inc. DOI: 10.1002/9781118135440, Jan 2012.

[33] Lagaly O. S. R. Z. G. , *Dispersionen und Emulsionen*, Darmstadt: Dietrich Steinkopff Verlag, 1997.

[34] Rosensweig R. E., *Ferrohydrodynamics*, Cambridge University Press, 1985.

[35] Liu Q., Wang Z. D., *Breakdown and Withstand Strengths of Ester Transformer Liquids in a Quasi-uniform Field under Impulse Voltages*, IEEE Transactions on Dielectrics and Electrical Insulation Vol. 20, No. 2; April 2013.

[36] Abernethy R. B., *The New Weibull Handbook*, published and distributed by Robert B. Abernethy, December 2006.

[37] Mettler-Toledo International, *GTPR - Good Titration Practice in Karl Fischer Titration*, 2011.

[38] Rzad S. J., Devins J. C. and R. J. Schwabe, *Transient behavior in transformer oils: prebreakdown and breakdown phenomena*,IEEE Transactions on Electrical Insulation Vol. ET-14, N.6, December 1979.

[39] Settles, Gary S., *Schlieren and shadowgraph techniques: visualizing phenomena in transparent media*, Springer Science & Business Media, 2012.

[40] Cristofolini, A., et al., *Schlieren imaging in a dielectric barrier discharge actuator for airflow control*, Journal of Applied Physics 111.3 (2012).

[41] Montgomery, Douglas, *Design and analysis of Experiments*, Eigth Edition, Wiley Press, 2013, Section 3.5.7.

[42] Current J. M., *Introduction to Data Analysis with R for forensic scientists*, CRC Press, 2009.

[43] Mazzanti G., Marzinotto M., *Extruded cables for high voltage direct current transmission: advances in research and development*, Wiley−IEEE press, 2013.

[44] Liu Q., Wang Z. D., Lesaint O., *Comparison of streamer propagation in mineral oils under lightning and step impulse voltages*, 2014 IEEE 18th International Conference on Dielectric Liquids (ICDL), DOI: 10.1109/ICDL.2014.6893151.

[45] Denat A., Lesaint O., Mc Cluskey F., *Streamer and breakdown phenomena under step and lightning impulses in various hydrocarbon liquids*, 2014 IEEE Conference on Electrical Insulation and Dielectric Phenomena (CEIDP), DOI: 10.1109/CEIDP.2014.6995862.

[46] Lesaint O., Tobazeon R., *Streamer generation and propagation in transformer oil under divergent field conditions*, 1987 Ninth International Conference on Conduction and Breakdown in Dielectric Liquids.

[47] Mason J. H., *Breakdown of solid dielectrics in divergent fields*, Proc. IEE B, Radio and Electronic Engineering, Vol.102, No.5, pp. 725727, 1955.

[48] Rajnak M., Kurimsky J., Dolnik B., Marton K., Tomco L., Taculescu A., Vekas L., Kovac J., Vavra I., Tothova J., Kopcansky P., Timko M., *Dielectric response of transformer oil based ferrofluid in low frequency range*, Journal of Applied Physics, 114, 034313 (2013).

[49] Miao J., Dong M., Ren M., Wu X., Shen L., *Effect of nanoparticle polarization on relative permittivity of transformer oil-based nanofluids*, Journal of Applied Physics, 113, 204103 (2013).

[50] Halpern B. and R. Gomer, *Field Emission in Liquids*, J. Chem. Phys. 51,1031 (1969).

[51] Linz P., *Analytical and Numerical Methods for Volterra Equations*, SIAM (Studies in Applied Mathematics), Philadelphia, 1985.

[52] IEC 60156, *Insulating liquidsDetermination of the breakdown voltage at power frequencyTest method*, 2003-11.

[53] Lesaint, O., *"'Streamers" in liquids: relation with practical high voltage insulation and testing of liquids*, IEEE Intern. Conf. Dielectr. Liquids (ICDL), Poitiers, France, pp.120-125, 2008.

[54] Dunne, O. J., *Multiple Comparisons Among Means*, Journal of the American Statistical Association. 56 (293): 5264. doi:10.1080/01621459.1961.10482090.

[55] Forster, E. O., *Partial discharges and streamers in liquid dielectrics-the significance of the inception voltage*, IEEE Trans. Electr. Insul., vol. 28, no. 6, pp. 941946, 1993.

[56] Hauschild W., Lemke E., *High-Voltage Test and Measuring Techniques*, Springer-Verlag Berlin Heidelberg, 2014.

[57] IEC 60270, *High-voltage test techniques - Partial discharge measurements*, 2000.

[58] Morshuis, P. H.F, *Partial discharge mechanism: mechanisms leading to breakdown analyzed by fast electrical and optical measurements*, PhD thesis, Delft University of Technology, 1993.

[59] Wang, L., *Physical model of PD behavior and relevant damage growth from micro cavities in polyethylene based material under AC voltage*, PhD thesis, Department of Electrical Engineering, University of Bologna, Italy, 2011.

[60] Wilhelm, H.M., Franch, V., Franch, A.F., *Compatibility of Transformer Construction Materials with Natural Ester-based Insulating Fluids*, IEEE Transactions on Dielectrics and Electrical Insulation, Vol. 22, Issue 5, Pag. 2703-2708, 2015.

[61] Pompili, M., Mazzetti, C., Bartnikas, R., *Phase relationship of PD pulses in dielectric liquids under ac conditions*, IEEE Transactions on Dielectrics and Electrical Insulation, Vol. 7, Issue 1, Pag. 113-117, 2000.

[62] Mazzetti, C., Pompili, M., Yamashita, H., *Comparison of streamer and partial discharge inception voltages in liquid dielectrics*, Sixth International Conference on Dielectric Materials, Measurements and Applications, 1992.

[63] Lewis, T. J., *A new model for the primary process of electrical breakdown in liquids*, IEEE Transactions on Dielectrics and Electrical Insulation, Vol. 5, Issue 3, Pag. 306-315, 1998.

[64] Niemeyer, L., *A generalized approach to partial discharge modeling*, IEEE Transactions on Dielectrics and Electrical Insulation, Vol. 2, Issue 4, Pag. 510-528, 2002.

[65] Lewis, T., *Interfaces are the dominant feature of dielectrics at the nanometric level*, IEEE Transactions on Dielectrics and Electrical Insulation, Vol. 11, No. 5, pp. 739-753, 2004.

[66] Rätzke, S., Kindersberger, J., *Role of interphase on the resistance to high-voltage arcing, on tracking and erosion of silicone/SiO_2 nanocomposites*, IEEE Trans. DEI, Vol. 17, No. 2, pp. 607-614, 2010.

[67] Tanaka, T., Kozako, M., Fuse, N., Ohki, Y., *Proposal of a multi-core model for polymer nanocomposite dielectrics*, IEEE Trans DEI, Vol. 12, No. 4, pp. 669-681, 2005.

[68] Andrisch, T., Kochetov, R., Morshuis P.H.F., *Proposal of the polymer chain alignment model*, Proc. IEEE CEIDP, pp. 624-627, 2011.

[69] Morshuis, P.H.F, *Interfaces: to be avoided or to be treasured?*, Proc. IEEE ICSD, pp. 1-9, 2013.

[70] Schwarz, G., *A theory of the low-frequency dielectric dispersion of the colloidal particles in elecrtolyte solutions*, J. Phys. Chem., 1962, 66 (12), pp 26362642.

[71] Butcher, M., Member, S., Neuber, A. et alia, *Conduction and Breakdown Mechanisms in Transformer Oil*, IEEE Transactions on Plasma Science, Vol. 34, No. 2, April 2006.

[72] Butcher, M., Neuber, A., Krompholz, H., Dickens, J., *Pre-breakdown current behavior in dc volume breakdown in transformer oil*, Proc. 14th IEEE Int. Pulsed Power Conf., vol. 1, Jun. 1518, 2003, pp.289292.

[73] Meek, J., Crags, J., *Electrical breakdown in gases*, Oxford at the Clarendon Press

[74] Kuffel, E., Zaengl, W. S., Kuffel, J., *High Voltage Engineering: Fundamentals*, Newnes, 2000.

[75] Jones, T. B., *Electromechanics of particles*, Cambridge University Press, Cambridge, 1995.

[76] Crank, J., Nicolson, P., *A practical method for numerical evaluation of solutions of partial differential equations of the heat conduction type*, Proc. Camb. Phil. Soc. 43 (1): 5067.

[77] Cavallini, A., Karthik, Negri, F., *The Effect of Magnetite, Graphene Oxide and Silicone Oxide Nanoparticles on Dielectric Withstand Characteristics of Mineral Oil*, IEEE Trans DEI, Vol. 22, No. 5, pp. 2592 - 2600, 2015.

[78] Azcarraga, C. G., *Partial Discharge Phenomena in Converter and Traction Transformers: Identification and Reliability*, Ph.D thesis, DEI Unibo, 2014.

[79] Schrodinger, E., *An Undulatory Theory of the Mechanics of Atoms and Molecules*, Physical Review, vol. 28, issue 6, 1926, pp. 10491070.

[80] Jin, H., Andritsch, T., Tsekmes, A., Kochetov, R., Morshuis, PHF., Smit, JJ., *Properties of mineral oil based silica nanofluids*, IEEE Transactions on Dielectrics and Electrical Insulation, Vol. 21, No. 3, 2014, p. 1100-1108.

[81] Du Yue fan, Lv Yu Zhen, Zhou Jian-quan, Chen Mu-tian, Li xiao- xin, Li cheng rong, *Effect of ageing on Insulating property of mineral oil based TiO2 nanofluids*, IEEE International Conference on Dielectric Liquids, pp. 1-4, 2011.

[82] Peppas, G.D., Bakandritsos, A., Charalampakos, V.P., Zboril, R., Gonos, I.F., *Ultrastable Natural Ester-Based Nanofluids for High Voltage Insulation Applications*, ACS Applied Materials and Interfaces 8 (38), pp. 25202-25209, 2016.

[83] Du, Y., Li, C., L, Y., Chen, M., Zhou, Y., *Insulating properties and charge characteristics of natural ester fluid modified by TiO_2 semiconductive nanoparticles*, IEEE Transactions on Dielectrics and Electrical Insulation 20 (1), 6451351, pp. 135-140, 2013.

[84] Li, J., Zhang, Z., Zou, P., Grzybowski, S., Zahn, M., *Preparation of a vegetable oil-based nanofluid and investigation of its breakdown and dielectric properties*, IEEE Electrical Insulation Magazine 28 (5), 6268441, pp. 43-50, 2012.

[85] Zou, P., Li, J., Sun, C.-X., Zhang, Z.-T., Liao, R.-J., *Dielectric properties and electrodynamic process of natural ester-based insulating nanofluid*, Modern Physics Letters B 25 (25), pp. 2021-2031, 2011.

[86] Aref, A.H., Entezami, A.A., Erfan-Niya, H., Zaminpayma, E., *Thermophysical properties of paraffin-based electrically insulating nanofluids containing modified graphene oxide*, Journal of Materials Science, 52 (5), pp. 2642-2660, 2017.

[87] Dalkilic, A.S., Kkyldrm, B.O., Akdogan Eker, A., (...), Jumpholkul, C., Wongwises, S., *Experimental investigation on the viscosity of Water-CNT and Antifreeze-CNT nanofluids*, International Communications in Heat and Mass Transfer, 80, pp. 47-59, 2017.